

Spring 1979

Noise performance of the Klapper-Kratt low delay FM detector

Allan Brown Tarbell

New Jersey Institute of Technology

Follow this and additional works at: <https://digitalcommons.njit.edu/dissertations>



Part of the [Electrical and Electronics Commons](#)

Recommended Citation

Tarbell, Allan Brown, "Noise performance of the Klapper-Kratt low delay FM detector" (1979). *Dissertations*. 1250.
<https://digitalcommons.njit.edu/dissertations/1250>

This Dissertation is brought to you for free and open access by the Theses and Dissertations at Digital Commons @ NJIT. It has been accepted for inclusion in Dissertations by an authorized administrator of Digital Commons @ NJIT. For more information, please contact digitalcommons@njit.edu.

Copyright Warning & Restrictions

The copyright law of the United States (Title 17, United States Code) governs the making of photocopies or other reproductions of copyrighted material.

Under certain conditions specified in the law, libraries and archives are authorized to furnish a photocopy or other reproduction. One of these specified conditions is that the photocopy or reproduction is not to be “used for any purpose other than private study, scholarship, or research.” If a user makes a request for, or later uses, a photocopy or reproduction for purposes in excess of “fair use” that user may be liable for copyright infringement,

This institution reserves the right to refuse to accept a copying order if, in its judgment, fulfillment of the order would involve violation of copyright law.

Please Note: The author retains the copyright while the New Jersey Institute of Technology reserves the right to distribute this thesis or dissertation

Printing note: If you do not wish to print this page, then select “Pages from: first page # to: last page #” on the print dialog screen

The Van Houten library has removed some of the personal information and all signatures from the approval page and biographical sketches of theses and dissertations in order to protect the identity of NJIT graduates and faculty.

INFORMATION TO USERS

This was produced from a copy of a document sent to us for microfilming. While the most advanced technological means to photograph and reproduce this document have been used, the quality is heavily dependent upon the quality of the material submitted.

The following explanation of techniques is provided to help you understand markings or notations which may appear on this reproduction.

1. The sign or "target" for pages apparently lacking from the document photographed is "Missing Page(s)". If it was possible to obtain the missing page(s) or section, they are spliced into the film along with adjacent pages. This may have necessitated cutting through an image and duplicating adjacent pages to assure you of complete continuity.
2. When an image on the film is obliterated with a round black mark it is an indication that the film inspector noticed either blurred copy because of movement during exposure, or duplicate copy. Unless we meant to delete copyrighted materials that should not have been filmed, you will find a good image of the page in the adjacent frame.
3. When a map, drawing or chart, etc., is part of the material being photographed the photographer has followed a definite method in "sectioning" the material. It is customary to begin filming at the upper left hand corner of a large sheet and to continue from left to right in equal sections with small overlaps. If necessary, sectioning is continued again—beginning below the first row and continuing on until complete.
4. For any illustrations that cannot be reproduced satisfactorily by xerography, photographic prints can be purchased at additional cost and tipped into your xerographic copy. Requests can be made to our Dissertations Customer Services Department.
5. Some pages in any document may have indistinct print. In all cases we have filmed the best available copy.

University
Microfilms
International

300 N. ZEEB ROAD, ANN ARBOR, MI 48106
18 BEDFORD ROW, LONDON WC1R 4EJ, ENGLAND

7920448

TARBELL, ALLAN BROWN
NOISE PERFORMANCE OF THE KLAPPER-KRATT LOW
DELAY FM DETECTOR.

NEW JERSEY INSTITUTE OF TECHNOLOGY,
D.ENG.SC., 1979

University
Microfilms
International 300 N. ZEEB ROAD, ANN ARBOR, MI 48106

NOISE PERFORMANCE OF THE KLAPPER-KRATT
LOW DELAY FM DETECTOR

BY

ALLAN B. TARBELL

A DISSERTATION
PRESENTED IN PARTIAL FULFILLMENT OF
THE REQUIREMENTS FOR THE DEGREE
OF
DOCTOR OF ENGINEERING SCIENCE IN ELECTRICAL ENGINEERING
AT
NEW JERSEY INSTITUTE OF TECHNOLOGY

This dissertation is to be used only with due regard to the rights of the author. Bibliographical references may be noted, but passages must not be copied without the permission of the College and without credit given in subsequent written or published work.

Newark, New Jersey

1979

ABSTRACT

In this dissertation the dual differentiator version of the Klapper-Kratt FM detector family is investigated with additive Gaussian noise. Prior analysis of this new detector family has been limited to the noiseless case.

The investigation was conducted both analytically and experimentally. First, the dual differentiator version of the Klapper-Kratt detector was mathematically analyzed, assuming an unmodulated carrier plus additive Gaussian noise. This analysis was verified by assembling the detector and measuring its performance in the laboratory.

It was discovered that the Klapper-Kratt detector without limiter performs identically to the conventional limiter discriminator in the linear improvement region. When compared to the limiter discriminator, threshold occurs at a higher CNR in the new detector (without limiter). When a limiter is added to the Klapper-Kratt detector, the new detector exhibits the same threshold as that of the limiter discriminator. The detector was found to have extremely low delay and wide bandwidth. The analytical and experimental results were nearly identical.

APPROVAL OF DISSERTATION

NOISE PERFORMANCE OF THE KLAPPER-KRATT
LOW DELAY FM DETECTOR

BY

ALLAN B. TARBELL

FOR

DEPARTMENT OF ELECTRICAL ENGINEERING
NEW JERSEY INSTITUTE OF TECHNOLOGY

BY

FACULTY COMMITTEE

APPROVED: _____ CHAIRMAN

NEWARK, NEW JERSEY

MAY 1979

ACKNOWLEDGEMENTS

The author gratefully acknowledges the guidance and assistance of the chairman of his doctoral committee, Dr. Jacob Klapper. He also expresses his gratitude to the other members of his committee, Dr. Joseph Frank, Dr. Solomon Rosenstark, and Dr. Walter Gilbert, for their aid.

The author also acknowledges the encouragement and understanding of Mr. William Fishbein, Chief of the Radar Division of the Army's Combat Surveillance and Target Acquisition Laboratory. Without his support this work would not have been possible.

TABLE OF CONTENTS

	<u>Page</u>
CHAPTER I: INTRODUCTION-FM AND ITS PROBLEMS	
1.1 FM and Its Problems	1
1.2 Limiter Discriminator - Above Threshold	1
1.3 Limiter Discriminator - Near Threshold	8
1.4 The Limiter Discriminator SNR vs CNR Relationship	8
References - Chapter I	13
CHAPTER II: A NEW FAMILY OF FM DETECTORS	
2.1 Background	14
2.2 Description of the New Detector	16
2.3 Integrator Initial Conditions	19
2.4 Description of the Dual Differentiator Detector	24
References - Chapter II	30
CHAPTER III: THE RESULTS OF PREVIOUS ANALYSIS OF THE KLAPPER-KRATT DETECTOR FAMILY	
3.1 Previous Art	31
3.2 Kratt's Results	31
3.3 Kersus' Results	36
3.4 Analytical Performance Comparisons of Two Versions of the Klapper-Kratt Detector	38
3.5 Threshold Comments of Kratt and Kersus	42
References - Chapter III	45

TABLE OF CONTENTS (Contd)

	<u>Page</u>
CHAPTER IV: PERFORMANCE OF THE KLAPPER-KRATT DETECTOR IN THE PRESENCE OF NOISE	
4.1 Introduction	46
4.2 Noise Representation	46
4.3 Noise Analysis	49
4.4 Special Case - High CNR	56
4.5 Threshold	57
4.6 RF Canceller	57
References - Chapter IV	60
CHAPTER V: EXPERIMENTAL VERIFICATION	
5.1 Introduction	61
5.2 Circuit Description and Operation	61
5.3 Experimental Performance Results	65
5.4 Comparison of the Experimental and Analytical Results for the Klapper-Kratt Demodulator	73
5.5 Comparison of the Klapper-Kratt Demodulator and the Limiter Discriminator	78
References - Chapter V	82
CHAPTER VI: CONCLUSIONS	
6.1 Conclusions	84
6.2 Future Efforts	85
References - Chapter VI	85

TABLE OF CONTENTS (Contd)

	<u>Page</u>
APPENDIX I: DETAILED DERIVATION OF SNR-CNR RELATIONSHIP	86
APPENDIX II: REAL AND IDEAL DIFFERENTIATORS	108
BIBLIOGRAPHY	111

TABLE OF CONTENTS (Contd)

LIST OF FIGURES

<u>Figure</u>	<u>Page</u>
1-1 FM System Performance	2
1-2 Limiter Discriminator	3
1-3 Conventional FM Demodulator	4
1-4 Graphical Representation of Carrier and Noise	6
1-5 $\theta(t)$ for High CNR	7
1-6 $\theta(t)$ for Low CNR	9
1-7 $\theta(t)$	10
1-8 Threshold $(\text{CNR})_{\text{AM}}$ vs IF To Twice Baseband Ratio	12
2-1 One Member of the New FM Detector Family	15
2-2 Coherent FM Discriminator	17
2-3 $\frac{1}{\omega} (\omega - \frac{1}{\omega})$ vs ω	18
2-4 A Second Member of the New Detector Family	20
2-5 A Third Member of the New Detector Family	21
2-6 A Fourth Member of the New Detector Family	22
2-7 Integrator Problem Under Wideband Conditions	23
2-8 Another Member of the New FM Detector Family	26
2-9 Coherent FM Discriminator	27
2-10 $\omega (\frac{1}{\omega} - \omega)$ vs ω	28
2-11 RF Canceller for the Dual Differentiator Detector	29
3-1 Park Detector	32
3-2 One Member of the New FM Detector Family	33
3-3 Dual Differentiator Member of the Klapper-Kratt Family	37

TABLE OF CONTENTS (Contd)

LIST OF FIGURES

<u>Figure</u>		<u>Page</u>
3-4	Limiter Discriminator Interference Characteristic Curve (Equation 3-22)	43
3-5	Klapper-Kratt Detector Interference Characteristic Curve (Equation 3-24)	44
4-1	Dual Differentiator Version of the New FM Detector Family	47
4-2	(a) PSD of $x(t)$ and $y(t)$ (b) Complete Detector	48
4-3	Demodulator Portion of FM Detector	50
4-4	Threshold $(CNR)_{AM}$ vs IF to Baseband Ratio	59
5-1	Demodulator Portion of FM Detector	62
5-2	(a) Demodulator Circuit Diagram (b) Test Point Waveforms	63 64
5-3	Output Voltage vs Input Frequency	66
5-4	Baseband Signal Superimposed on Multiplier Output for Various Baseband Waveforms	67
5-5	Test Equipment for Measurement of SNR - CNR Characteristic	68
5-6	Predetection Filter Response	70
5-7	Postdetection Filter Response	71
5-8	Experimental Performance of Klapper- Kratt Demodulator with no Limiter	72
5-9	Experimental Performance of Klapper-Kratt Demodulator with no Limiter (Expanded Scale)	74
5-10	Limiter Schematic	75
5-11	Experimental Performance of Klapper- Kratt Demodulator with Limiter	76

TABLE OF CONTENTS (Contd)

LIST OF FIGURES

<u>Figure</u>		<u>Page</u>
5-12	Experimental Performance of Klapper-Kratt Demodulator with Limiter (Expanded Scale)	77
5-13	Analytical and Experimental Comparison of the Klapper-Kratt and Limiter Discriminator Demodulators	79
5-14	Discriminator Block Diagram	80
5-15	Comparison of Klapper-Kratt (with Limiter) Demodulator and Limiter Discriminator Near Threshold	83
I-1	Dual Differentiator Version of Klapper-Kratt Family	87
II-1	Ideal Differentiator	109
II-2	Real Differentiator	109
II-3	Block Diagram of Real Differentiator with Phase Correction	110
II-4	Phasor Diagram for Real Differentiator with Phase Correction	110

TABLE OF CONTENTS (Contd)

LIST OF TABLES

<u>Table</u>		<u>Page</u>
3-1	RMS Distortion - Figure 3-2	40
3-2	RMS Distortion - Figure 3-3	41
5-1	Summary of Analytical and Experimental Results for Klapper-Kratt Detector	73
5-2	Comparison of the Limiter Discriminator with the Klapper-Kratt Detector	81

CHAPTER I

INTRODUCTION - FM AND ITS PROBLEMS1.1 FM and its Problems

FM operation is characterized by the curve shown in Figure 1-1 (Ref. 1). Three distinct regions are indicated: (1) The FM improvement region; (2) the below threshold region; and (3) the distortion limited region.

The FM improvement region is the portion normally used. It is in this region that the signal to noise ratio at the output can be improved over the input carrier to noise ratio (CNR).

The below threshold region is characterized by a rapid deterioration in SNR at the demodulator output. The "threshold point" is usually defined as the point at which the SNR has dropped 1 dB more than predicted by the linear improvement region.

Above a certain level the output of an FM system fails to improve, due to various possible distortions. This region is referred to as the distortion limited region.

1.2 Limiter Discriminator - Above Threshold

Let us begin with a review of the operation of a conventional limiter discriminator. One of the many possible forms of the limiter discriminator is shown in Figure 1-2. Operationally, the limiter discriminator might be represented as in Figure 1-3. An FM signal can be defined as

$$e_i(t) = A \cos \left[\omega_c t + \phi(t) \right] \quad (1-1)$$

where A is the carrier amplitude, ω_c is the carrier frequency, and $\phi(t)$ represents the integral of the modulating signal. Applying this signal to the demodulator of Figure 1-3 yields at the limiter output,

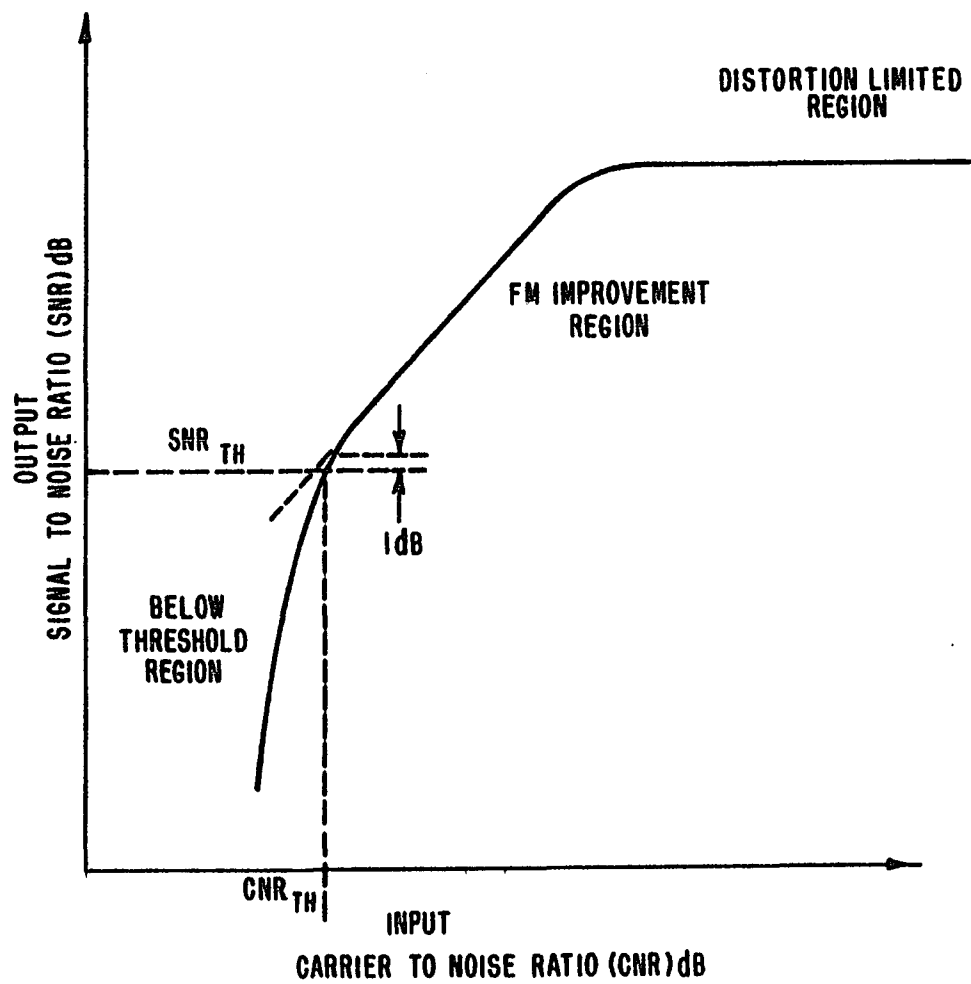


FIGURE I-1. FM SYSTEM PERFORMANCE

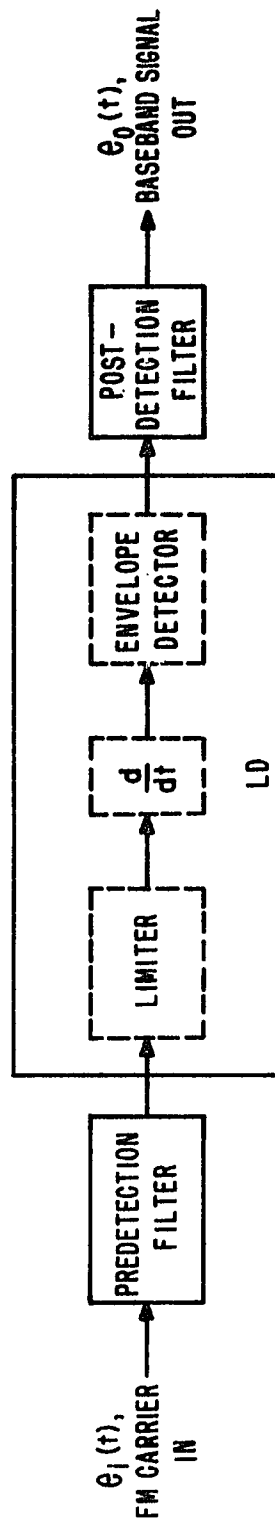


FIGURE I-3. CONVENTIONAL FM DEMODULATOR

$$A' \cos [\omega_c t + \phi(t)], \quad (1-2)$$

and at the differentiator output

$$- [\omega_c + \dot{\phi}(t)] A' \sin [\omega_c t + \phi(t)]. \quad (1-3)$$

Notice that the differentiation transformed the FM signal into AM.

Next, the AM is demodulated by the envelope detector and filtered.

The filtered output is

$$e_o(t) = A'' \dot{\phi}(t) \quad (1-4)$$

which is proportional to the baseband modulating signal, $0(t)$.

Equation (1-5) describes an unmodulated carrier with additive narrow-band noise.

$$e_i(t) = A \cos \omega_c t + x(t) \cos \omega_c t - y(t) \sin \omega_c t \quad (1-5)$$

This equation can be represented by phasors, as in Figure 1-4 (Ref. 2). From Figure 1-4,

$$\phi(t) = \tan^{-1} \frac{y(t)}{[A + x(t)]} \quad (1-6)$$

For the high CNR case where $x(t)$ and $y(t)$ are small compared to A , Equation 1-6 becomes

$$\phi(t) \cong \frac{y(t)}{A} \quad (1-7)$$

For this case, $\phi(t)$ can be illustrated by Figure 1-5.

The perturbations of $\phi(t)$ about the time axis are produced by the random nature of the noise. The output of the detector is proportional to the derivative of the input phase angle, or,

$$e_o(t) \propto \frac{\dot{y}(t)}{A} \quad (1-8)$$

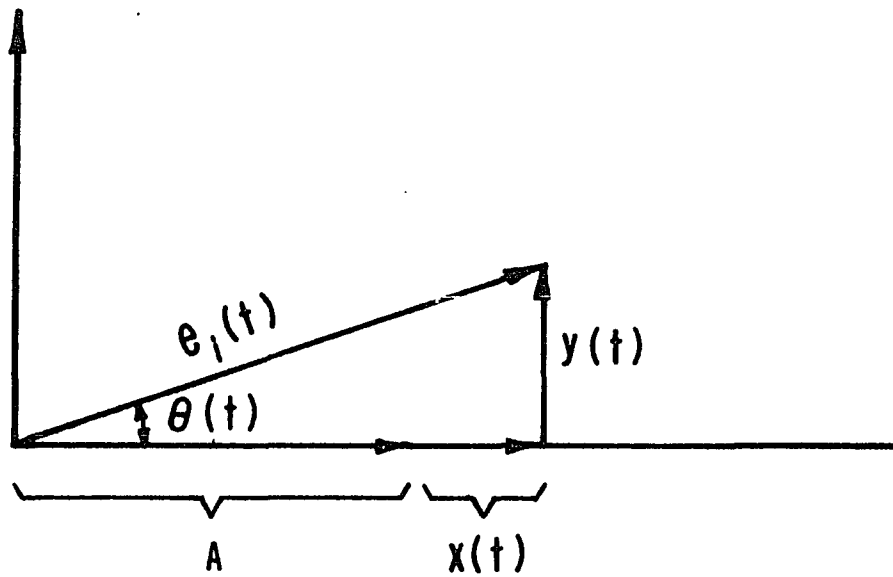


FIGURE 1-4. GRAPHICAL REPRESENTATION OF CARRIER AND NOISE

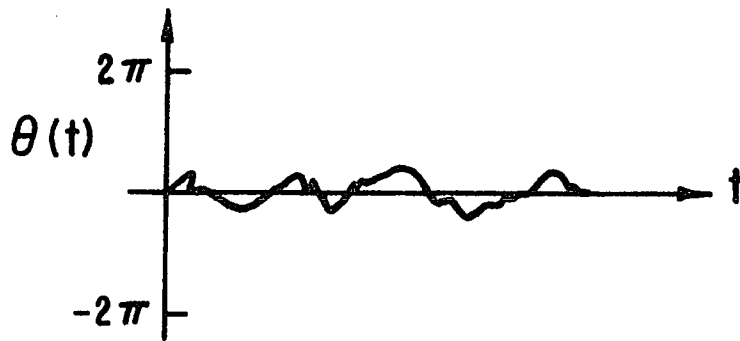


FIGURE 1-5. $\theta(t)$ FOR HIGH CNR

1.3 Limiting Discriminator - Near Threshold

Rice shows that, as the CNR is decreased, a significant number of fast step discontinuities in $\hat{\theta}(t)$ occur randomly, as in Figure 1-6 (Ref. 2). These steps may be explained as follows: If the amplitude of the random variable, $|x(t)|$, becomes greater than the signal amplitude, A , and $x(t)$ is negative, and if at the same time $y(t)$ goes from positive to negative, an encirclement of the origin takes place in the phasor representation of Figure 1-4. This encirclement produces a 2π step in $\hat{\theta}(t)$. The output from a conventional discriminator, (t) , appears as shown in Figure 1-7. The step discontinuities in $\hat{\theta}(t)$ produced by encirclements appear as spikes or clicks in the receiver output. The number of these "clicks" per second is related to how often the magnitude of $x(t)$ is greater than A , which in turn is related to the input CNR.

More quantitatively, for the case of an unmodulated carrier corrupted by additive Gaussian noise and centered in a power spectral density (PSD) with arithmetic symmetry,

$$N = \# \text{ Spikes/Sec} = r \left[1 - \text{erf} (\text{CNR})^{\frac{1}{2}} \right], \text{ (Ref. 2)} \quad (1-9)$$

where r is the radius of gyration of the noise PSD defined by

$$r^2 = \frac{\int_{-\infty}^{\infty} (f - f_c)^2 W(f) df}{\int_{-\infty}^{\infty} W(f) df} \quad (1-10)$$

The PSD of the resulting spikes is essentially flat. The SNR at the receiver output is substantially degraded by these spikes at or below threshold. The point at which the output SNR is degraded by these spikes by 1 dB from the expected linear FM improvement region SNR is commonly defined as the threshold point. Threshold is the limiting factor in all FM systems that prevents unlimited trading of power versus bandwidth.

1-4. The Limiter Discriminator SNR vs CNR Relationship

A few words concerning the determination of output SNR as a function of input CNR for the conventional limiter discriminator are



FIGURE I-6. $\theta(t)$ FOR LOW CNR

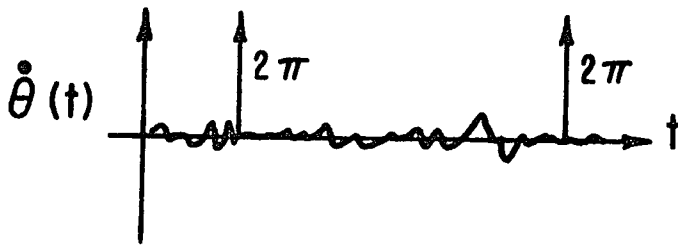


FIGURE 1-7. $\dot{\theta}(t)$

appropriate. The FM system performance curve in Figure 1-1 is deceptively simple. For an actual system, the curve is very complex when the threshold effect enters. The equations describing it are very complex. These equations have been derived by Middleton (Ref. 3) and Stumpers (Ref. 4). Middleton assumes Gaussian pre- and post-detection filters; Stumpers assumes rectangular filters. The difference is minor and their results compare quite closely. The analytical results of Middleton and Stumpers are complicated and evaluating their equations is extremely difficult, with errors being hard to avoid. However, a simple relationship exists between the SNR at the output and the input CNR (Ref. 5) for operation above threshold

$$(\text{SNR})_{\text{TT}} = 3\beta^2 (\text{CNR})_{\text{AM}} \quad (1-11)$$

where TT indicates reference to a test tone output, β is the modulation index, and $(\text{CNR})_{\text{AM}}$ refers to the carrier to noise ratio, with the noise measured in a bandwidth of twice the base bandwidth (in this case, the test tone frequency is equal to the base bandwidth).

Threshold CNR may be readily determined using a result plotted by Enloe (Ref. 7), which is reproduced in Figure 1-8. The actual points were taken by Enloe from an unpublished memo of J. O. Replogle. For more detailed analytical performance data for the limiter discriminator, the complex results of Middleton or Stumpers must be utilized.

Much work has been done with phase locked loops and frequency feedback loops to reduce the CNR at which threshold occurs. The new family of demodulators, not having some of the nonlinearities of the conventional limiter discriminator, and not having the feedback of the phase locked loop or frequency feedback loop, has been conjectured to offer a new avenue to threshold extension. However, we show in this dissertation that no threshold advantages appear to exist. The next chapter describes and defines the salient features of the

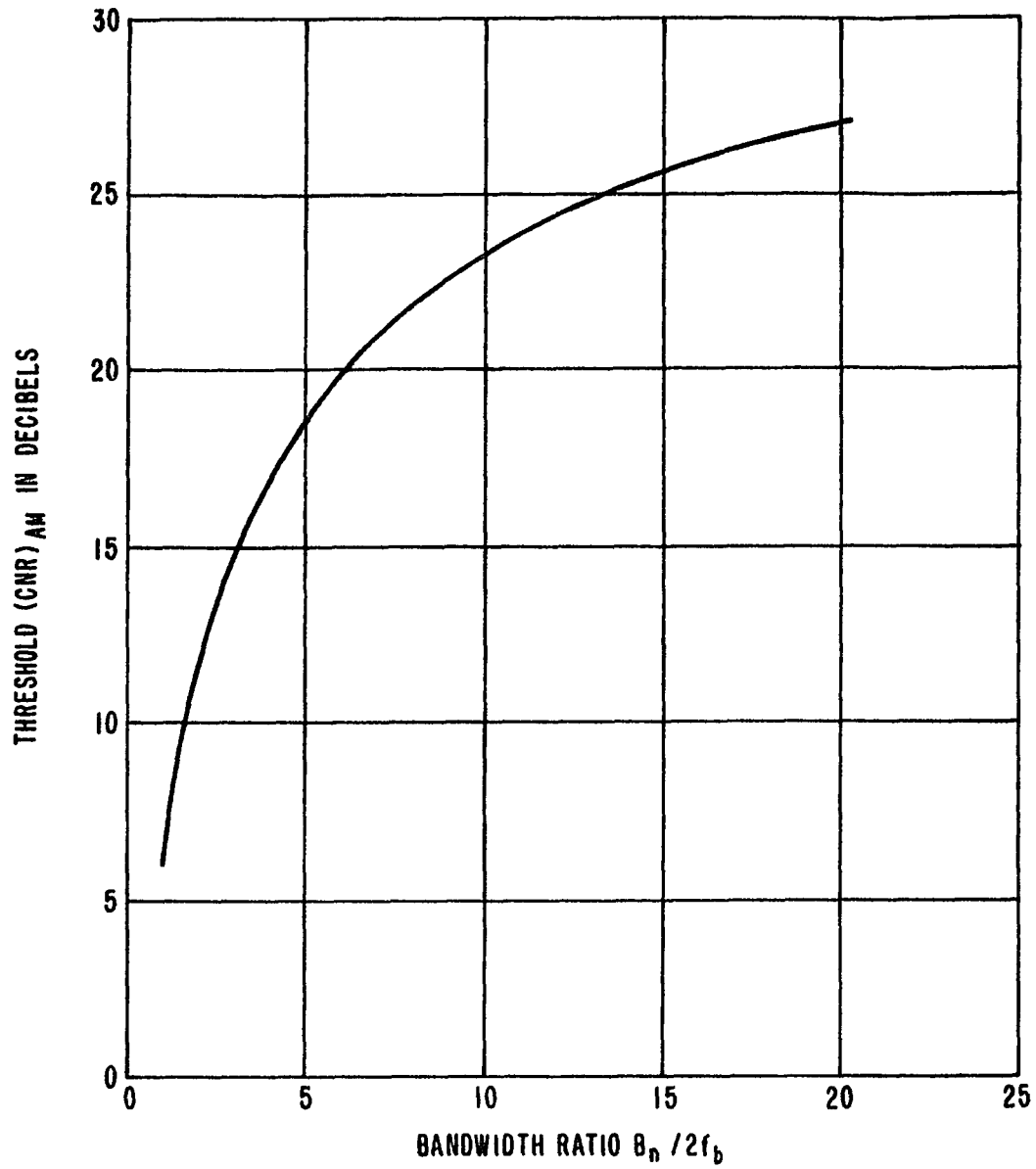


FIGURE 1-8. THRESHOLD (CNR)_{AM} VS IF-TO-TWICE BASE BAND RATIO

Klapper-Kratt demodulator family. Details of past analyses are presented in Chapter 3.

References - Chapter I

1. Klapper & Frankle, Phase Locked and Frequency Feedback Systems, Chpt. 3, Fig. 3-1, Academic Press, 1972.
2. S.O. Rice, "Noise in FM Receivers," in Selected Papers on Frequency Modulation, (J. Klapper, ed.), Dover Press, 1970.
3. D. Middleton, "On the Theoretical Signal-to-Noise Ratios in FM Receivers: A Comparison with AM," *Journal of Applied Physics*, Vol. 20, April, 1949.
4. F. Stumpers, "Theory of FM Noise," *Proc. IRE*, Vol. 36, No. 9, Sept, 1948.
5. M. Schwartz, Information Transmission, Modulation, and Noise, Section 6-3, McGraw-Hill, 1959.
6. Klapper & Frankle, Phase Locked and Frequency Feedback Systems, Chpt. 3, pp. 29, Academic Press, 1972.
7. L. Enloe, "The Synthesis of Frequency Feedback Demodulators," *Proc. Nat. Electron: Conf.* 18; 477, 1962.
8. Klapper & Frankle, Phase Locked and Frequency Feedback Systems, Chpt. 5, pp. 105-110, Academic Press, 1972.
9. Enloe, "Decreasing the Threshold in FM by Frequency Feedback", *Proc. IRE*, Vol. 50, No. 1, pp. 18-30, Jan 1962.
10. Klapper & Frankle, Phase Locked and Frequency Feedback Systems, Chpt. 4, pp. 69-72, Academic Press, 1972.
11. Klapper & Frankle, Phase Locked and Frequency Feedback Systems, Chpt. 3, Fig. 3-8, Academic Press, 1972.

CHAPTER II

A NEW FAMILY OF FM DETECTORS2.1 Background

The development of this new family of detectors resulted from a requirement to demodulate FM signals with extremely low delay and good sensitivity. The early work performed on these demodulators was accomplished by Dr. Jacob Klapper and Edward Kratt and is described in their paper presented at the National Telecommunications Conference - 1975 (Ref. 1). Some later analysis was performed by Gerald Kersus during the course of his Master's Project at NJIT under the guidance of Dr. Klapper (Ref. 2).

Theoretically, integrators, differentiators, summers, and multipliers are low delay (zero group delay) circuits. Circuits such as lowpass filters and bandpass filters would normally not be low delay circuits. Their finite bandwidth limits the rate at which their output can change. Up to the present, all FM detectors have incorporated low pass circuitry to filter undesired high frequency components generated in the detection process, and, typically, a tuned circuit for the FM to AM conversion. Even previous FM detectors using integrators and differentiators incorporate lowpass filters in their output circuitry (Refs. 3, 4, and 5).

Klapper and Kratt's solution to the delay problem utilizes an integrator, differentiator, and summer for the FM to AM conversion. A synchronous demodulator is then used to detect the amplitude modulation. No delay occurs, and the only undesirable signal produced is the second harmonic of the carrier frequency. This second harmonic could be eliminated by the use of a notch filter with some inherent delay. Better yet, the inventors developed a method using another integrator and multiplier to generate a cancelling signal.

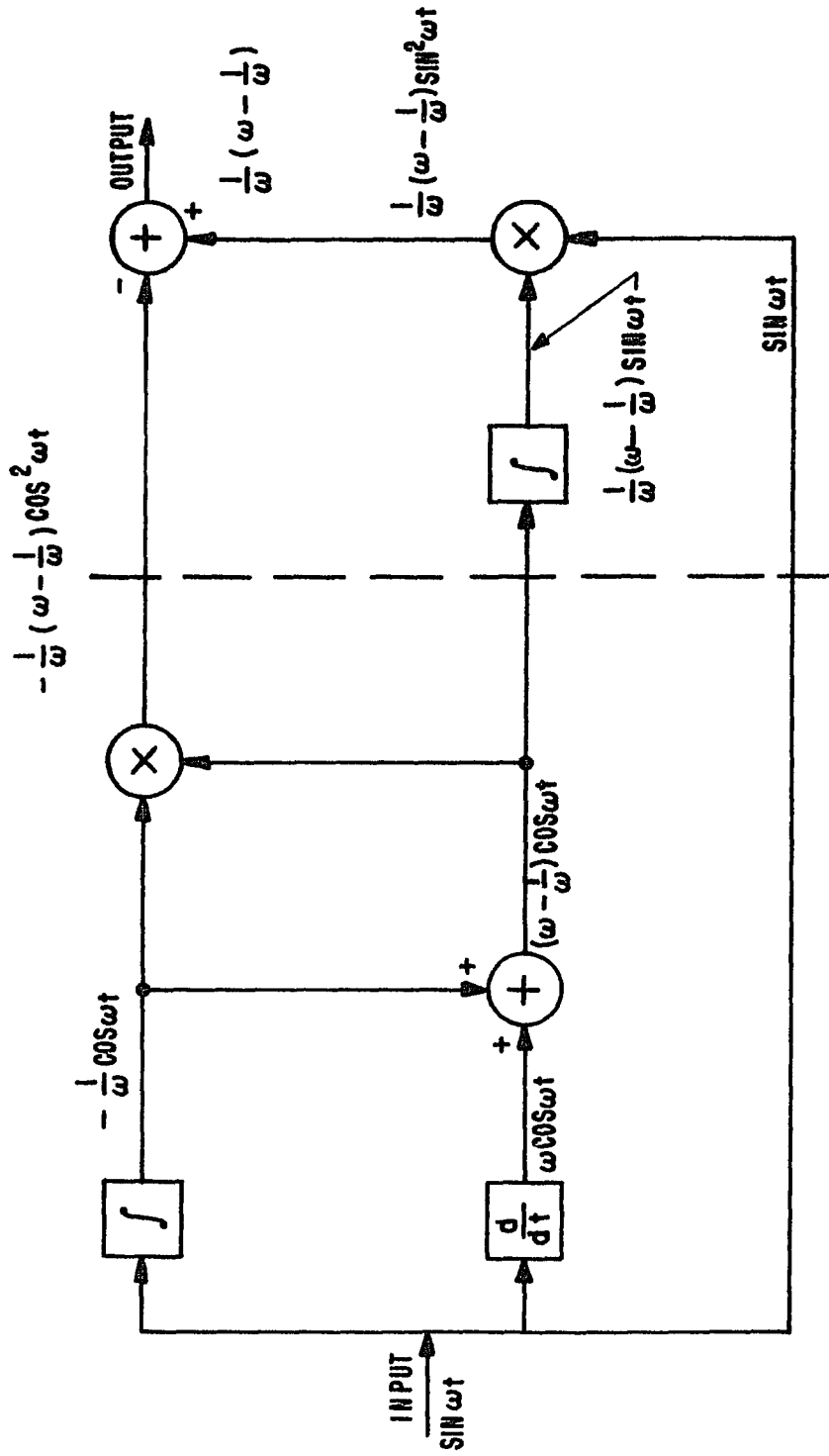


FIGURE 2-1. ONE MEMBER OF THE NEW FM DETECTOR FAMILY

2.2 Description of the New Detector

Figure 2-1 shows one of the forms of this new family of detectors. It is made up of integrators, a differentiator, summers, and multipliers, all theoretically zero delay components.

The detector may be divided into two basic functions: (A) a coherent FM discriminator, and (B) an RF canceller. The dashed line in Figure 2-1 separates these functions.

(A) Coherent FM Discriminator

The FM to AM conversion is performed by the portion of the detector shown in Figure 2-2. The input signal, $\sin \omega t$, is applied to the input of I_1 and D_1 . The integrator produces a -90° phase shift, while the differentiator produces a $+90^\circ$ phase shift. This results in two signals with a 180° phase difference. The integrator and differentiator are adjusted to give unity gain at some frequency, ω_0 . These two signals are then applied to the summer, S_1 , the output of which will be zero when $\omega = \omega_0$. Above and below this frequency, the summer has an increasing amplitude. Below ω_0 the integrator output dominates, while above ω_0 the differentiator output dominates.

Coherent detection is performed by M_1 . M_1 multiplies the output of the summer with the output of the integrator. The output of the multiplier contains the demodulated baseband signal plus a second harmonic of the input signal.

The waveforms present at each stage are indicated in Figure 2-2. Assuming a steady state frequency offset input signal, $\sin \omega t$, where the frequency is normalized with respect to the center frequency (i.e., $\omega_0 = 1$). The output is proportional to

$$\frac{1}{\omega} \left(\omega - \frac{1}{\omega} \right) \quad (2-1)$$

This expression is plotted in Figure 2-3. Some nonlinearity is clearly present near the center frequency ($\omega = 1$). However, the nonlinearity is very small in usual applications where the center

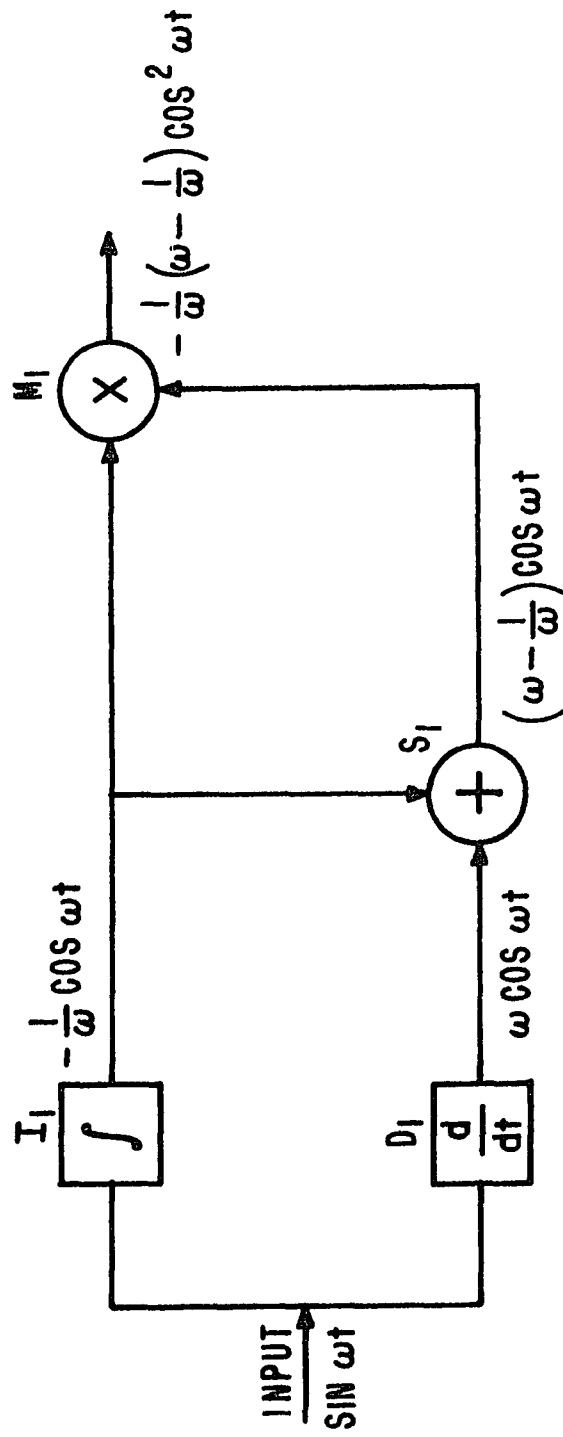


FIGURE 2-2. COHERENT FM DISCRIMINATOR

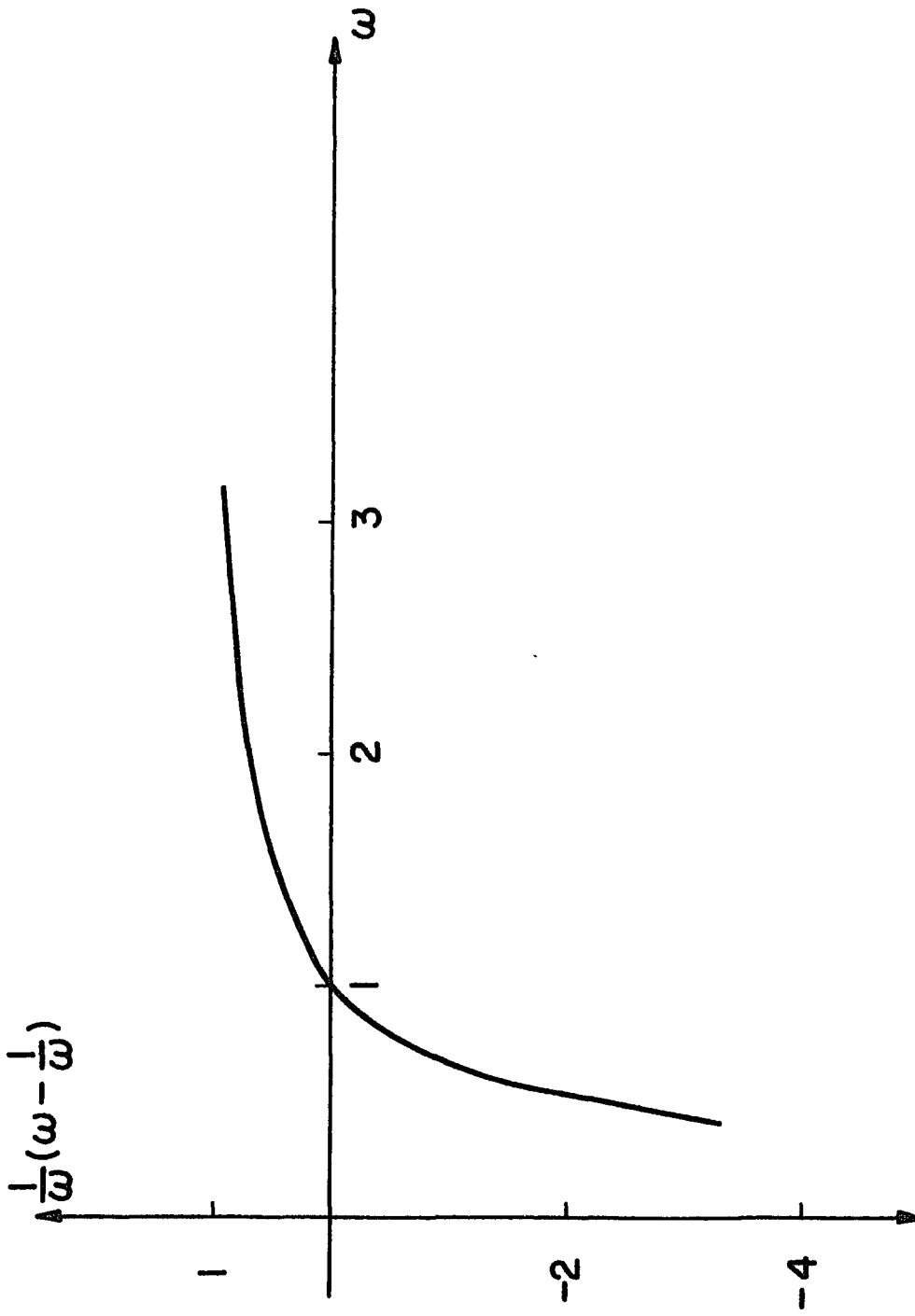


FIGURE 2-3. $\frac{1}{\omega}(\omega - \frac{1}{\omega})$ VS ω

frequency is much greater than the deviation.

All the components in Figure 2-2 are capable of wideband operation. It is important to note that previous FM demodulators perform the balancing operation at baseband requiring high gain, low drift, DC amplification. In the Klapper-Kratt demodulator the balance is accomplished at the carrier frequency, permitting high gain AC amplification which eliminates the complication of high gain DC amplifiers.

(B) RF Cancellation.

Referring back to Figure 2-1, the portion to the right of the dashed line provides RF suppression. The integrator and multiplier generate a quadrature signal proportional to $\sin^2 \omega t$. The outputs of the two multipliers are summed.

Since

$$\cos^2 \omega t + \sin^2 \omega t = 1, \quad (2-2)$$

the second harmonic is cancelled with zero delay. The equations in Figure 2-1 describe this cancellation.

2.3 Integrator Initial Conditions.

There are many other members of this new family of detectors. Figures 2-4, 5, and 6 detail some of these other forms. Notice that all of the forms shown up to this time have integrators utilized in the FM to AM conversion. Referring back to Figure 2-1, no DC component should be present at the inputs of the multipliers if the detector is to perform as previously described. If this condition is violated, a considerable amount of the fundamental carrier will appear at the output. This potential problem can result from the initial conditions of the integrators (which drive the multipliers) at the time of a rapid input frequency change.

A worst case condition is shown in Figure 2-7. Assume the input signal, $e_i(t)$, doubles its frequency instantaneously at t_0 . The

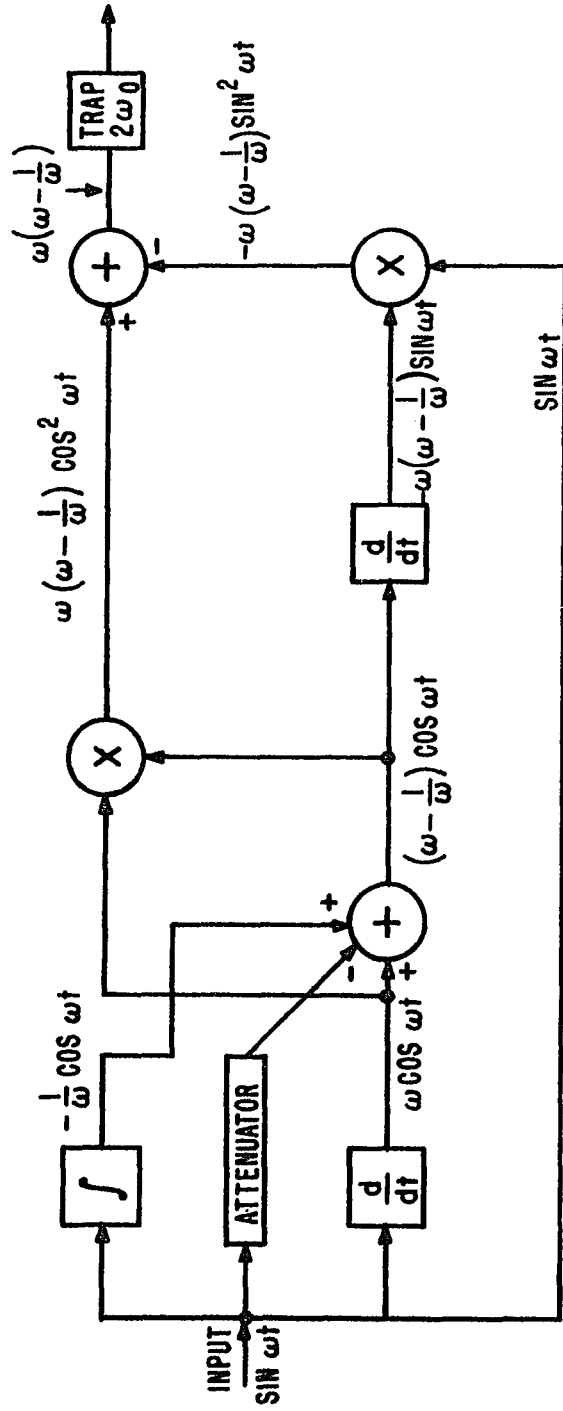


FIGURE 2-4. A SECOND MEMBER OF THE NEW DETECTOR FAMILY

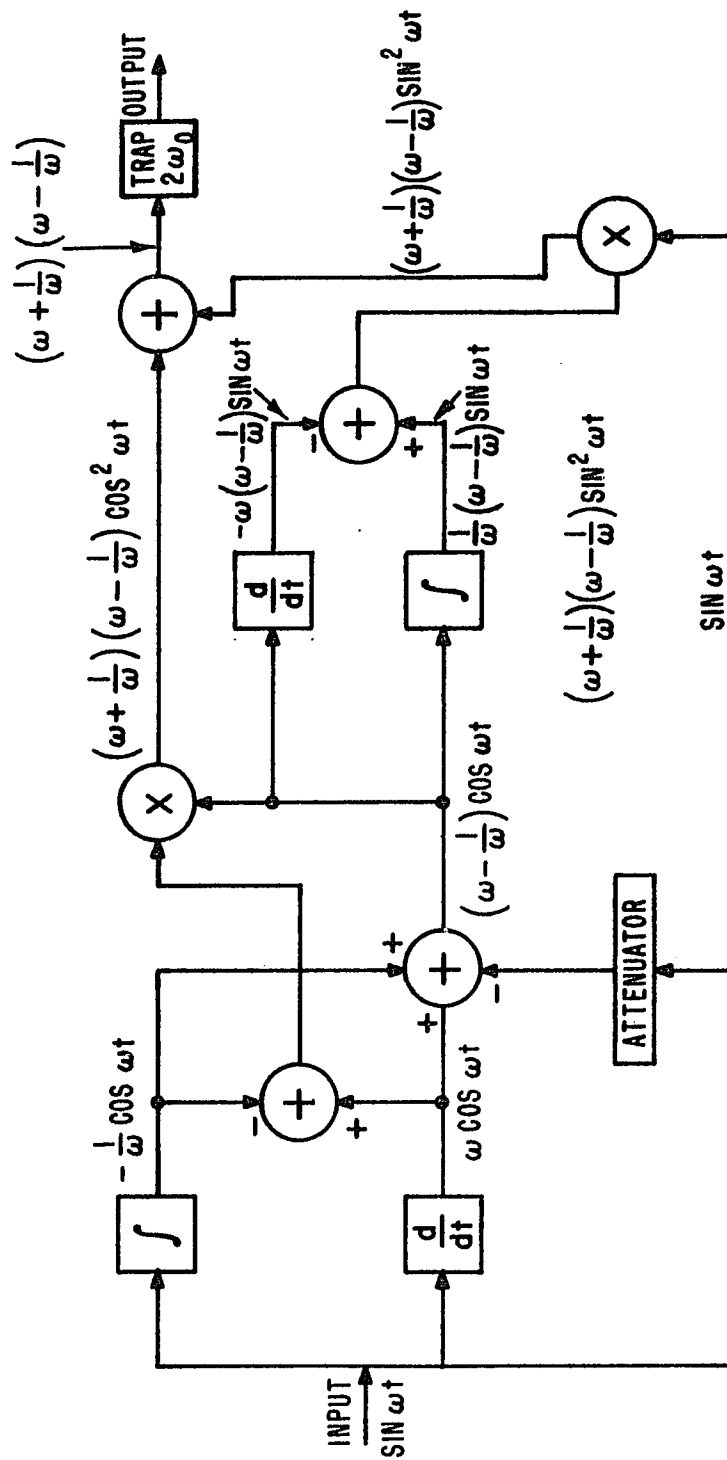


FIGURE 2-5. A THIRD MEMBER OF THE NEW DETECTOR FAMILY

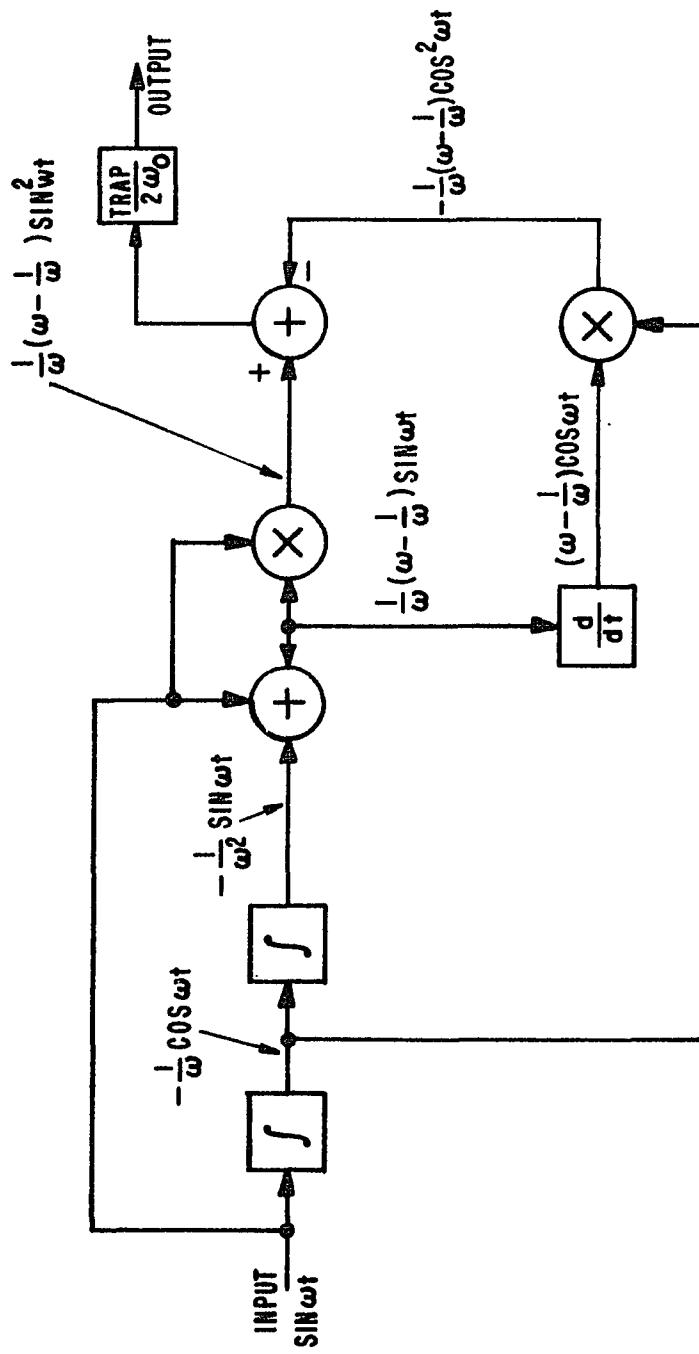


FIGURE 2-6. A FOURTH MEMBER OF THE NEW FM DETECTOR FAMILY

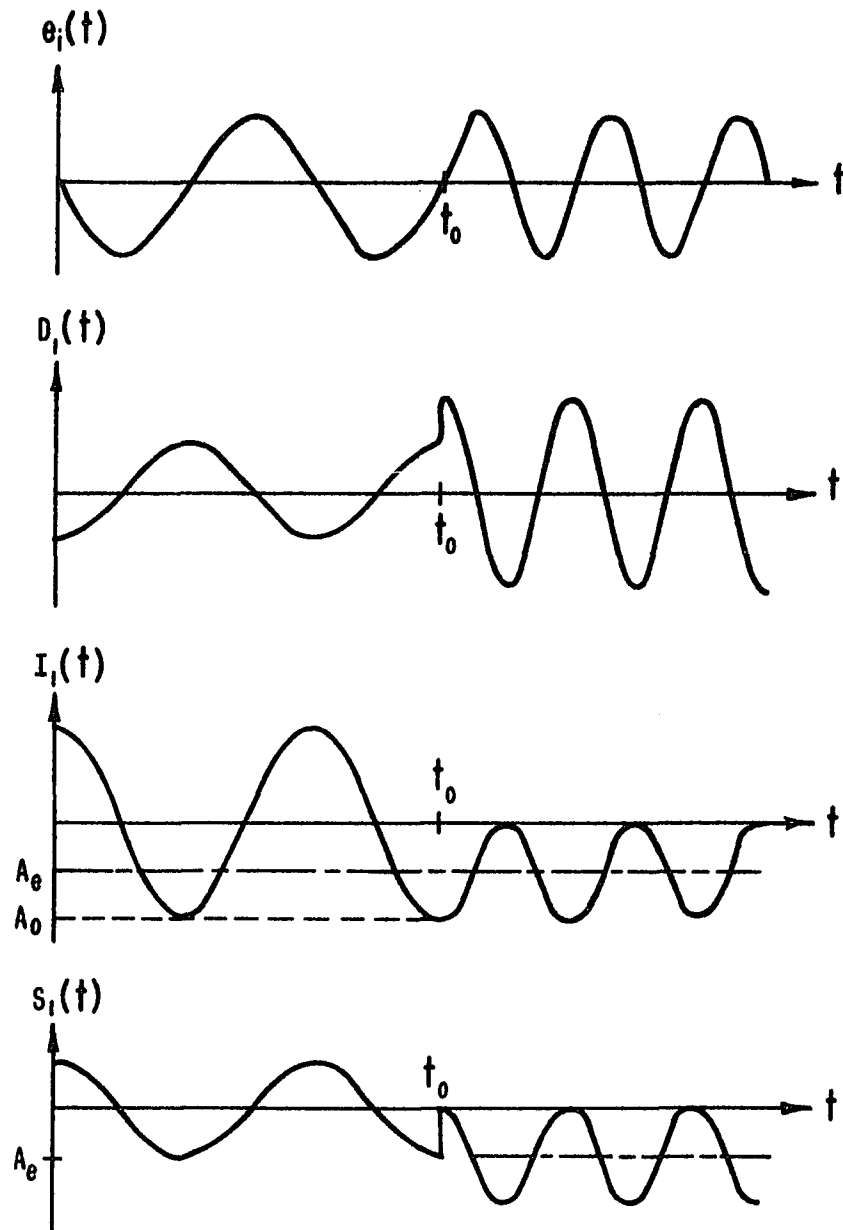


FIGURE 2-7. INTEGRATOR PROBLEM UNDER WIDE BAND CONDITIONS [REF 1]

outputs, with reference to Figure 2-1, of D_1 , I_1 , and S_1 are shown in Figure 2-7. At $t = t_0$ the output of I_1 is A_0 , which becomes the effective initial condition on the integrator output. After $t = t_0$ the amplitude of the integrator output is half what it was previous to $t = t_0$. A DC term of value A_e is produced. The output of S_1 is no longer balanced symmetrically about zero. When $S_1(t)$ is multiplied by $I_1(t)$, a considerable amount of the fundamental carrier will be present in the multiplier output. The magnitude of the DC error will, of course, depend on the time at which the frequency change occurs. For example, if the change occurs when the integrator output is crossing the axis, A_e is zero, and no error is produced (Ref. 1).

There are ways of solving this problem, but they require complication in the modulator and/or demodulator. In practice, actual integrators are imperfect and will automatically maintain zero DC at their output if the input frequency changes are relatively slow. This assumes the baseband signal is reasonably narrow band; but what if it is really wideband? How can the integration problem be circumvented? Fortunately, other forms of the detector do not utilize an integrator in the discriminator section.

Figure 2-8 is one of these forms. It consists of two differentiators, one integrator, two summers, and two multipliers.

2.4 Description of the Dual Differentiator Detector.

The coherent FM discriminator portion of Figure 2-8 is shown in Figure 2-9. The input signal is applied to differentiator, D_1 . The output of D_1 is fed into differentiator, D_2 . Each differentiation produces a $+90^\circ$ phase shift resulting in a 180° total phase shift at the output of D_2 (with respect to the input signal phase). As was the case in the previous analysis, two signals are present with a 180° phase difference. The differentiator gains in Figure 2-9 are adjusted to give unity gain at some frequency, ω_0 . Thus, when $\omega = \omega_0$, the equal amplitude, opposite polarity signals cancel at the output of the summer, S_1 . Above and below ω_0 , the summer has an increasing amplitude.

Below ω_0 the output of S_1 is dominated by the input signal, while above ω_0 the output of S_1 is dominated by the output of differentiator, D_2 .

Coherent detection is accomplished by the multiplier. M_1 multiplies the output of the summer with the input signal. For a steady state, frequency offset input signal, the waveforms present at each stage are shown in Figure 2-8, where the frequency, ω , is normalized with respect to the center frequency (i.e., $\omega_0 = 1$).

The output of the discriminator portion is proportional to $(\frac{1}{\omega} - \omega)$ and contains the demodulated baseband signal plus a second harmonic of the input carrier. The expression, $(\frac{1}{\omega} - \omega)$ is plotted in Figure 2-10. All the components of Figure 2-8 are capable of wideband operation. The second harmonic component may be cancelled, as shown in Figure 2-11. The output of M_1 is proportional to $\sin^2 \omega t$. A quadrature signal proportional to $\cos^2 \omega t$ is developed by I_1 and M_2 . The two signals are summed by S_2 cancelling the RF, leaving

$$(\frac{1}{\omega} - \omega)$$

The RF cancellation is imperfect for a modulated input signal. This appears to be true for all forms of the Klapper-Kratt Detector Family. Kersus delves into this problem in his project (Ref. 2). It appears, however, that the imbalance is small enough to be ignored in most applications.

Recall that for most FM demodulators, as the discriminator bandwidth is widened, the sensitivity is reduced. This results from the fact that previous demodulators have been balanced at baseband. Due to the difficulty in amplifying the resultant low level DC signals, a lower limit on discriminator sensitivity is effectively set. However, in all the Klapper-Kratt detectors balance is accomplished at RF, permitting accurate high gain AC amplification of the low level wide band signals.

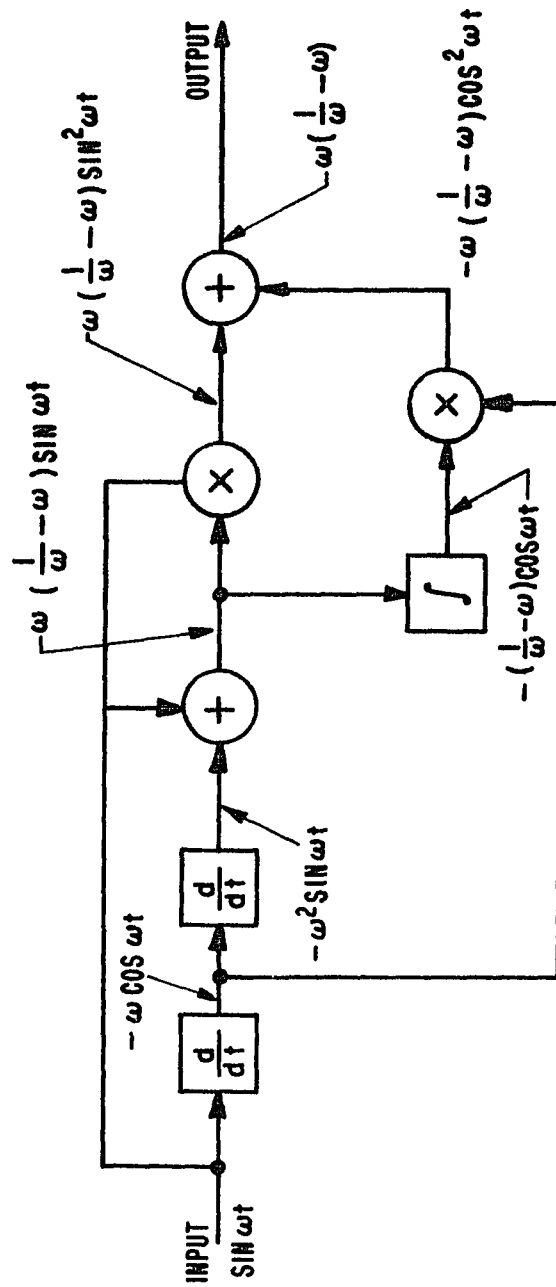


FIGURE 2-8. ANOTHER MEMBER OF THE NEW FM DETECTOR FAMILY

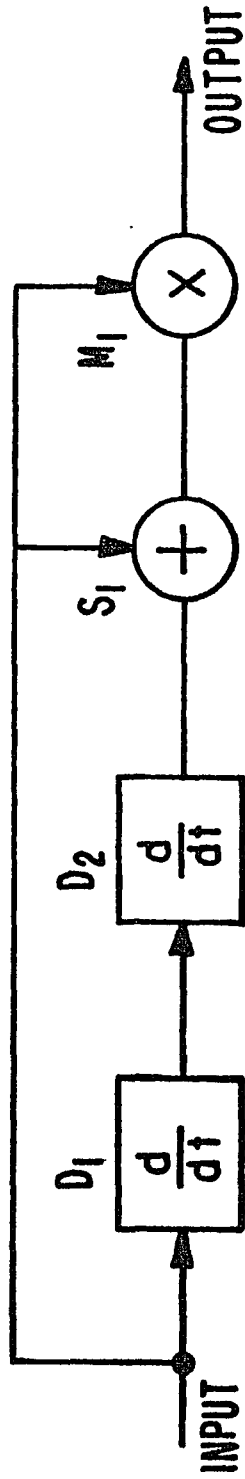
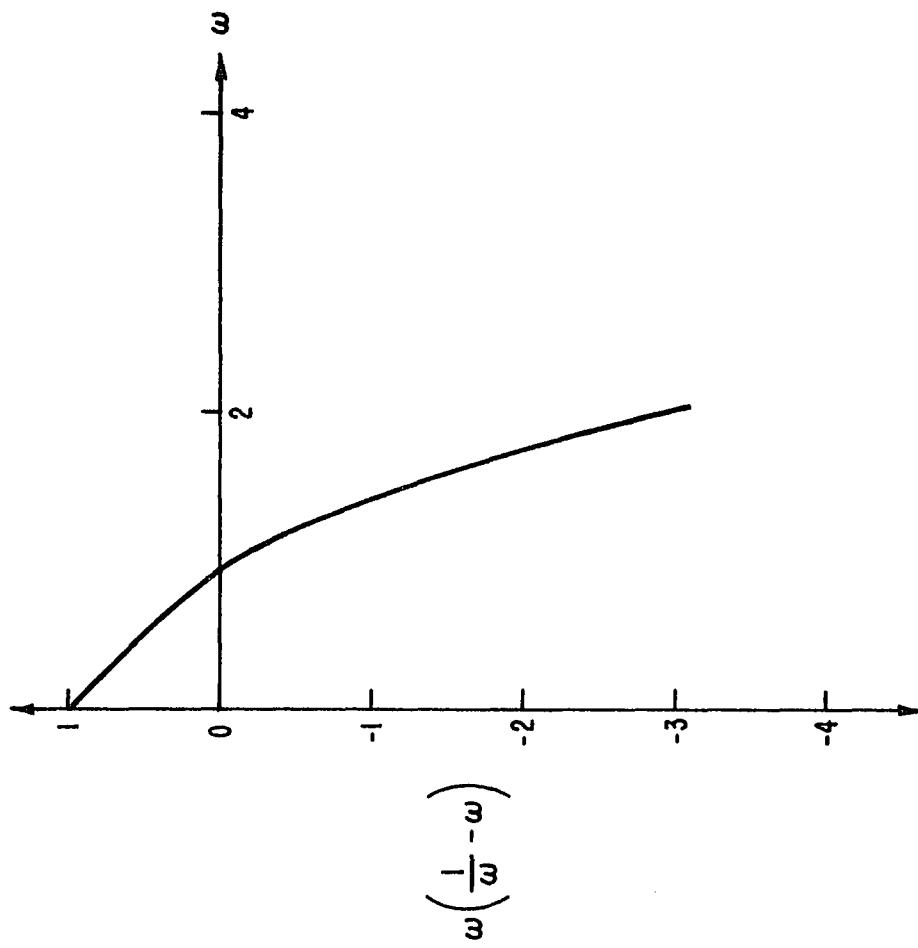


FIGURE 2-9. COHERENT FM DISCRIMINATOR

FIGURE 2-10. $\omega \left(\frac{1}{\omega} - \omega \right)$ VS ω

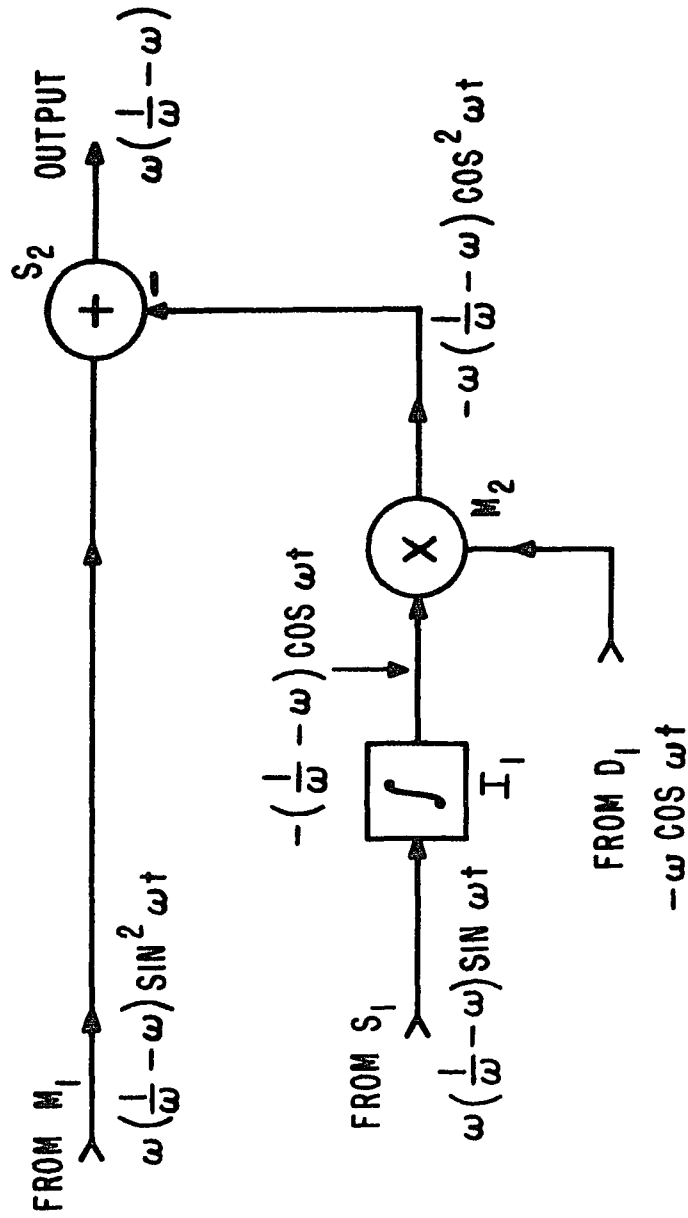


FIGURE 2-11. RF CANCELLER FOR DUAL DIFFERENTIATOR DETECTOR

References - Chapter II

1. J. Klapper & E. Kratt, "A New Family of Low Delay FM Detectors," NTC-1975.
2. G. Kersus, "Analysis of the Klapper-Kratt FM Detector," NJIT Master's Project, Newark, NJ, 1976.
3. K. Clarke & D. Hess, "Communications Circuits: Analysis and Design," Addison-Wesley, 1971.
4. E. Patronis, "A Frequency Modulation Detector using Operational Amplifiers," Audio Magazine, Feb 1970.
5. J. Park, "An FM Detector for Low S/N," IEEE Transactions on Communication Technology, VOL. COM-18, No. 2, April 1970.

CHAPTER III

THE RESULTS OF PREVIOUS ANALYSIS OF THE KLAPPER-KRATT DETECTOR FAMILY3.1 Previous Art

Earlier analyses of members of the Klapper-Kratt detector family have been described in the Master's Project of Edward Kratt (Ref. 1) and the Master's Project of Gerald Kersus (Ref. 2). The details of their results will be presented shortly. An extensive search of the literature produced no other previous work on the Klapper-Kratt detector forms. However, a paper by J. H. Park, Jr. (Ref. 3) did describe another detector scheme that, like the Klapper-Kratt family, converts the FM to AM and then synchronously detects the AM. Figure 3-1 shows the Park detector. As in the Klapper-Kratt design, the detector does not require a limiter. Park, however, does not balance at RF and removes the unwanted products of detection in a narrowband fashion.

The analysis of Park's circuit is much easier than that of the Klapper-Kratt, due to the presence of high order autocorrelation terms in the latter. In the linear improvement region with modulation, Park shows that his detector (without normalization) is worse in performance than the limiter discriminator. Park's analysis shows his detector to be superior to the limiter discriminator at and below threshold, due to the lack of "clicks".

3.2 Kratt's Results

Kratt presented the results of his analysis in his Master's Project (Ref. 1). In this thesis he analyzes the operation of one of the detector forms described in Chapter II. This detector is redrawn in Figure 3-2. Kratt describes the scheme for instantaneous cancellation of the unwanted RF by developing a quadrature cancelling signal.

Kratt derives the resultant output of Figure 3-2 for a tone modulated input signal with small modulation index. The input signal is

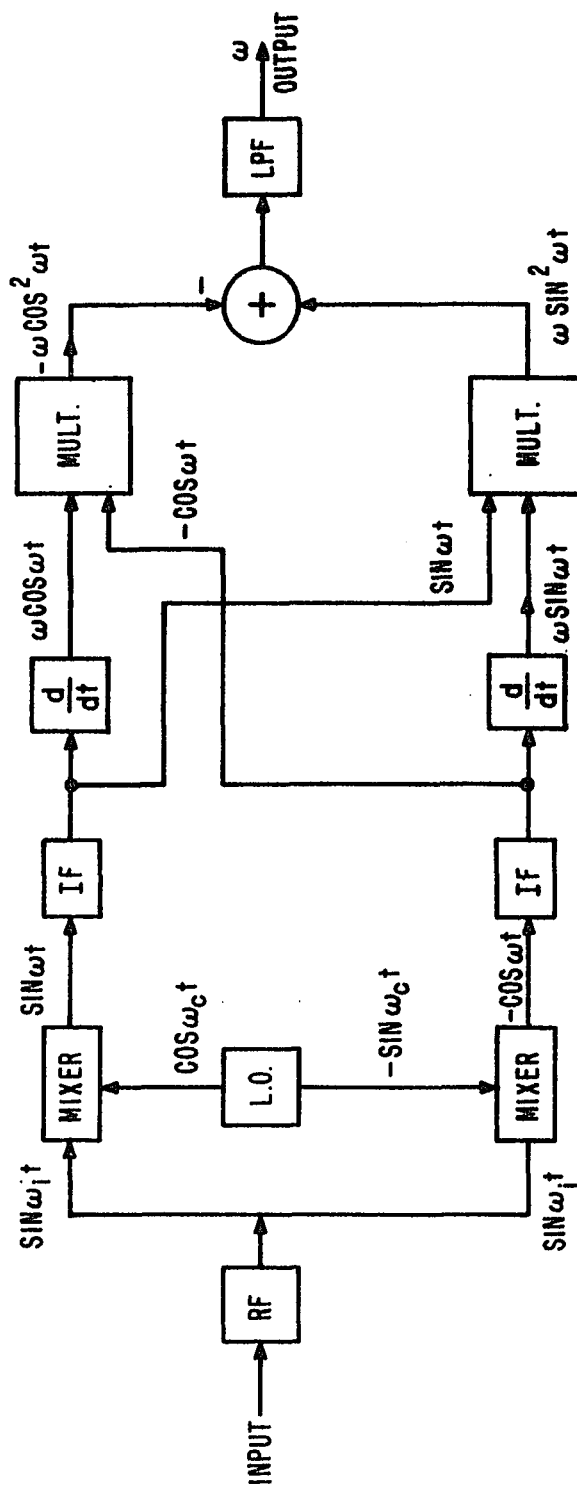


FIGURE 3-1. PARK DETECTOR [REF. 3]

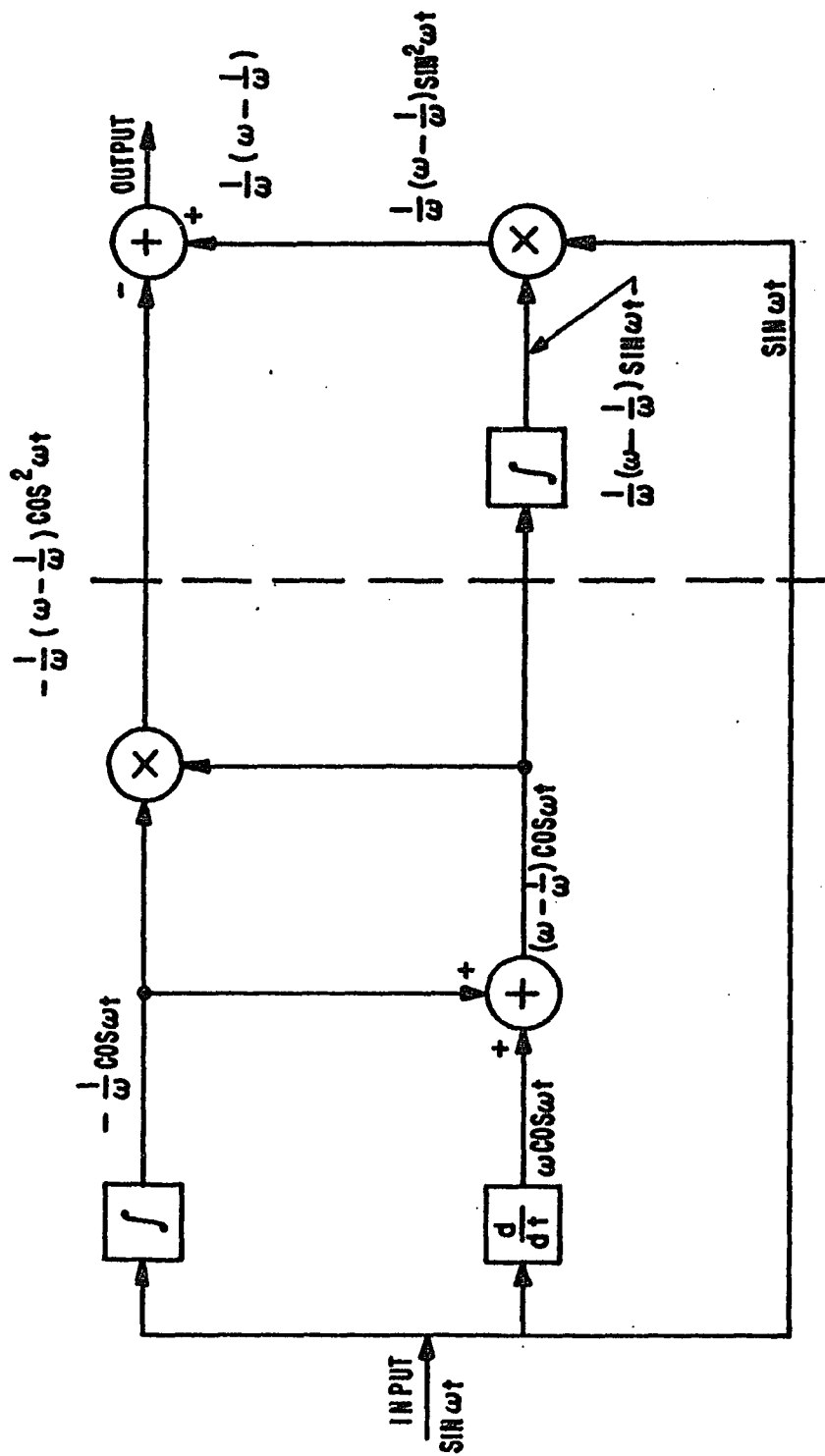


FIGURE 3-2. ONE MEMBER OF THE NEW FM DETECTOR FAMILY

modeled as the sum of three components -- the carrier and a pair of sidebands:

$$e_i(t) = A \left[\cos \omega_0 t - \frac{K}{2} \cos (\omega_0 - \omega_m)t + \frac{K}{2} \cos (\omega_0 + \omega_m)t \right], \quad (3-1)$$

where A is the input signal amplitude,
 K is related to the modulation index,
 ω_0 is the carrier frequency, and
 ω_m is the modulating tone frequency.

Kratt finds the output of this detector (assuming Equation 3-1 as the input) to be

$$\begin{aligned} e_o(t) = & \frac{A^2 kR}{4(1-R^2)^2} \left[2(4 - 3R^2 + R^4) \cos \omega_m t \right. \\ & + 2 kR(2 - R^2) \cos^2 \omega_m t \\ & + R(2 + 3R - R^3) \cos(2 \omega_0 - \omega_m)t \\ & - R(2 - 3R + R^3) \cos(2 \omega_0 + \omega_m)t \\ & \left. - 2 kR(3 - R^2)(1 - \cos 2 \omega_0 t) \right] \end{aligned} \quad (3-2)$$

where $R = \frac{\omega_m}{\omega_0}$

If R is small (i.e., $R \ll 1$), the expression in Equation 3-2 may be approximated by

$$\begin{aligned} e_o(t) = & A^2 kR \left[2 \cos \omega_m t + kR \cos 2 \omega_m t \right. \\ & + \frac{R}{4} (2 + 3R) \cos (2 \omega_0 - \omega_m)t \\ & - \frac{R}{4} (2 - 3R) \cos (2 \omega_0 + \omega_m)t \\ & \left. - \frac{3}{2} kR (1 - \cos 2 \omega_0 t) \right] \end{aligned} \quad (3-3)$$

From Equation 3-3, it is observed that the demodulated output consists of an undistorted baseband term, a low level component of

twice the baseband frequency, a low level component of first order sidebands about twice the center frequency, and low level components at DC and twice the center frequency. The amplitudes of the distortion components become smaller as R becomes smaller. Assuming the integrator initial condition problem discussed in Chapter II is solved, Kratt's analysis can be readily extended to the wideband case.

In his project Kratt also considers the effects of sine wave interference. Consider the situation where the input consists of a desired carrier at frequency, ω_d , and an interfering carrier at frequency, ω_i , or,

$$e_i(t) = A \cos \omega_d t + B \cos \omega_i t . \quad (3-4)$$

$$\text{where } \omega_d = \omega_o + \omega_c$$

$$\omega_i = \omega_o + \omega_r$$

The baseband output is derived by Kratt:

$$\begin{aligned} e_o(t) \approx & 2A^2 \frac{\omega_c}{\omega_o} \left(1 - \frac{\omega_c}{\omega_o}\right) + 2B^2 \frac{\omega_r}{\omega_o} \left(1 - \frac{\omega_r}{\omega_o}\right) \\ & + AB \left[2 \left(\frac{\omega_c}{\omega_o} + \frac{\omega_r}{\omega_o} \right) - \left(\frac{\omega_c}{\omega_o} + \frac{\omega_r}{\omega_o} \right)^2 \right] \cos (\omega_r - \omega_c) t \\ & - AB \left(\frac{\omega_c}{\omega_o} - \frac{\omega_r}{\omega_o} \right)^2 \cos (\omega_d + \omega_i) t \end{aligned} \quad (3-5)$$

The first term is the desired DC output. The remaining terms are interference DC and beat frequency outputs, respectively.

If $\omega_c = 0$, the output reduces to

$$e_o(t) \approx \frac{\omega_r}{\omega_o} \left(\frac{B}{A}\right)^2 + \frac{\omega_r}{\omega_o} \frac{B}{A} \cos \omega_r t, \quad \frac{\omega_r}{\omega_o} \ll 1 \quad (3-6)$$

Corrington (Ref. 4) has derived the equivalent output for a conventional limiter discriminator for $\omega_c = 0$,

$$e_o(t) = \frac{\frac{\omega_R}{\omega_o} (\cos \omega_R t + \frac{B}{A})}{2 \cos \omega_R t + \frac{A}{B} + \frac{B}{A}} \quad (3-7)$$

Comparing the last two equations, observe that at high desired to interference carrier ratios ($A \gg B$), both discriminators produce approximately the same output. However, as the interfering signal increases, the Klapper-Kratt detector has a much higher output purity. Kratt concludes from these promising sine wave interference results and from the absence of limiting that this new demodulator may exhibit a threshold reduction capability when compared to the limiter discriminator.

3.3 Kersus' Results

In his project, Gerald Kersus (Ref. 2) performs an analysis similar to that of Kratt. Kersus chose to analyze the detector form first shown in Figure 2-8 and repeated in Figure 3-3. Kersus, as did Kratt, derives the output from the detector for both a narrow band input and for an interfering carrier input.

The narrow band, tone modulated input signal of Equation 3-1 will be considered first. For this input signal, Kersus shows the demodulator output to be

$$e_o(t) = \frac{A^2 K}{4} \left\{ -2 R^2 K - 2R \left[\frac{3 R^2 - 4}{R^2 - 1} \right] \cos \omega_m t \right. \quad (3-8)$$

$$+ \left[\frac{2 R^2 K (R^2 - 2)}{R^2 - 1} \right] \cos 2\omega_o t + \left[\frac{R^2 (R - 2)}{R - 1} \right] \cos (2\omega_o - \omega_m)t$$

$$\left. - \left[\frac{R^2 (R + 2)}{R + 1} \right] \cos (2\omega_o + \omega_m)t \right\}$$

where A , K , ω_o , ω_m , and R are defined as in Equations 3-1 and 3-2. For $R \ll 1$,

$$e_o(t) \approx \frac{A^2 K R}{2} \left[-4 \cos \omega_m t - R K \cos 2\omega_m t \right]$$

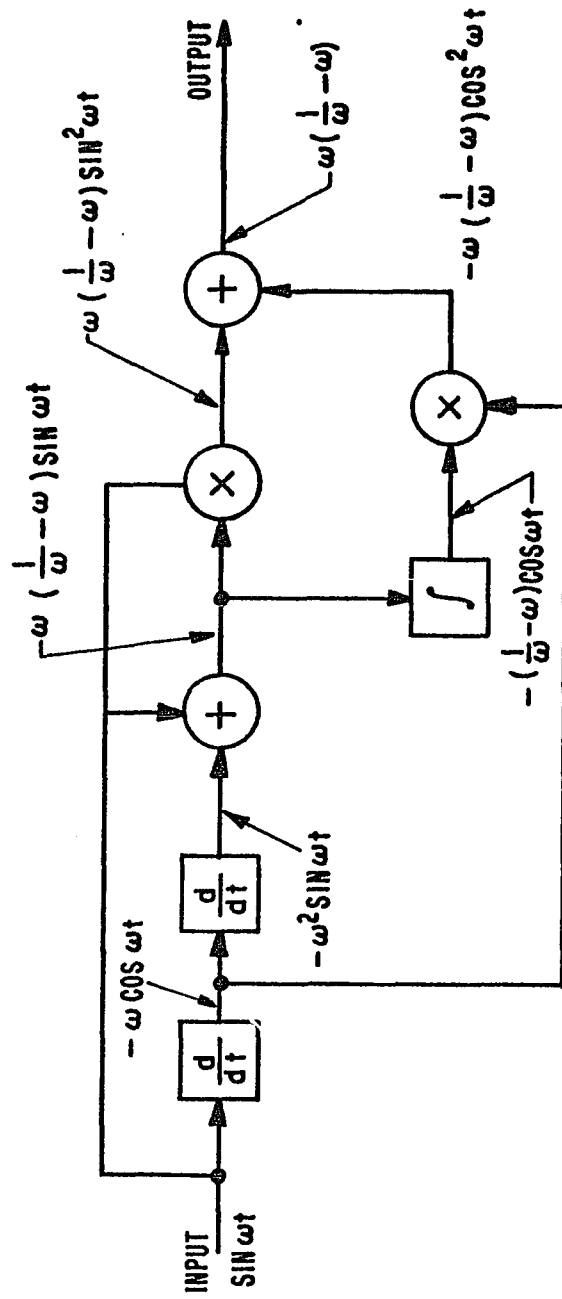


FIGURE 3-3. DUAL DIFFERENTIATOR MEMBER OF KLAPPER-KRATT FAMILY

$$\begin{aligned}
& - RK (1 - 2 \cos 2 \omega_0 t) + R \cos (2 \omega_0 - \omega_m) t \\
& - R \cos (2 \omega_0 + \omega_m) t \Big]. \quad (3-9)
\end{aligned}$$

This output, similar to Kratt's, consists of a desired baseband component, a low level component of first order sidebands around twice the center frequency, low level components at DC, at twice the center frequency, and at twice the modulating frequency.

Next Kersus considers the effects of sine wave interference. As was done previously, let the input signal consist of a desired carrier at frequency ω_d and an interference carrier at ω_i . Then

$$E_i(t) = A \cos \omega_d t + B \cos \omega_i t \quad (3-10)$$

$$\text{where } \omega_d = \omega_0 + \omega_c$$

$$\omega_i = \omega_0 + \omega_r$$

For the above detector input Kersus derived the output to be approximately

$$e_o(t) \approx 2 A^2 \frac{\omega_c}{\omega_0} - 2B^2 \frac{\omega_r}{\omega_0} - 2 AB \left[\frac{\omega_r}{\omega_0} + \frac{\omega_c}{\omega_0} \right] \cos (\omega_r - \omega_c) t. \quad (3-11)$$

If $\omega_c = 0$, the normalized output of the detector reduces to

$$e_o(t) \approx \frac{\omega_r}{\omega_0} \left(\frac{B}{A} \right)^2 - \frac{\omega_r}{\omega_0} \frac{B}{A} \cos \omega_r t \quad (3-12)$$

3.4 Analytical Performance Comparisons of Two Versions of the Klapper-Kratt Detector

No description of the performance of the Klapper-Kratt detectors would be complete without comparing the results with the conventional limiter discriminator. Recall from Chapter I, Equation 1-3, the output (assuming no noise) from a limiter discriminator is

$$e(t) = - \left[\omega_c + \phi(t) \right] A'' \sin \left[\omega_c t + \phi(t) \right]. \quad (3-13)$$

And, after post detection filtering, the output becomes

$$e_o(t) = A'' \dot{\phi}(t) \quad (3-14)$$

where A'' is the limiter discriminator sensitivity. For a cosinusoidal modulating signal Equation (3-13) becomes

$$e(t) = \left[-\omega_c + K\omega_m \cos \omega_m t \right] A'' \sin \left[\omega_c t + K \sin \omega_m t \right], \quad (3-15)$$

where K represents the modulation index, and Equation 3-14 becomes

$$e_o(t) = A'' K \omega_m \cos \omega_m t \quad (3-16)$$

Hence, the output for this ideal limiter discriminator consists only of the undistorted baseband modulating signal with an amplitude proportional to the modulating frequency and the modulation index.

In Equations 3-3 and 3-9, it was found that the Klapper-Kratt detectors have several small distortion components in the output. At first it appears the limiter discriminator is superior to the Klapper-Kratt detector in view of the foregoing distortion analysis. However, it must be remembered that, for wideband systems, it is very difficult to approximate an ideal limiter discriminator with real components. On the other hand, the Klapper-Kratt detector of Figure 3-3 has been built using off-the-shelf components. Its operation closely approximates the ideal Klapper-Kratt detector. This circuit and its operation is described in detail in Chapter V.

To gain a quantitative feel for the actual amount of distortion present in the ideal Klapper-Kratt detectors, the resultant RMS distortion voltages may be readily calculated from the results of Equations 3-3 and 3-9. Recall that Equations 3-3 and 3-9 are the outputs (for the narrowband case) of the Klapper-Kratt demodulators shown in Figures 3-2 and 3-3, respectively.

From Equation 3-3 the desired component is

$$2 \cos \omega_m t \quad (3-17)$$

The remainder of Equation 3-3 is distortion --

$$\begin{aligned} & KR \cos 2 \omega_m t + \frac{R}{4} (2 + 3R) \cos (2 \omega_0 - \omega_m) t \\ & - \frac{R}{4} (2 - 3R) \cos (2 \omega_0 + \omega_m) t - \frac{3}{2} KR (1 - \cos 2 \omega_0 t) \end{aligned} \quad (3-18)$$

Calculating the RMS distortion yields,

$$d = \frac{\frac{1}{2} (RK)^2 + \frac{1}{2} \left[\frac{R}{4} (2+3R) \right]^2 + \frac{1}{2} \left[\frac{R}{4} (2-3R) \right]^2 + \left(\frac{3}{2} RK \right)^2 + \frac{1}{2} \left(\frac{3}{2} RK \right)^2}{\left[\frac{1}{2} (2)^2 \right]^{\frac{1}{2}}} \quad (3-19)$$

$$= \frac{\left[2.6 (RK)^2 + 2R^2 \right]^{\frac{1}{2}}}{4} \quad (3-20)$$

The amount of distortion with $R = \frac{\omega_m}{\omega_0}$ and with $K = .1$ is presented in Table 3-1.

TABLE 3-1
RMS DISTORTION - FIGURE 3-2

<u>R</u>	<u>d</u> (dB relative to desired output)
.001	-77.5
.005	-63.5
.01	-57.5
.05	-43.5
.10	-37.5

A similar analysis has been performed for the dual differentiator version of the Klapper-Kratt detector. From Equation 3-9 the demodulated output is

$$\begin{aligned} e_o(t) = & \frac{A^2 KR}{2} \left[-4 \cos \omega_m t - RK \cos 2 \omega_m t \right. \\ & \left. - RK (1 - 2 \cos 2 \omega_0 t) + R \cos (2 \omega_0 - \omega_m) t \right] \end{aligned}$$

$$- R \cos (2 \omega_0 + \omega_m t) \Big]. \quad (3-9)$$

The undistorted output component is $4 \cos \omega_m t$. The remaining terms are distortion components. The rms distortion can be easily calculated.

$$d = \frac{\left[\frac{1}{2} (RK)^2 + 3 (RK)^2 + R^2 \right]^{\frac{1}{2}}}{\left[\frac{1}{2} 4^2 \right]^{\frac{1}{2}}} = \frac{\left[7 (RK)^2 + 2 R^2 \right]^{\frac{1}{2}}}{4} \quad (3-21)$$

Equation 3-21 is presented in tabular form in Table 3-2 ($K = .1$). Upon comparing the results in Tables 3-1 and 3-2, it is evident that the amounts of distortion in these two versions of the detector are similar and very small.

TABLE 3-2
RMS DISTORTION - FIGURE 3-3

<u>R</u>	<u>d</u> (dB relative to desired output)
.001	-77.9
.005	-63.9
.01	-57.9
.05	-43.9
.10	-37.9

Next, the performance of the limiter discriminator and the two Klapper-Kratt detectors in the presence of sinusoidal interference will be compared. For the input signal described by Equation 3-4, Corrington (Ref. 4) has derived the RMS output of the limiter-discriminator. From Corrington,

$$e_o(t)_{\text{RMS}} = \frac{\left[\left(\frac{B}{A} \right)^2 \left(\frac{\omega_R}{\omega_0} \right)^2 \right]^{\frac{1}{2}}}{\left\{ 2 \left[1 - \left(\frac{B}{A} \right)^2 \right]^{\frac{1}{2}} \right\}} \quad (3-22)$$

for $\omega_c = 0$, and $B/A < 1$.

Curves of Equation 3-22 for various values of B/A and ω_R/ω_0 are shown in Figure 3-4. The output is symmetrical about $\omega_R/\omega_0 = 0$. Therefore, only positive values of ω_R/ω_0 are plotted.

Previously, the output of the Klapper-Kratt detector of Figure 3-2 with sinewave interference was derived. This result is repeated below.

$$e_o(t) \approx \frac{\omega_R}{\omega_0} \left(\frac{B}{A}\right)^2 + \frac{\omega_R}{\omega_0} \frac{B}{A} \cos \omega_R t \quad (3-23)$$

Hence,

$$e_o \text{ RMS} = \left\{ \left[\frac{\omega_R}{\omega_0} \left(\frac{B}{A}\right)^2 \right]^2 + \frac{1}{2} \left[\frac{\omega_R}{\omega_0} \frac{B}{A} \right]^2 \right\}^{1/2} \quad (3-24)$$

For the Klapper-Kratt detector of Figure 3-3, a similar analysis yields the same result. Curves of Equation 3-24 are presented in Figure 3-5. Observe that the performance of the Klapper-Kratt detectors is nearly identical to that of the limiter discriminator for small values of B/A . However, as the interfering signal increases ($B/A \geq 1$), the Klapper-Kratt detector has a much higher output purity.

Curves of Equations 3-24 and 3-26 are presented in Figures 3-5 and 3-6, respectively. Observe that the performance of the detector of Figure 3-2 is nearly identical to that of the limiter discriminator in the presence of sine wave interference, and that the Klapper-Kratt detector in Figure 3-2 is 3 dB better than the detector in Figure 3-3.

3.5 Threshold Comments of Kratt and Kersus

Both Kratt and Kersus state their suspicions that threshold reduction may be possible with the Klapper-Kratt designed demodulators. They base their comments on the absence of limiters in this new family of detectors, and on the use of synchronous detection.

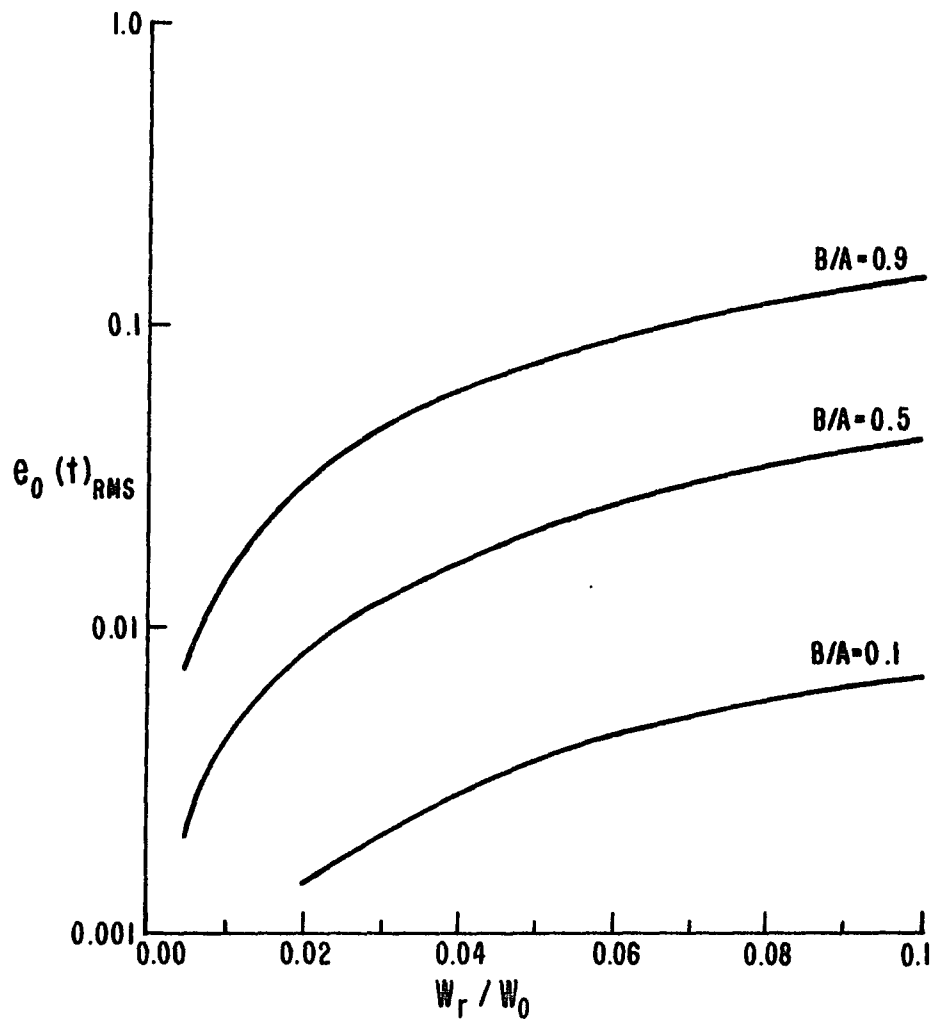


FIGURE 3-4. LIMITER DISCRIMINATOR INTERFERENCE CHARACTERISTIC CURVE (EQUATION 3-22)

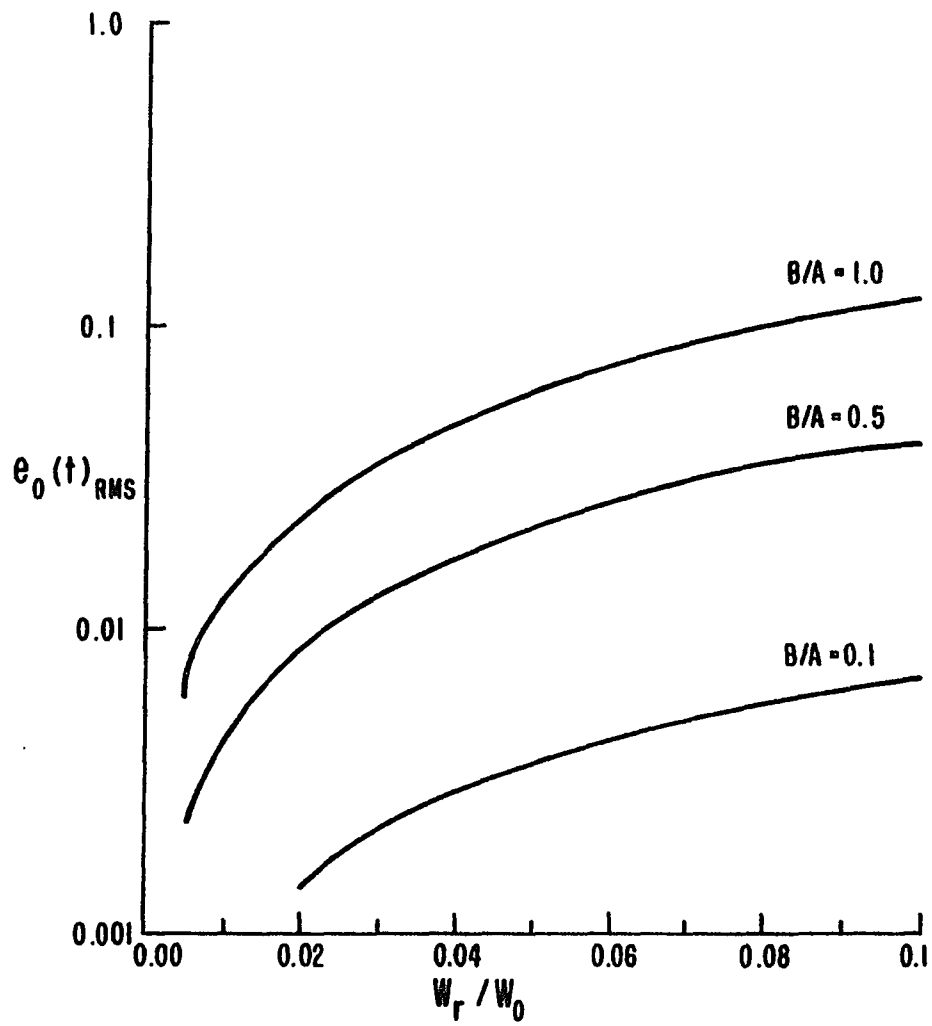


FIGURE 3-5. KLAPPER-KRATT DETECTOR INTERFERENCE CHARACTERISTIC CURVE (EQUATION 3-24)

Chapter IV is a detailed analysis of the Klapper-Kratt detector in the presence of noise. This analysis demonstrates that, while performance above threshold is identical to that of the limiter discriminator, threshold reduction does not occur, as was previously suspected. The experimental results of Chapter V verify this conclusion.

References - Chapter III

1. E. Kratt, NJIT Master's Project, Newark NJ.
2. G. Kersus, "An Analysis of the Klapper-Kratt EM Detector," NJIT Master's Project, Newark, NJ, 1976.
3. J. Park, "An FM Detector for Low S/N," IEEE Transactions on Communications Technology, Vol. COM-18, No. 2, April 1970.
4. M. Corrington, "Frequency Modulation Caused by Common-and-Adjacent-Channel Interference," RCA Review, Vol 7, No. 4, pp. 1051-1092, Dec. 1946.

CHAPTER IV

PERFORMANCE OF THE KLAPPER-KRATT DETECTOR IN THE PRESENCE OF NOISE4.1 Introduction

There are many forms of the Klapper-Kratt detector. It would be impractical to perform a noise analysis on all of them. The version shown earlier in Figures 2-8 and 3-3 was chosen to be analyzed in detail. This detector is again presented in Figure 4-1. The primary reason for this choice was determined by the lack of an integrator in the demodulator portion of this detector. With no integrators, the potential integrator initial condition problem previously described is nonexistent, resulting in a detector with true wideband performance.

4.2 Noise Representation

Before proceeding with the analysis, it is worthwhile to discuss the properties of the assumed noise and its representation. The noise will be considered to be narrowband. Its bandwidth can be no wider than twice the RF center frequency. Such noise can be modeled as

$$n(t) = x(t) \cos \omega_0 t - y(t) \sin \omega_0 t \quad (4-1)$$

Equation 4-1 describes a carrier at the center frequency, ω_0 , modulated by two random variables, $x(t)$ and $y(t)$. The random variables, $x(t)$ and $y(t)$, are assumed to have the following properties:

- (1) Lowpass, rectangular power spectral density (PSD) of bandwidth, B , and amplitude, η (Figure 4-2a).
- (2) Zero mean.
- (3) Gaussian distribution.
- (4) $\sigma_{n(t)}^2 = \sigma_{x(t)}^2 = \sigma_{y(t)}^2$.
- (5) $x(t)$ and $y(t)$ are independent.

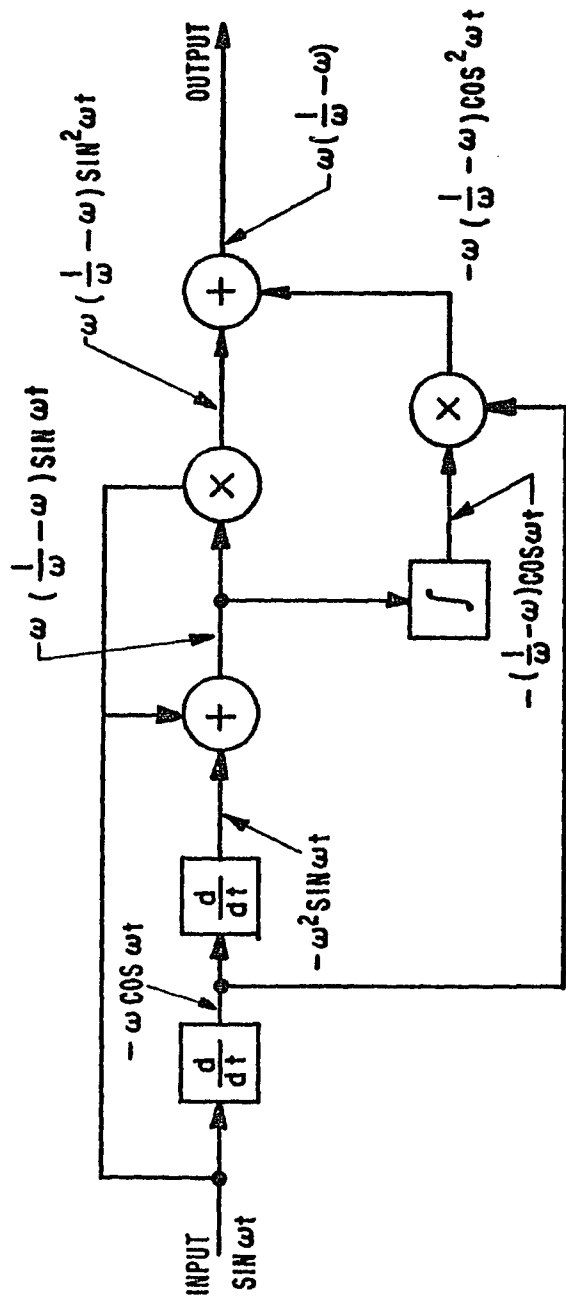


FIGURE 4-1. DUAL DIFFERENTIATOR VERSION OF THE NEW FM DETECTOR FAMILY

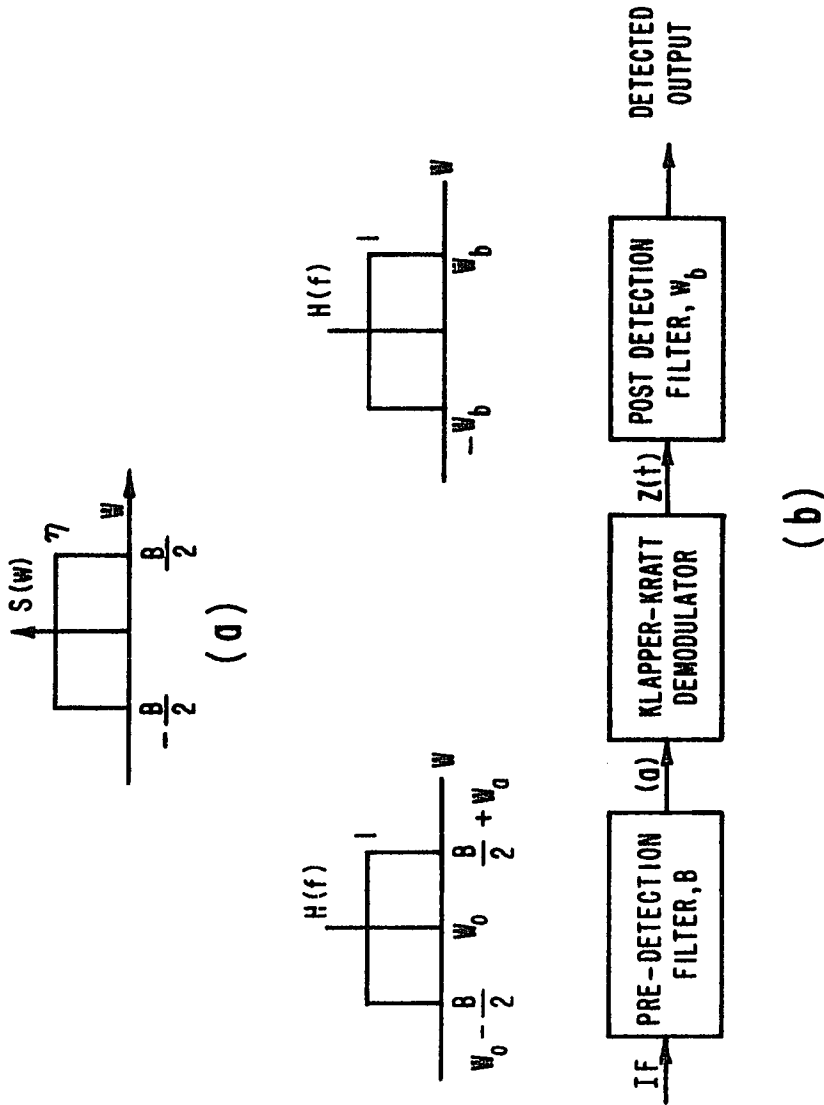


FIGURE 4-2. (a) PSD OF $X(t)$ AND $Y(t)$
 (b) COMPLETE DETECTOR

4.3 Noise Analysis

The output of the detector will be derived as a function of time. The autocorrelation of this time function will be computed, and transformed to output power spectral density (PSD). The output PSD will be used to derive an SNR versus CNR relationship. This result will be compared to that of a conventional limiter discriminator in this chapter and in Chapter V.

The demodulator portion of Figure 4-1 is drawn in Figure 4-3. Various points in the signal flow path have been labeled to aid in the following derivation. The input signal consists of an unmodulated carrier with the additive noise of Equation 4-1. The derivation of the SNR versus CNR relationship is quite lengthy. What follows is an outline of this derivation. The detailed derivation is included in Appendix I.

$$\text{Input} = A \sin \omega_0 t + x(t) \cos \omega_0 t - y(t) \sin \omega_0 t, \quad (4-2)$$

where ω_0 is the RF (or IF) center frequency,
and A is the amplitude of the signal carrier.

At the output of the first differentiator, (b), we obtain

$$(b) = \frac{1}{\omega_0} \left[\omega_0 A \cos \omega_0 t + \dot{x}(t) \cos \omega_0 t - \omega_0 x(t) \sin \omega_0 t - \dot{y}(t) \sin \omega_0 t - \omega_0 y(t) \cos \omega_0 t \right]. \quad (4-3)$$

The $1/\omega_0$ term is necessary to cancel the gain factor of ω_0 inherent in the differentiation. Another $1/\omega_0$ term is necessary in the second differentiation.

At the output of the second differentiator,

$$(c) = \frac{1}{\omega_0^2} \left[-\omega_0^2 A \sin \omega_0 t + \ddot{x}(t) \cos \omega_0 t - \omega_c \dot{x}(t) \sin \omega_0 t - (\omega_0 \dot{x}(t) \sin \omega_0 t) \right]$$

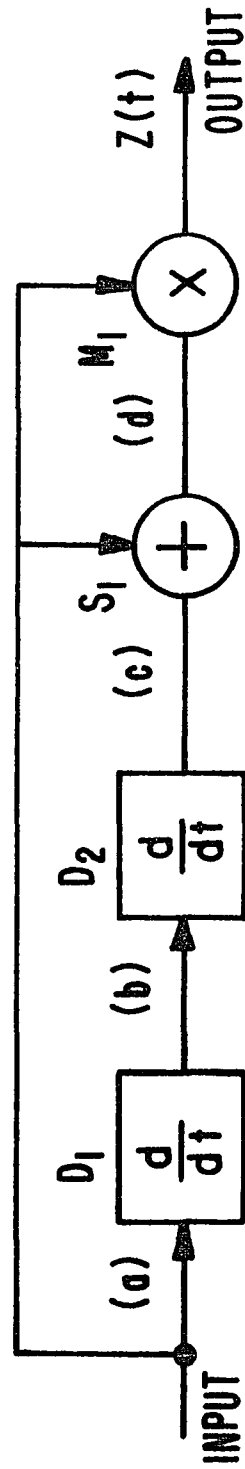


FIGURE 4-3. DEMODULATOR PORTION OF FM DETECTOR

$$\begin{aligned}
& - \omega_0^2 x(t) \cos \omega_0 t - \ddot{y}(t) \sin \omega_0 t - \omega_0 \dot{y}(t) \cos \omega_0 t \\
& - \omega_0 \dot{y}(t) \cos \omega_0 t + \omega_0^2 y(t) \sin \omega_0 t
\end{aligned} \tag{4-4}$$

At point (d),

$$\begin{aligned}
(d) &= A \sin \omega_0 t + x(t) \cos \omega_0 t - y(t) \sin \omega_0 t - A \sin \omega_0 t \\
&+ 1/\omega_0^2 \ddot{x}(t) \cos \omega_0 t - 2/\omega_0 \dot{x}(t) \sin \omega_0 t - x(t) \cos \omega_0 t - 1/\omega_0^2 \ddot{y}(t) \\
&\quad \sin \omega_0 t - 2/\omega_0 \dot{y}(t) \cos \omega_0 t + y(t) \sin \omega_0 t
\end{aligned} \tag{4-5}$$

$$\begin{aligned}
&= \frac{\ddot{x}(t)}{\omega_0^2} \cos \omega_0 t - \frac{2}{\omega_0} \dot{x}(t) \sin \omega_0 t \\
&- \frac{\ddot{y}(t)}{\omega_0^2} \sin \omega_0 t - \frac{2\dot{y}(t)}{\omega_0} \cos \omega_0 t.
\end{aligned} \tag{4-6}$$

The output, $Z(t)$, is the product of (a) and (d). After multiplication and simplification,

$$\begin{aligned}
Z(t) &= \left[-\frac{2A\dot{x}(t)}{\omega_0} - \frac{A\ddot{y}(t)}{\omega_0^2} + \frac{2y(t)\dot{x}(t)}{\omega_0} + \frac{y(t)\ddot{y}(t)}{\omega_0^2} \right] \sin^2 \omega_0 t \\
&+ \left[\frac{x(t)\ddot{x}(t)}{\omega_0^2} - \frac{2x(t)\dot{y}(t)}{\omega_0} \right] \cos^2 \omega_0 t \\
&+ \left[A \frac{\ddot{x}(t)}{\omega_0^2} - \frac{2A\dot{y}(t)}{\omega_0} - \frac{2x(t)\dot{x}(t)}{\omega_0} - \frac{x(t)\dot{y}(t)}{\omega_0^2} - \frac{y(t)\ddot{x}(t)}{\omega_0^2} \right. \\
&\quad \left. + \frac{2y(t)\dot{y}(t)}{\omega_0} \right] \sin \omega_0 t \cos \omega_0 t.
\end{aligned} \tag{4-7}$$

Using appropriate trigonometric identities, $Z(t)$ becomes

$$\begin{aligned}
Z(t) &= \left[\frac{-A\dot{x}(t)}{\omega_0} - \frac{2A\ddot{y}(t)}{2\omega_0^2} + \frac{y(t)\dot{x}(t)}{\omega_0} + \frac{y(t)\ddot{y}(t)}{2\omega_0^2} \right] \\
&- \left[\frac{A\dot{x}(t)}{\omega_0} - \frac{A\ddot{y}(t)}{2\omega_0^2} + \frac{y(t)\dot{x}(t)}{\omega_0} + \frac{y(t)\dot{y}(t)}{2\omega_0^2} \right] \cos 2 \omega_0 t
\end{aligned}$$

$$\begin{aligned}
& + \left[\frac{x(t)\ddot{x}(t)}{2\omega_0^2} - \frac{x(t)\dot{y}(t)}{\omega_0} \right] + \left[\frac{x(t)\dot{x}(t)}{2\omega_0^2} - \frac{x(t)\dot{y}(t)}{\omega_0} \right] \cos 2\omega_0 t \\
& + \left[\frac{A\ddot{x}(t)}{2\omega_0^2} - \frac{A\dot{y}(t)}{\omega_0} - \frac{x(t)\dot{x}(t)}{\omega_0} - \frac{x(t)\ddot{y}(t)}{2\omega_0^2} - \frac{y(t)\dot{x}(t)}{2\omega_0^2} + \frac{y(t)\dot{y}(t)}{\omega_0} \right] \\
& \sin 2\omega_0 t. \tag{4-8}
\end{aligned}$$

Taking baseband terms only, the demodulator output reduces to

$$\begin{aligned}
Z(t) = & - \frac{A\dot{x}(t)}{\omega_0} - \frac{A\dot{y}(t)}{2\omega_0^2} + \frac{y(t)\dot{x}(t)}{\omega_0} + \frac{y(t)\dot{y}(t)}{2\omega_0^2} \\
& + \frac{x(t)\dot{x}(t)}{2\omega_0^2} - \frac{x(t)\dot{y}(t)}{\omega_0} \tag{4-9}
\end{aligned}$$

Assuming $\omega_0^2 \gg \omega_0$, Equation 4-9 may be approximated by

$$Z(t) \cong - \frac{A\dot{x}(t)}{\omega_0} + \frac{y(t)\dot{x}(t)}{\omega_0} - \frac{x(t)\dot{y}(t)}{\omega_0} \tag{4-10}$$

Next, the autocorrelation of $Z(t)$ is defined by

$$R_{ZZ}(\tau) = E \{ Z(t) Z(t + \tau) \} \tag{4-11}$$

From Equation 4-10

$$\begin{aligned}
R_{ZZ}(\tau) = & E \left\{ \left[- \frac{A\dot{x}(t)}{\omega_0} + \frac{y(t)\dot{x}(t)}{\omega_0} - \frac{x(t)\dot{y}(t)}{\omega_0} \right] \right. \\
& \left. \left[- \frac{A\dot{x}(t+\tau)}{\omega_0} + \frac{y(t+\tau)\dot{x}(t+\tau)}{\omega_0} - \frac{x(t+\tau)\dot{y}(t+\tau)}{\omega_0} \right] \right\} \tag{4-12}
\end{aligned}$$

Equation 4-12 may be rewritten as the sum of expected values and simplified.

$$\begin{aligned}
R_{ZZ}(\tau) = & E \left[\frac{A^2}{\omega_0^2} \dot{x}(t) \dot{x}(t + \tau) \right] + E \left[\frac{1}{\omega_0^2} y(t) \dot{x}(t) y(t + \tau) \dot{x}(t + \tau) \right] \\
& - E \left[\frac{1}{\omega_0^2} y(t) \dot{x}(t) x(t + \tau) \dot{y}(t + \tau) \right] - E \left[\frac{1}{\omega_0^2} x(t) \dot{y}(t) y(t + \tau) \right]
\end{aligned}$$

$$\dot{x}(t + \tau) \Big] + E \left[\frac{1}{\omega_0} x(t) x(t + \tau) \dot{y}(t) \dot{y}(t + \tau) \right]. \quad (4-13)$$

Further simplification yields

$$R_{ZZ}(\tau) = \frac{A^2}{\omega_0} R_{\dot{X}\dot{X}}(\tau) + 2 D^2 R_{YY}(\tau) R_{\dot{X}\dot{X}}(\tau) - (2 D^2) E \left[x(t) \dot{x}(t + \tau) \right] \quad (4-14)$$

$$= \frac{A^2}{\omega_0} \frac{d^2 R_{XX}(\tau)}{d\tau^2} + \frac{2}{\omega_0} R_{YY}(\tau) R_{\dot{X}\dot{X}}(\tau) - \frac{2}{\omega_0} \left[\frac{d R_{XX}(\tau)}{d\tau} \right]^2 \quad (4-15)$$

The Fourier transform of $R_{ZZ}(\tau)$ will produce the output power spectral density,

$$R_{ZZ}(\tau) \longleftrightarrow S_{ZZ}(f) \text{ watts/Hz} \quad (4-16)$$

$$\text{or, } S_{ZZ}(\omega) = \frac{A^2}{\omega_0} \left[\omega^2 S(\omega) \right] + \frac{2}{\omega_0} \left\{ \int \left[R_{YY}(\tau) R_{\dot{X}\dot{X}}(\tau) \right] \right\} - \frac{2}{\omega_0} \int \left\{ \left[\frac{d R_{XX}(\tau)}{d\tau} \right]^2 \right\} \quad (4-17)$$

Where $S(\omega)$ is as shown in Figure 4-2a.

The second and third terms of Equation 4-17 may be evaluated using convolution techniques. After much manipulation, the output spectral density becomes

$$S_{ZZ}(\omega) = \frac{A^2}{\omega_0} \left[\omega^2 S(\omega) \right] + \frac{1}{\pi \omega_0} \left[\begin{array}{l} \frac{\eta^2}{3} \left[(\omega + \frac{B}{2})^2 + (\frac{B}{2})^3 \right] - B \leq \omega < 0 \\ \frac{\eta^2}{3} \left[(-\omega + \frac{B}{2})^3 + (\frac{B}{2})^3 \right] \quad 0 \leq \omega \leq B \end{array} \right]$$

$$-\frac{1}{\pi\omega_0^2} \left[\begin{array}{l} \eta^2 \left[2/3 \left(\frac{B}{2}\right)^3 + \left(\frac{B}{2}\right)^2 \omega - \frac{\omega^3}{6} \right], \quad -B \leq \omega \leq -\frac{B}{2} \\ \eta^2 \left[\frac{\omega^3}{2} - 2 \frac{\left(\frac{B}{2}\right)^3}{3} - \left(\frac{B}{2}\right)^2 \omega \right], \quad -\frac{B}{2} \leq \omega \leq 0 \\ \text{(Symmetric in Positive Half Plane)} \end{array} \right] \quad (4-18)$$

where η is the amplitude of the PSD of $x(t)$ and $y(t)$, and B is the bandwidth of the predetection filter (Figure 4-3).

Total noise power at the detector output is equal to the integral of the noise power spectral density, $S_{ZZ}(\omega)$, over the post detection filter bandwidth. Hence,

$$\text{Noise Power} = \frac{1}{2\omega} \int_{-\omega_b}^{\omega_b} S_{ZZ}(\omega) d\omega, \quad (4-19)$$

Since the units of $S_{ZZ}(\omega)$ are watts/Hz, the $1/2\pi$ factor is necessary when integrating over ω (radians/second).

$$\begin{aligned} \text{Noise Power} = \frac{1}{2\pi} \left\{ \frac{A^2}{\omega_0^2} \int_{-\omega_b}^{\omega_b} \omega^2 S(\omega) d\omega + \frac{2\eta^2}{3\pi\omega_0^2} \int_{-\omega_b}^0 \left[\left(\omega + \frac{B}{2}\right)^3 \right. \right. \\ \left. \left. + \left(\frac{B}{2}\right)^3 \right] d\omega - \frac{2\eta^2}{\omega_0^2\pi} \int_{-\omega_b}^0 \left[\frac{\omega^3}{2} - \frac{2\left(\frac{B}{2}\right)^3}{3} - \left(\frac{B}{2}\right)^2 \omega \right] d\omega \right\}, \quad (4-20) \end{aligned}$$

assuming $\omega_b < \frac{B}{2}$.

Completing the integration results in

$$\text{NOISE POWER} = \frac{A^2 \eta \omega_b^3}{3 \pi \omega_0^2} + \frac{\eta^2 \omega_b^4}{2 \cdot 4\eta^2 \omega_0^2} + \frac{\eta^2 \omega_b^3 B}{6 \pi^2 \omega_0^2}$$

$$- \frac{\eta^2 \omega_b^2 B^2}{4 \eta^2 \omega_0^2} + \frac{\eta^2 \omega_b B^3}{6 \pi^2 \omega_0^2} \cdot \quad (4-21)$$

In order to obtain the output signal to noise ratio, the signal output power from the demodulator must also be obtained. Single tone modulation is a common standard of comparison. Assuming single tone modulation, the input signal can be written as

$$\text{Input Signal} = A \cos(\omega_0 t + \beta \sin \omega_m t) \quad (4-22)$$

where β = modulation index,

ω_m = frequency of modulating signal.

Passing this signal through the demodulator yields

$$\frac{\text{Output Signal}}{\text{Power RMS}} = \frac{A^4 \beta^2 \omega_m^2}{2 \omega_0^2} \quad (4-23)$$

(The details of this operation are presented in Appendix II.)

The SNR at the detector output is simply the ratio of Equation 4-23 and Equation 4-21, assuming that the signal and noise terms can be considered additive. This assumption held sufficiently well in the analyses of previous investigators, except when deep below threshold; therefore,

$$\text{SNR} = \frac{\frac{A^4 \beta^2 \omega_m^2}{2 \omega_0^2}}{\frac{A^2 \eta \omega_b^3}{3 \pi \omega_0^2} + \frac{2 b^4}{4 \eta^2 \omega_0^2} + \frac{\eta^2 \omega_b^3 B}{6 \pi^2 \omega_0^2} - \frac{2 b^2 B^2}{4 \pi^2 \omega_0^2} - \frac{\eta^2 \omega_b B^3}{7 \pi^2 \omega_b^2}} \cdot \quad (4-24)$$

Dividing the numerator and denominator of Equation 4-24 by

$$\frac{A^2 \eta \omega_b^3}{3 \pi \omega_0^2}$$

and recalling that

$$\text{CNR} \equiv \frac{A^2/2}{\eta \left(\frac{B}{2\pi}\right)} = \frac{\pi A^2}{\eta B} \quad (4-25)$$

yields

$$\text{SNR} = \frac{\frac{3}{2} (\text{CNR}) B \beta^2 \frac{\omega_m^2}{\omega_b^3}}{1 + \frac{1}{8x(\text{CNR})} + \frac{1}{2(\text{CNR})} - \frac{3x}{4(\text{CNR})} + \frac{x^2}{2(\text{CNR})}} \quad (4-26)$$

$$\text{where } x = \frac{B}{\omega_b}$$

Equation 4-26 was derived for quite general circumstances. Only the following assumptions were made:

- (1) $\omega_0^2 \gg \omega_0$
- (2) $\omega_b < \frac{B}{2}$.
- (3) Signal and noise terms are additive.

4.4 Special Case -- High CNR

For the high CNR situation, the last four terms in the denominator of Equation 4-26 will become negligible. Hence,

$$\text{SNR (High CNR)} \approx \frac{3}{2} (\text{CNR}) B \beta^2 \frac{\omega_m^2}{\omega_b^3} \quad (4-27)$$

For best performance set $\omega_m = \omega_b$, then

$$\text{SNR (High CNR)} = \frac{3}{2} (\text{CNR}) \frac{B\beta^2}{\omega_b} \quad (4-28)$$

Recall that

$$\text{CNR}_{AM} = \text{CNR} \left(\frac{B}{2\omega_b}\right) \quad (4-29)$$

$$\text{or } \text{CNR} = (\text{CNR}_{AM}) \frac{2\omega_b}{B} \quad (4-30)$$

Inserting Equation 4-30 into 4-28 produces

$$\text{SNR (High CNR)} = 3/2 (\text{CNR}_{\text{AM}}) \frac{2\omega_b}{B} \frac{B\beta^2}{\omega_b} = 3 \beta^2 \text{CNR}_{\text{AM}} \quad (4-31)$$

Equation 4-31 describes the SNR improvement expected in the linear improvement region. This expression is identical to the expression derived for the conventional limiter discriminator in Chapter I, Equation 1-11. Hence, the performance of the Klapper-Kratt detector above threshold is identical to that of the limiter discriminator above threshold, without the use of a limiter. A conventional discriminator, however, has a highly degraded performance without a limiter.

4.5 Threshold

Equation 4-26 may be used to determine threshold occurrence for a specified ω_b and B . Equation 4-26 has been evaluated for threshold for various values of the ratio $B/2\omega_b$, and the result is plotted in Figure 4-4. This result is compared to data for the conventional limiter discriminator (Ref. 1). Apparently no threshold improvement exists, as was previously thought. However, the new detector, without the additional complexity of a limiter, will perform nearly as well as the limiter discriminator in many cases.

4.6 RF Canceller

Up to this point of the analysis, the RF cancelling portion of the detector has been ignored. It has been assumed that the canceller simply eliminates the undesired high frequency products of detection, and has no effect on the output signal to noise ratio. This assumption is, in fact, true, as will now be demonstrated.

From Equation 4-6, the output of the first summer in Figure 4-1 is

$$(d) = \frac{\ddot{x}(t)}{\omega_0} \cos \omega_0 t - \frac{2}{\omega_0} \dot{x}(t) \sin \omega_0 t$$

$$- \frac{\ddot{y}(t)}{\omega_0^2} \sin \omega_0 t - \frac{2\dot{y}(t)}{\omega_0} \cos \omega_0 t \quad (4-32)$$

For high ω_0 Equation 4-32 becomes

$$(d) \approx \frac{2}{\omega_0} \dot{x}(t) \sin \omega_0 t - \frac{2}{\omega_0} \dot{y}(t) \cos \omega_0 t \quad (4-33)$$

Similarly, for high ω_0 , the output from the first differentiator (Equation 4-3) is

$$(b) \approx A \cos \omega_0 t - x(t) \sin \omega_0 t - y(t) \cos \omega_0 t \quad (4-34)$$

Hence, the output of the second multiplier in Figure 4-1 is

$$\begin{aligned} & - 2 \left[\int (\dot{x} \sin \omega_0 t + \dot{y} \cos \omega_0 t) dt \right] \left[A \cos \omega_0 t - x \sin \omega_0 t - y \cos \omega_0 t \right] \\ & = - 2 A \cos \omega_0 t \int (\dot{x} \sin \omega_0 t + \dot{y} \cos \omega_0 t) dt \\ & \quad + 2 x \sin \omega_0 t \int (\dot{x} \sin \omega_0 t + \dot{y} \cos \omega_0 t) dt \quad (4-35) \end{aligned}$$

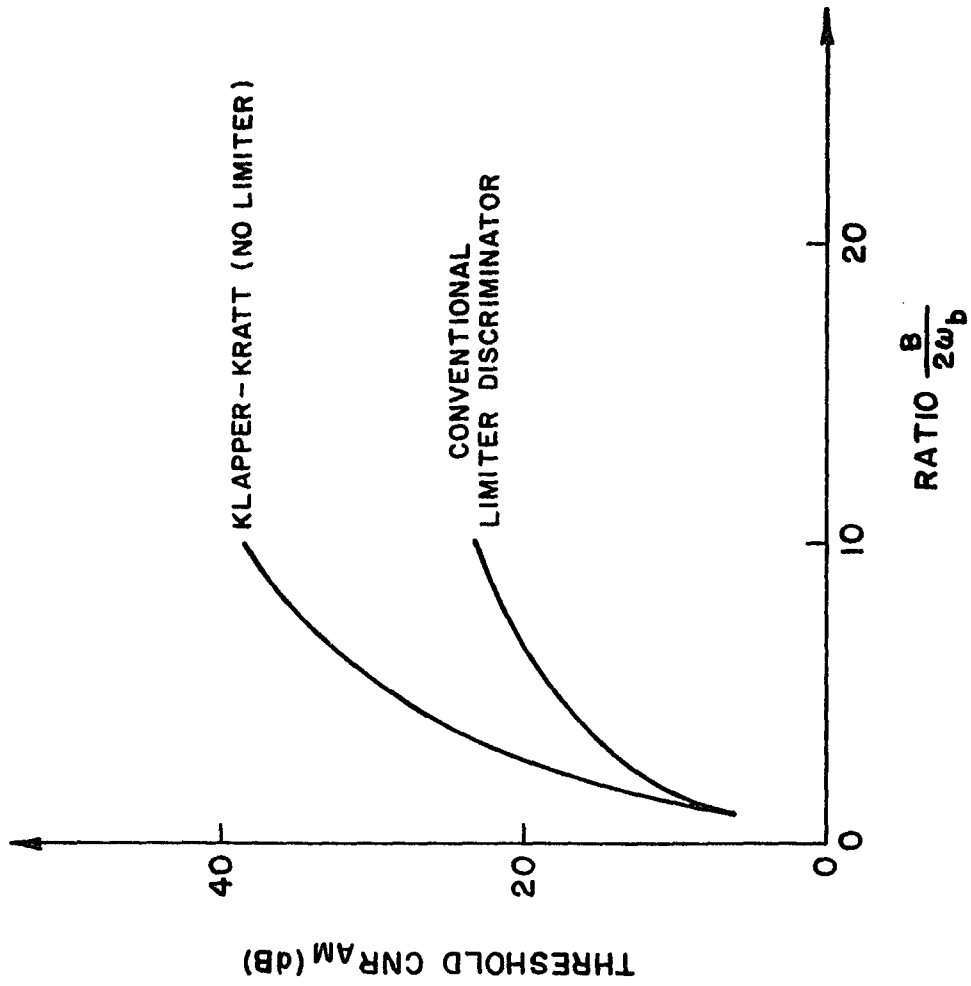
$$+ 2 y \cos \omega_0 t \int (\dot{x} \sin \omega_0 t + \dot{y} \cos \omega_0 t) dt. \quad (4-36)$$

Multiple integrations by parts (assuming high ω_0) solve the above integral.

$$\begin{aligned} \int (x \sin \omega_0 t + y \cos \omega_0 t) dt \approx & \left[- \frac{\dot{x}}{\omega_0} \cos \omega_0 t + \frac{\ddot{x}}{\omega_0^2} \sin \omega_0 t \right. \\ & \left. + \frac{\dot{y}}{\omega_0} \sin \omega_0 t + \frac{\ddot{y}}{\omega_0^2} \cos \omega_0 t \right] \quad (4-37) \end{aligned}$$

Substitution of Equation 4-37 into Equation 4-36, followed by grouping of terms, produces

$$\begin{aligned} & \left[\frac{A\dot{x}}{\omega_0} - \frac{A\dot{y}}{\omega_0^2} - \frac{y\dot{x}}{\omega_0} + \frac{y\ddot{y}}{\omega_0^2} + \frac{x\dot{y}}{\omega_0} + \frac{x\ddot{x}}{\omega_0^2} \right] \\ & + \left[\frac{A\dot{x}}{\omega_0} - \frac{A\dot{y}}{\omega_0^2} - \frac{y\dot{x}}{\omega_0} + \frac{y\ddot{y}}{\omega_0^2} - \frac{x\dot{y}}{\omega_0} - \frac{x\ddot{x}}{\omega_0^2} \right] \cos 2 \omega_0 t \end{aligned}$$

FIGURE 4-4. THRESHOLD CNR_{AM} VS IF TO BASE BAND RATIO

$$+ \left[-\frac{A\ddot{x}}{\omega_0^2} - \frac{A\dot{y}}{\omega_0} - \frac{x\dot{x}}{\omega_0} + \frac{x\dot{y}}{\omega_0^2} + \frac{y\ddot{x}}{\omega_0^2} + \frac{y\dot{y}}{\omega_0} \right] \sin 2\omega_0 t. \quad (4-38)$$

Subtracting the output of the second multiplier (Equation 4-38) from the output of the first multiplier (Equation 4-8) yields the output from the canceller circuit, i.e., the final detector output. This result is shown below.

$$\begin{aligned} \text{Canceller Output} &= \frac{-2AX(t)}{\omega_0} + \frac{A\dot{Y}(t)}{2\omega_0^2} + \frac{2y(t)\dot{x}(t)}{\omega_0} - \frac{y(t)\ddot{y}(t)}{2\omega_0^2} \\ &\quad - \frac{2x(t)\dot{y}(t)}{\omega_0} - \frac{x(t)\ddot{x}(t)}{2\omega_0^2} \end{aligned} \quad (4-39)$$

For high ω_0 , the contribution of the $1/\omega_0^2$ terms may be considered to be negligible. Eliminating the $1/\omega_0^2$ terms, the canceller output is

$$- \frac{2A\ddot{X}(t)}{\omega_0} + \frac{2y(t)\dot{x}(t)}{\omega_0} - \frac{2x(t)\dot{y}(t)}{\omega_0} \quad (4-40)$$

The unwanted harmonic terms are gone. Equation 4-40 is identical to the earlier derived output, $Z(t)$, in Equation 4-10, with the exception of a factor of two. This factor of two does not effect the SNR at the detector output, since both the signal and the noise will be multiplied by it.

References - Chapter IV

1. J. Klapper & J.T. Frankle, "Phased Locked and Frequency Feedback Systems", Chpt. 7, Figure 7-14, Academic Press, 1972.
2. N. Blachman, "Noise and Its Effect on Communication", Chpt. 6, McGraw-Hill, 1966.

CHAPTER V

EXPERIMENTAL VERIFICATION5.1 Introduction

The demodulator portion of the dual differentiator version of the Klapper-Kratt detector has been built and is operational. Data taken with this demodulator are presented for comparison with the analytical results of Chapter IV and with the conventional limiter discriminator. The block diagram of this demodulator is shown in Figure 5-1. It is only necessary to build the demodulator portion of this detector to determine detector performance in the presence of noise. Recall that, in Chapter IV, it was demonstrated that the cancelling portion of the detector does not effect the CNR-SNR relationship of the Klapper-Kratt detector.

5.2 Circuit Description and Operation

The circuitry, assembled with silicon monolithic integrated circuits, is presented in Figure 5-2. Each stage is labeled and photographs of the actual waveforms at various test points are shown. These waveforms were recorded with a sinewave modulated FM input signal centered at 1000 Hz. Such a low IF frequency permits the use of off-the-shelf operational amplifiers and multipliers. These integrated components make initial assembly and later modification easier than if discrettes were used exclusively. A peak frequency deviation of ± 75 Hz about the 1000 Hz carrier was established, resulting in truly wideband performance.

The modulated input signal is produced by a function generator. This input signal consists of a 1000 Hz carrier deviated ± 75 Hz by a 25 Hz sinewave. This signal is applied to the demodulator input, TP (A). After amplification, the signal is differentiated. The differentiated output appears at TP (C), where it is applied to the second differentiator. Practical differentiators are imperfect, due to their inherent frequency limitations. To circumvent this

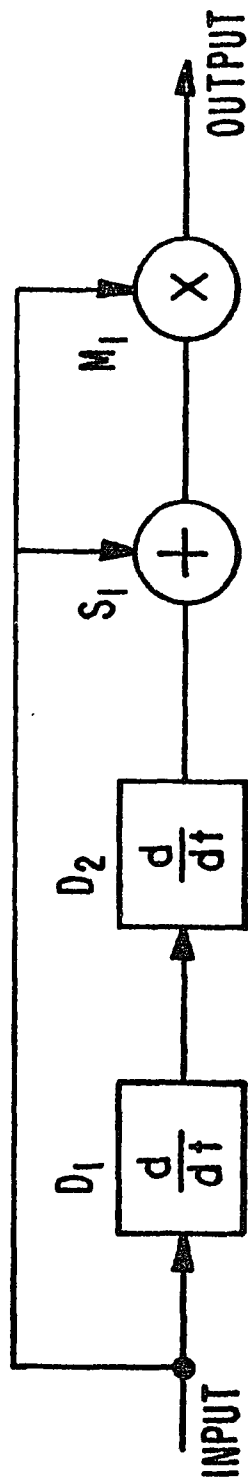
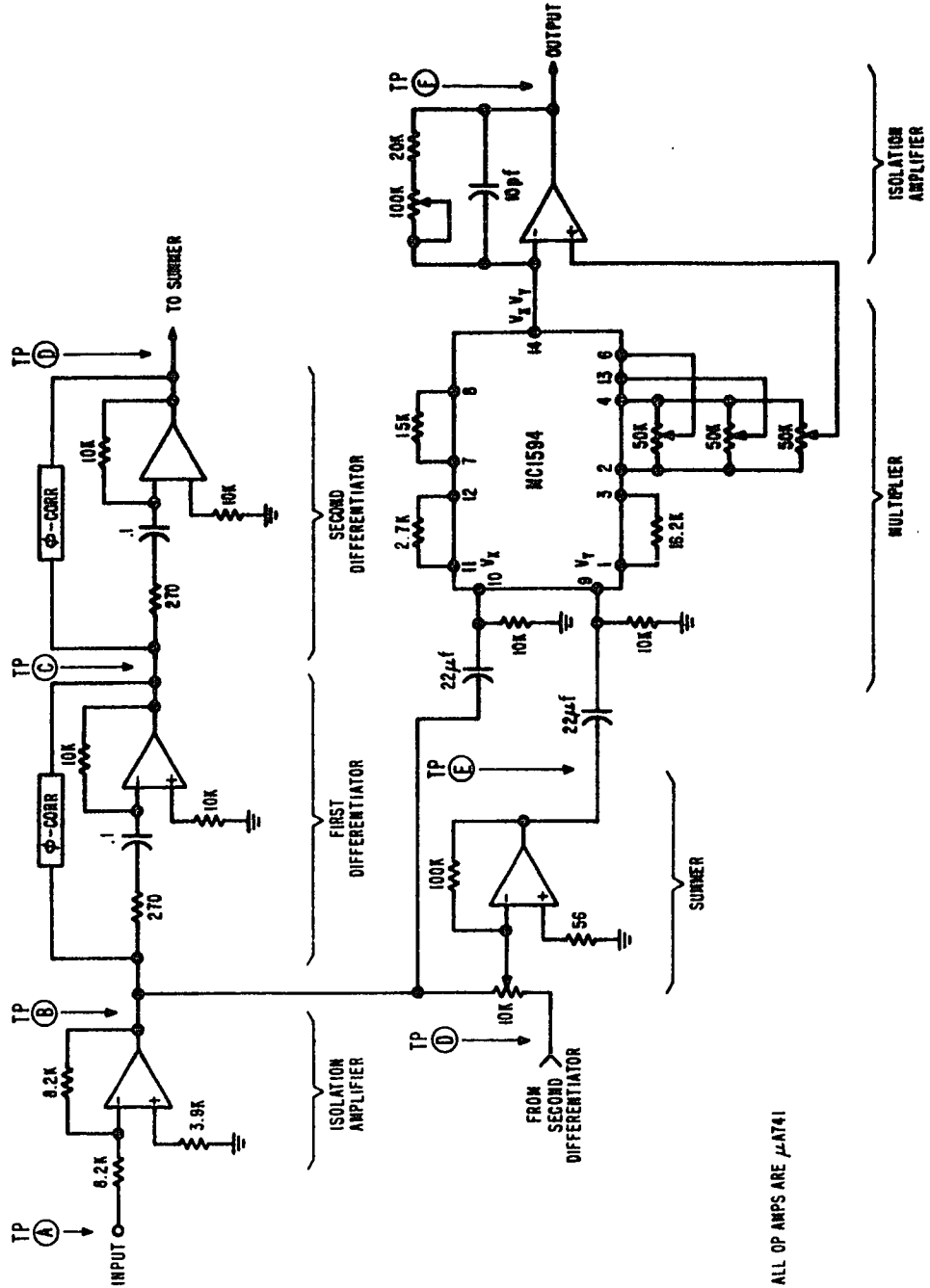
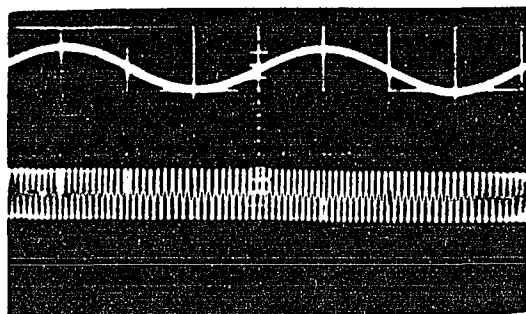


FIGURE 5-1. DEMODULATOR PORTION OF FM DETECTOR

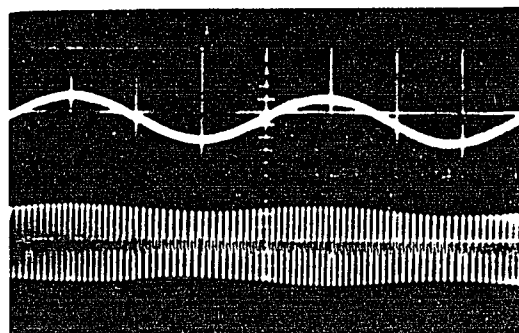


ALL OP AMPS ARE μ A741

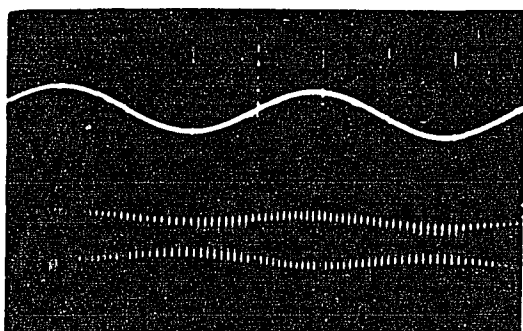
FIGURE 5-2a DEMODULATOR CIRCUIT DIAGRAM



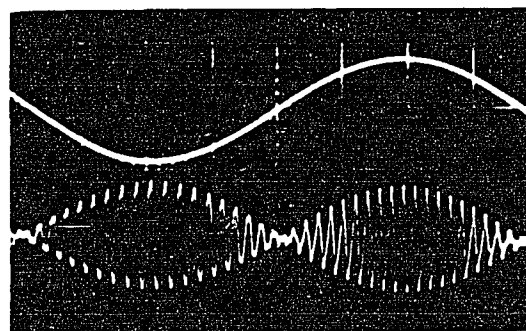
TP A: BASEBAND MODULATION COMPARED TO
FM MODULATED CARRIER (10ms/div)



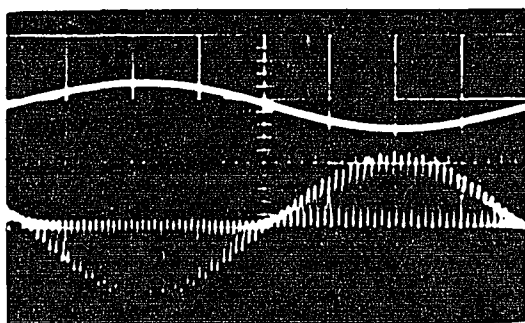
TP C: BASEBAND MODULATION COMPARED TO
FIRST DIFFERENTIATOR OUTPUT
(10ms/div)



TP D: BASEBAND MODULATION COMPARED TO
SECOND DIFFERENTIATOR OUTPUT
(10ms/div)



TP E: BASEBAND MODULATION COMPARED TO
SUMMER OUTPUT (5ms/div)



TP F: BASEBAND MODULATION COMPARED TO
MULTIPLIER OUTPUT (5ms/div)

FIGURE 5-2b. TEST POINT WAVEFORMS

characteristic, a correction element is placed across each differentiator. This element is actually an adjustable resistor which provides a cancellation voltage at the differentiator output. This cancellation technique was first used by Klapper and Kratt, and a detailed explanation of the technique is provided in Appendix III.

The output of the second differentiator is summed with a sample of the input signal. The summer output appears at TP (E). The summer output is then multiplied with the input signal, and the demodulated output appears at TP (F). The various fixed resistors and capacitors determine the gains and time constants for the various stages. A number of variable resistors are provided to adjust the demodulator for optimum performance.

5.3 Experimental Performance Results

Prior to making any noise measurements, the linearity of the demodulator and the demodulator response to signal-only were recorded. The steady state input frequency versus output voltage for the circuit in Figure 5-2 is plotted in Figure 5-3. Figure 5-3 shows substantial linearity over a 20% bandwidth.

Next, the function generator was adjusted to produce a 1000 Hz carrier FM modulated by a 25 Hz sinusoidal baseband signal (± 75 Hz deviation). The baseband signal is shown superimposed on the demodulator output in Figure 5-4a. Results assuming other baseband waveforms are shown in Figures 5-4b and 5-4c. In each case, the envelope of the multiplier output closely resembles the baseband waveform. These waveforms also verify that this version of the Klapper-Kratt detector can handle very wideband signals.

Before meaningful noise measurements can be made, the test configuration and predetection and post detection filters must be specified. The test equipment layout for the measurements of SNR versus CNR for the Klapper-Kratt demodulator (without limiter) is diagrammed in Figure 5-5.

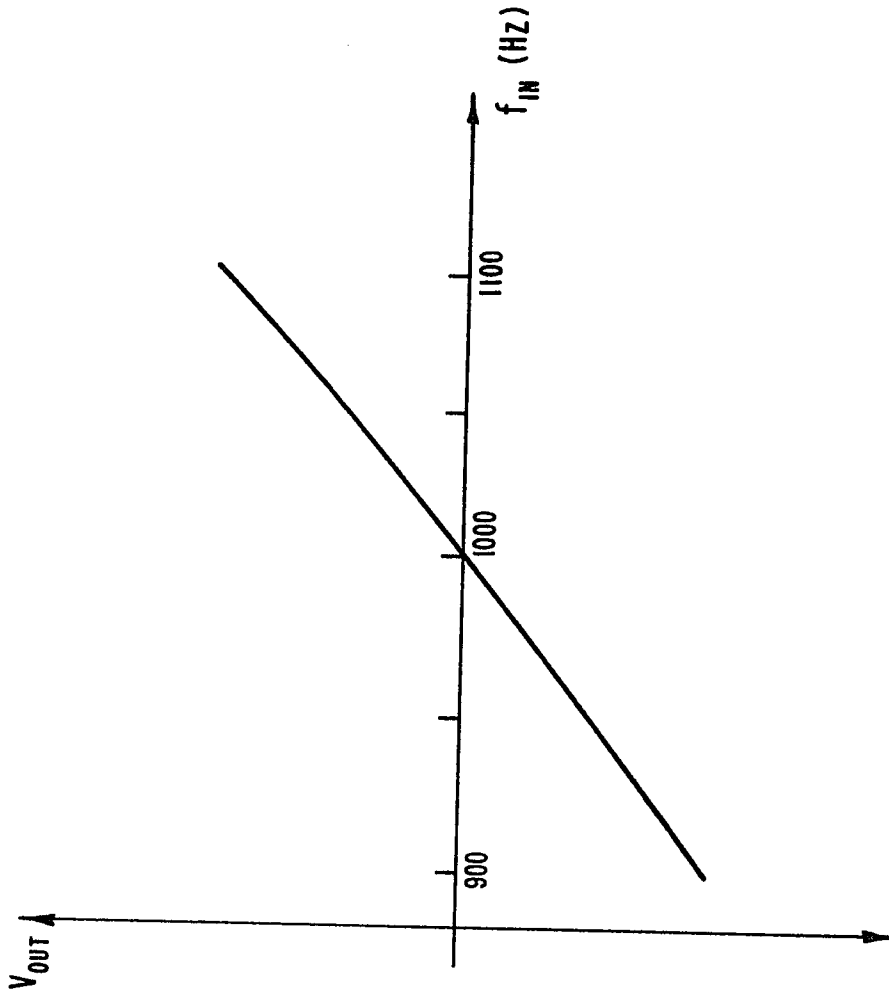
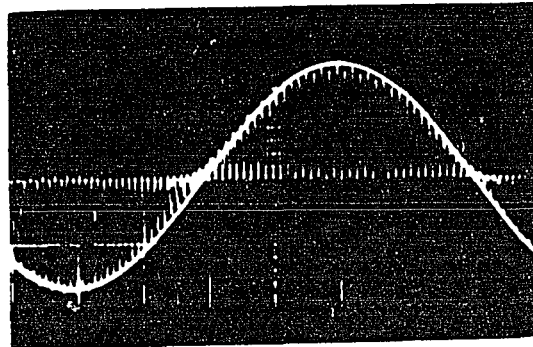
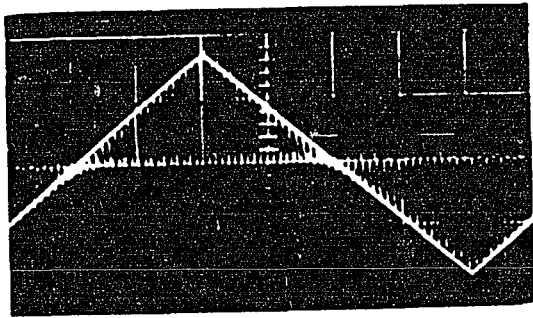


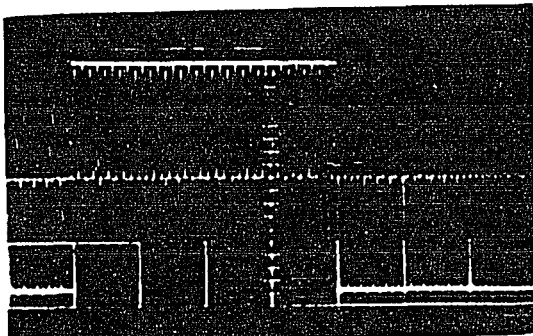
FIGURE 5-3. OUTPUT VOLTAGE VS INPUT FREQUENCY



(A) SINUSOIDAL BASEBAND (10ms/div)



(B) TRIANGULAR BASEBAND (10ms/div)



(C) SQUARE BASEBAND (10ms/div)

FIGURE 5-4. BASEBAND SIGNAL SUPERIMPOSED ON MULTIPLIER OUTPUT FOR VARIOUS BASEBAND WAVEFORMS

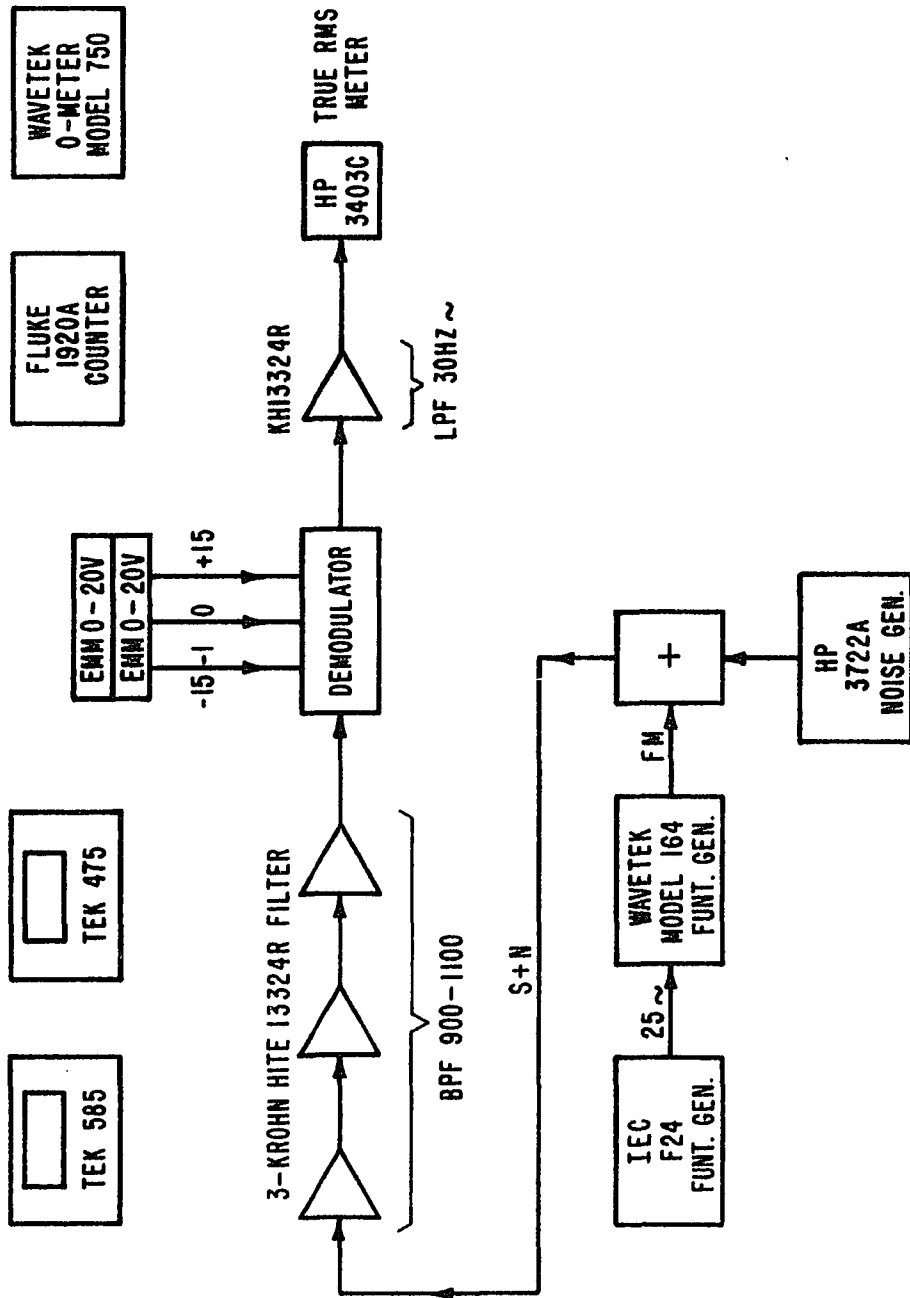


FIGURE 5-5. TEST EQUIPMENT FOR MEASUREMENT OF SNR-CNR CHARACTERISTIC

This diagram shows an Interstate Electronics (IEC) function generator FM modulating a Wavetek generator with a 25 Hz sinewave. The IEC generator output level is adjusted to produce ± 75 Hz deviation. The Hewlett-Packard 3722A noise generator produces Gaussian noise within the bandwidth of interest. The noise power can be adjusted on the HP 3722A. The signal and noise are summed, and the resultant signal plus noise is applied to the predetection bandpass filter. This filter consists of three Krohn-Hite active filter units in cascade. Together they produce the response in Figure 5-6. The predetection filter output is applied to the demodulator. The output from the demodulator is then lowpass filtered. A single Krohn-Hite filter unit serves as the post detection filter. This filter response is presented in Figure 5-7. The output power from the post detection filter is measured with an HP 3403C true RMS meter.

Klapper and Frankle describe two techniques for measuring SNR as a function of CNR (Ref. 1). One technique allows measurement of the output noise with modulation present. However, this requires the addition of a narrowband reject filter ahead of the true RMS power meter to remove the tone modulation. The other method requires the least equipment, but provides CNR versus SNR information in the absence of modulation. Measurement of data for this chapter utilized this latter method. The effect of modulation on threshold is ignored, as in the analytical part of this dissertation. Using this technique, the noise output is measured with the RMS power meter at each value of CNR (no modulation). A reference signal output from which SNR calculations are made is obtained by removing the noise and adding tone modulation to the carrier at some specified deviation. To insure accuracy near threshold, twenty measurements were averaged for each input CNR.

A plot of the measured SNR versus CNR characteristic for the Klapper-Kratt demodulator is shown in Figure 5-8. The term $(\text{CNR})_{\text{AM}}$ is the carrier to noise power ratio with the noise measured in a

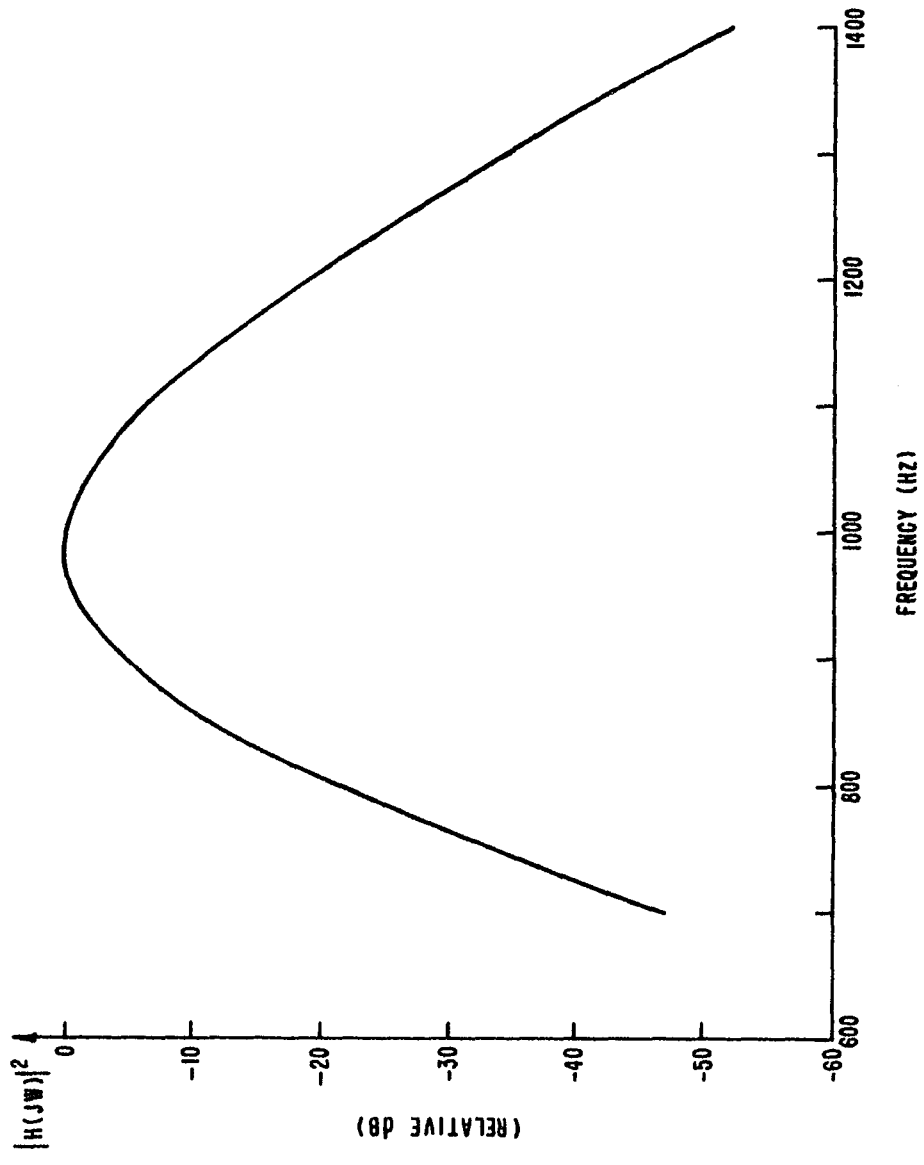


FIGURE 5-6. PREDETECTION FILTER RESPONSE

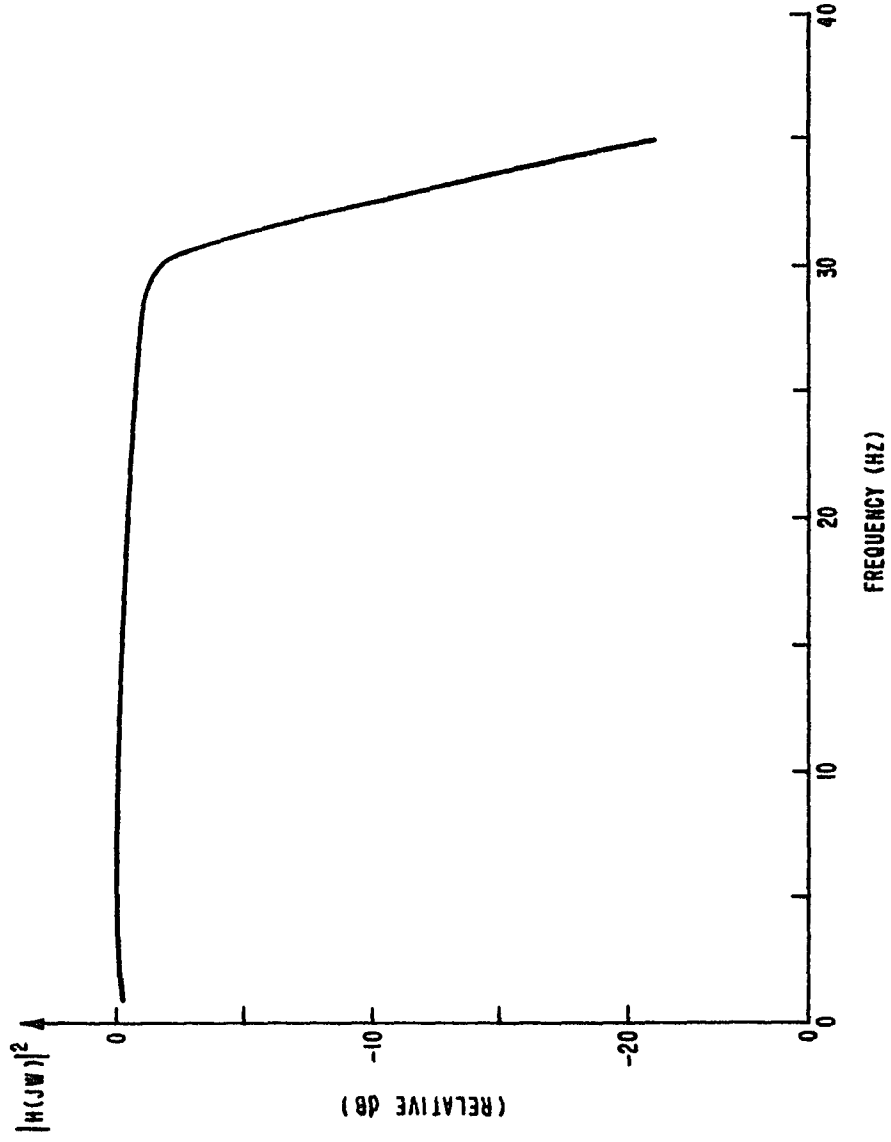


FIGURE 5-7. POSTDETECTION FILTER RESPONSE

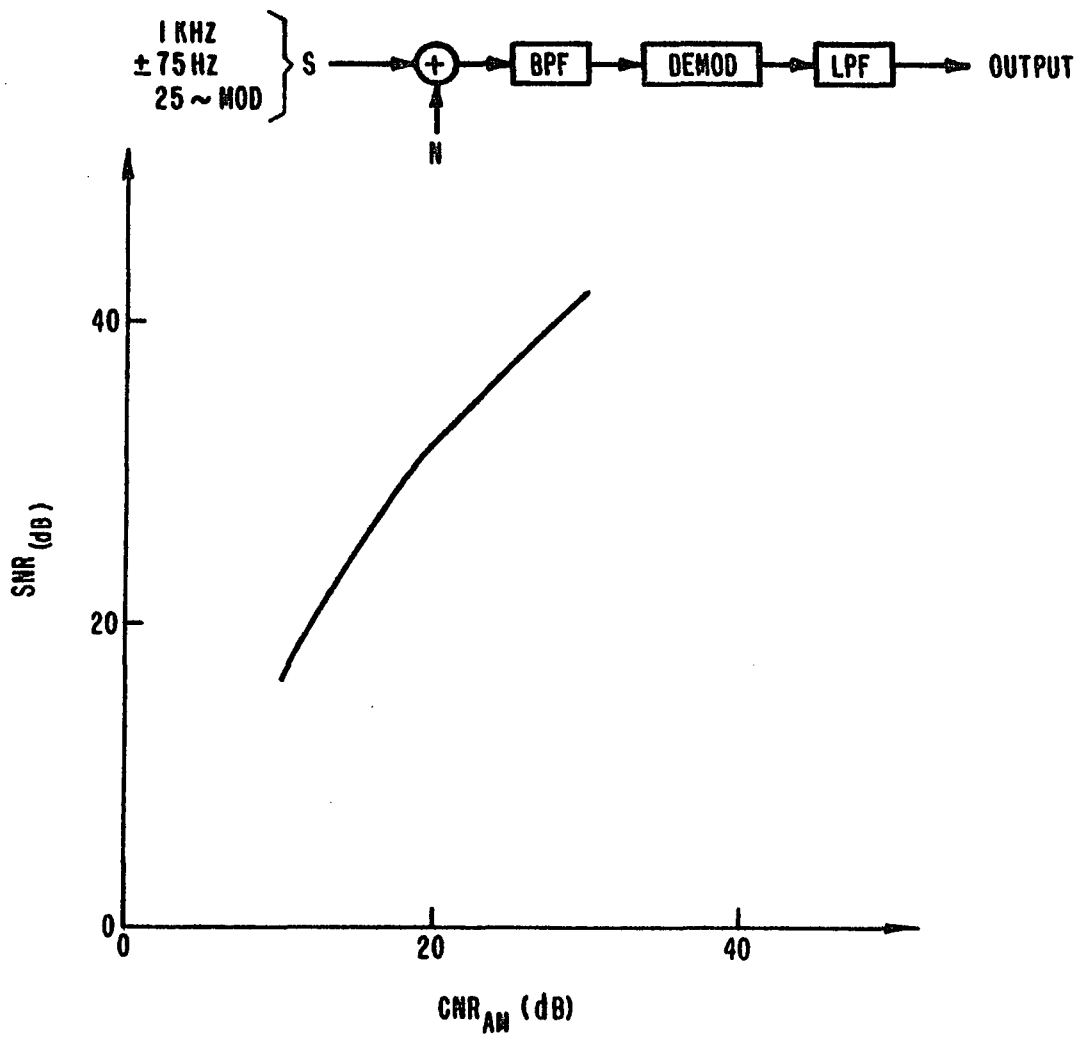


FIGURE 5-8.

EXPERIMENTAL PERFORMANCE OF KLAPPER-KRATT DEMODULATOR WITHOUT LIMITER

filter bandwidth of twice the basebandwidth, or

$$(\text{CNR})_{\text{AM}} = (\text{CNR}) \frac{B}{2\omega_b}$$

Figure 5-9 is an expanded portion of Figure 5-8. Figure 5-9 shows threshold occurring at $(\text{CNR})_{\text{AM}} = 16.9$ dB. The SNR improvement above threshold is 12.3 dB.

Next, a limiter was added between the output of the predetection filter and the input of the demodulator. The active limiter in Figure 5-10 was designed for this task. Actually, the circuit of Figure 5-10 contains two cascaded limiters, followed by a lowpass filter. Two limiters insure hard limiting on small signals. The lowpass filter is used to remove the harmonics generated in the limiting process. The SNR-CNR relationship for the Klapper-Kratt demodulator with limiter is presented in Figures 5-11 and 5-12. Threshold occurs at $(\text{CNR})_{\text{AM}} = 11.2$ dB. The SNR improvement above threshold is 12.6 dB. Hence, the addition of the limiter improves threshold performance by 3.5 dB. The linear improvement region is not significantly changed. The apparent .3 dB improvement could well be the result of errors in the measuring equipment.

5.4 Comparison of the Experimental and Analytical Results for the Klapper-Kratt Demodulator

Table 5-1 summarizes the analytical and experimental results for the Klapper-Kratt detector in terms of $(\text{CNR})_{\text{AM}}$ dB:

Table 5-1

	Analytical		Experimental	
	Improvement	Threshold	Improvement	Threshold
No Limiter	12.2	19.9	12.3	16.9
With Limiter	--	--	12.6	11.2

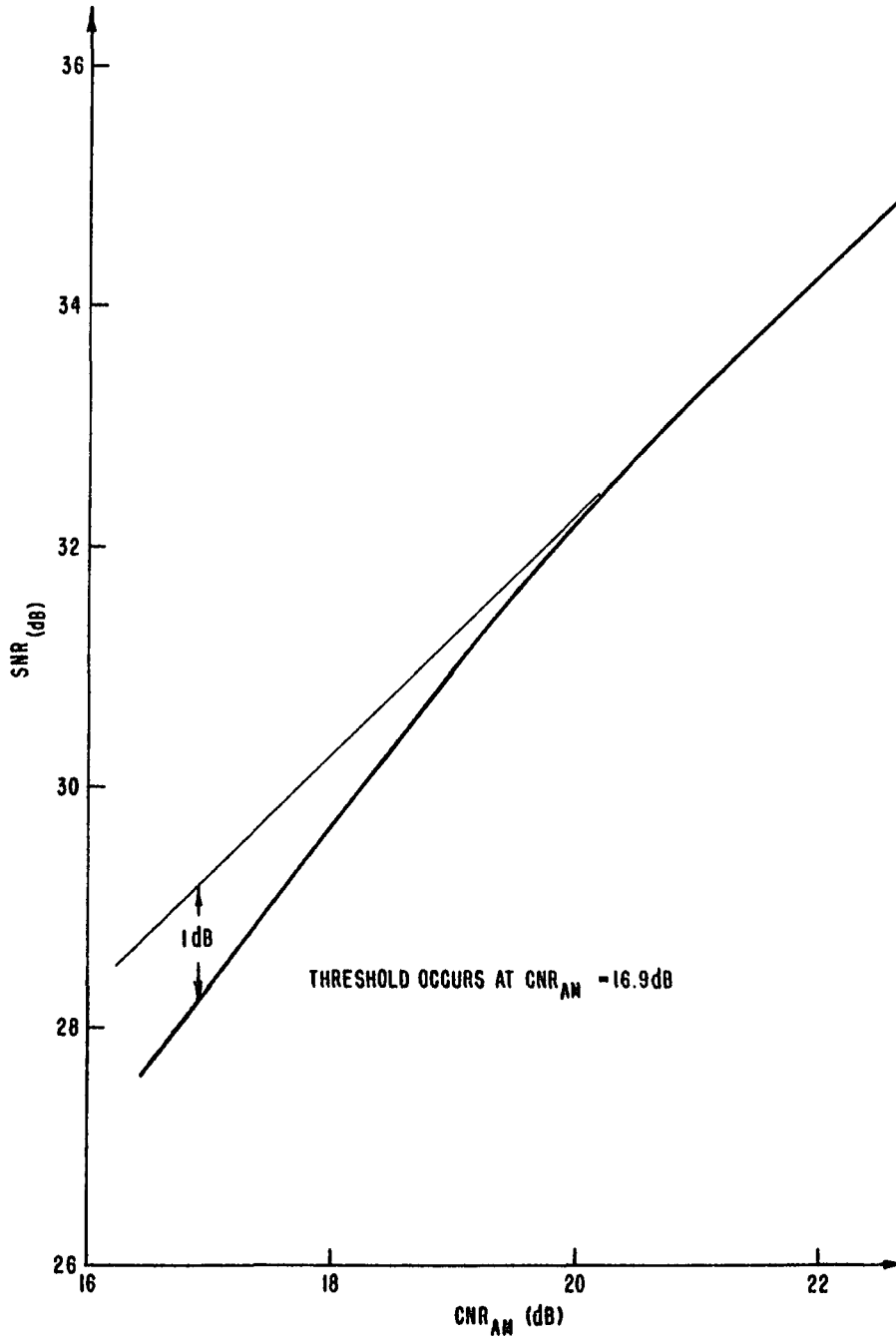


FIGURE 5-9. EXPERIMENTAL PERFORMANCE OF KLAPPER-KRATT DEMODULATOR WITHOUT LIMITER (EXPANDED SCALE)

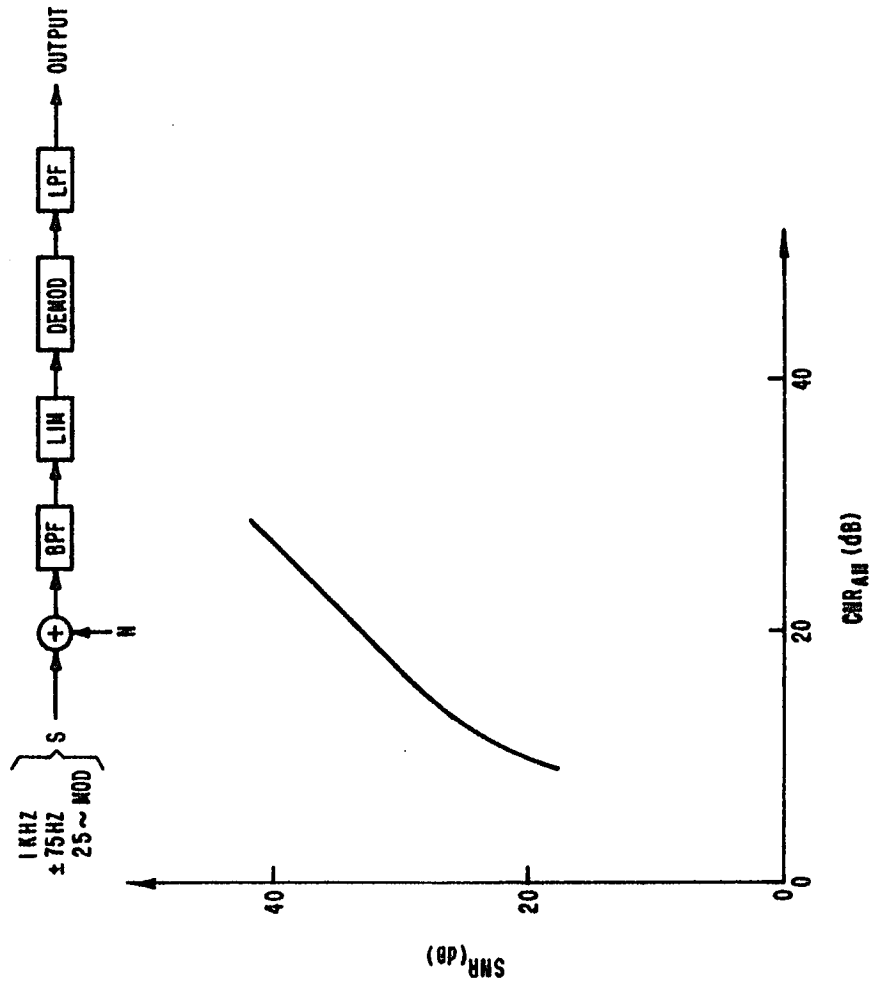


FIGURE 5-11. EXPERIMENTAL PERFORMANCE OF KLAPPER-KRATT DEMODULATOR WITH LIMITER

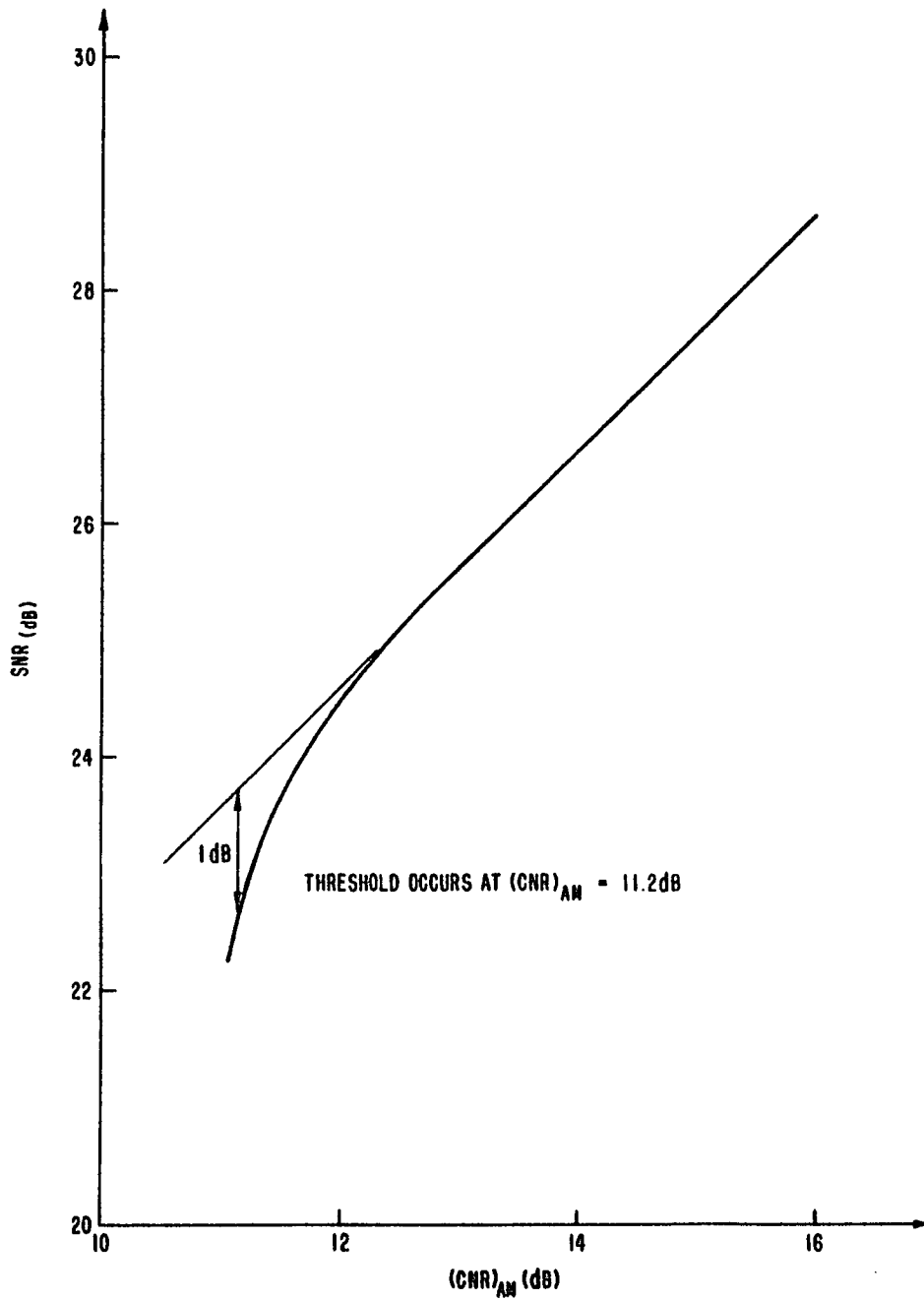


FIGURE 5-12. EXPERIMENTAL PERFORMANCE OF KLAPPER-KRATT DEMODULATOR WITH LIMITER (EXPANDED SCALE)

The analytical performance figures in Table 5-1 were derived using the results of Chapter IV. Equation 4-26 provides the amount of improvement expected in the linear improvement region, and is sufficient to derive the threshold $(\text{CNR})_{\text{AM}}$. For these calculations, the experimental parameters of this chapter were used, i.e., $B = 2\pi(165)$, $\omega_b = 2\pi(32)$, and $\omega_d = 2\pi(75)$. Analysis of the Klapper-Kratt detector with a limiter has not been accomplished.

A graphical comparison of the analytical and experimental results for the Klapper-Kratt demodulator with no limiter are presented in Figure 5-13. Agreement well above threshold and well below threshold is excellent—the two curves coincide. These same curves, while not coincident, are quite similar in the vicinity of threshold. The small (<1.0 dB) differences between the measured and analytical SNRs produce the 3.0 dB difference in the experimental versus analytical threshold CNR. The effect of these small differences in measured SNR is magnified by the very gradual "break" near threshold. Hence, small changes in measured SNR can substantially effect the measured threshold point. Comparison of the Klapper-Kratt demodulator results with those for the limiter discriminator in Figure 5-13 shows the substantially sharper "break" of the limiter discriminator at threshold.

5.5 Comparison of the Klapper-Kratt Demodulator and the Limiter Discriminator

For the purpose of obtaining comparison data, the discriminator in Figure 5-14 was assembled. The signal input to this discriminator was taken from the output of the limiter used in the Klapper-Kratt detector. By switching the post detection filter (described in Section 5.3) between the limiter discriminator and the Klapper-Kratt detector, near simultaneous data were available. The experimental performance curve for the limiter discriminator is presented in Figure 5-13. For comparison, the theoretical limiter discriminator performance predicted by Stumpers (Ref. 2) is included in Figure 5-13. The agreement of the limiter discriminator experimental and theoretical data is similar to that of the Klapper-Kratt data, i.e., excellent

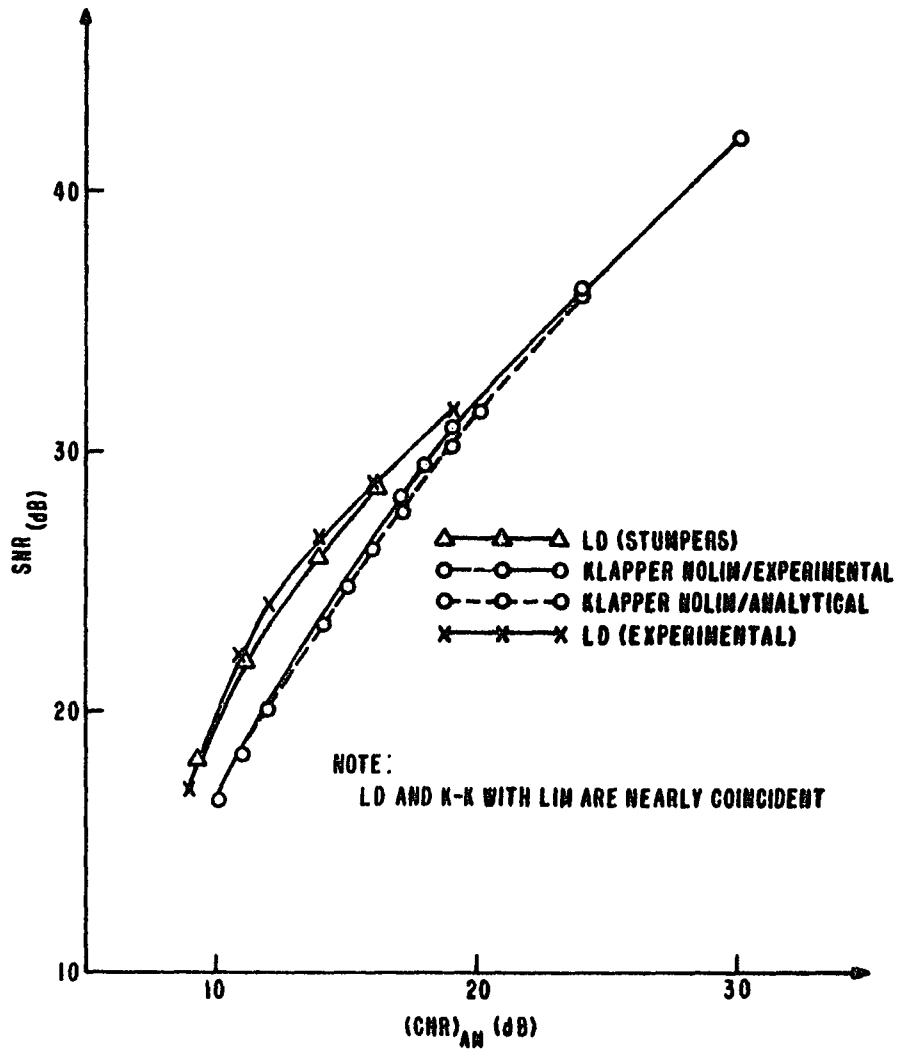


FIGURE 5-13 ANALYTICAL AND EXPERIMENTAL COMPARISON OF THE KLAPPER-KRATT AND LIMITER DISCRIMINATOR DEMODULATORS

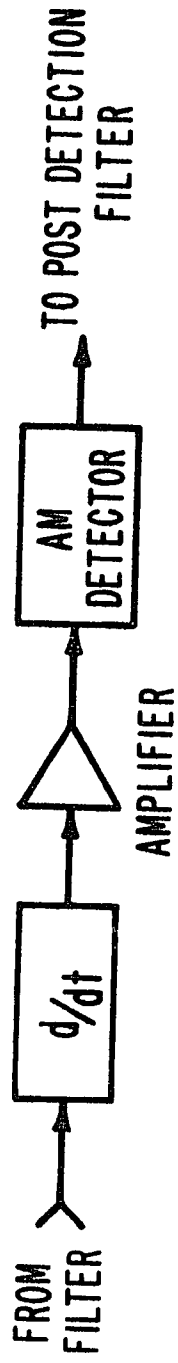


FIGURE 5-14. DISCRIMINATOR BLOCK DIAGRAM

agreement exists above and below threshold. However, near threshold, small differences (<1.0 dB) between the measured and theoretical values for SNR exist. These limiter discriminator results are summarized in Table 5-2. The differences in measured versus theoretical SNRs result in a 1.0 dB difference between the experimental and theoretical limiter discriminator thresholds.

Table 5-2 also compares the conventional limiter discriminator performance with that of the Klapper Kratt demodulator. Performance of the Klapper-Kratt detector (with or without a limiter) in the linear improvement region is the same as that of the limiter discriminator. Threshold performance of the Klapper-Kratt detector with a limiter is slightly better than that of the limiter discriminator.

Table 5-2
Comparison of the Limiter Discriminator
with the Klapper-Kratt Demodulator

CNR _{AM} (dB)	Analytical		Experimental	
	Improvement Threshold		Improvement Threshold	
Limiter Discriminator	12.2	12.5	12.6	11.5
No Klapper Kratt Limiter	12.2	19.9	12.3	16.9
With Limiter	--	--	12.6	11.2

However, threshold performance of the Klapper-Kratt detector with no limiter is worse than that of the conventional limiter discriminator.

An expanded scale comparison of the Klapper-Kratt demodulator with limiter and the limiter discriminator is provided in Figure 5-15.

References - Chapter V

1. J. Klapper & J. T. Frankle, Phase Locked and Frequency Feedback Systems, Chapter 10, p. 329, Academic Press, 1972.
2. L. Stumpers, "Theory of Frequency Modulation Noise", Proc. IRE, Vol. 36, No. 9, p. 1081-1092, September, 1948.

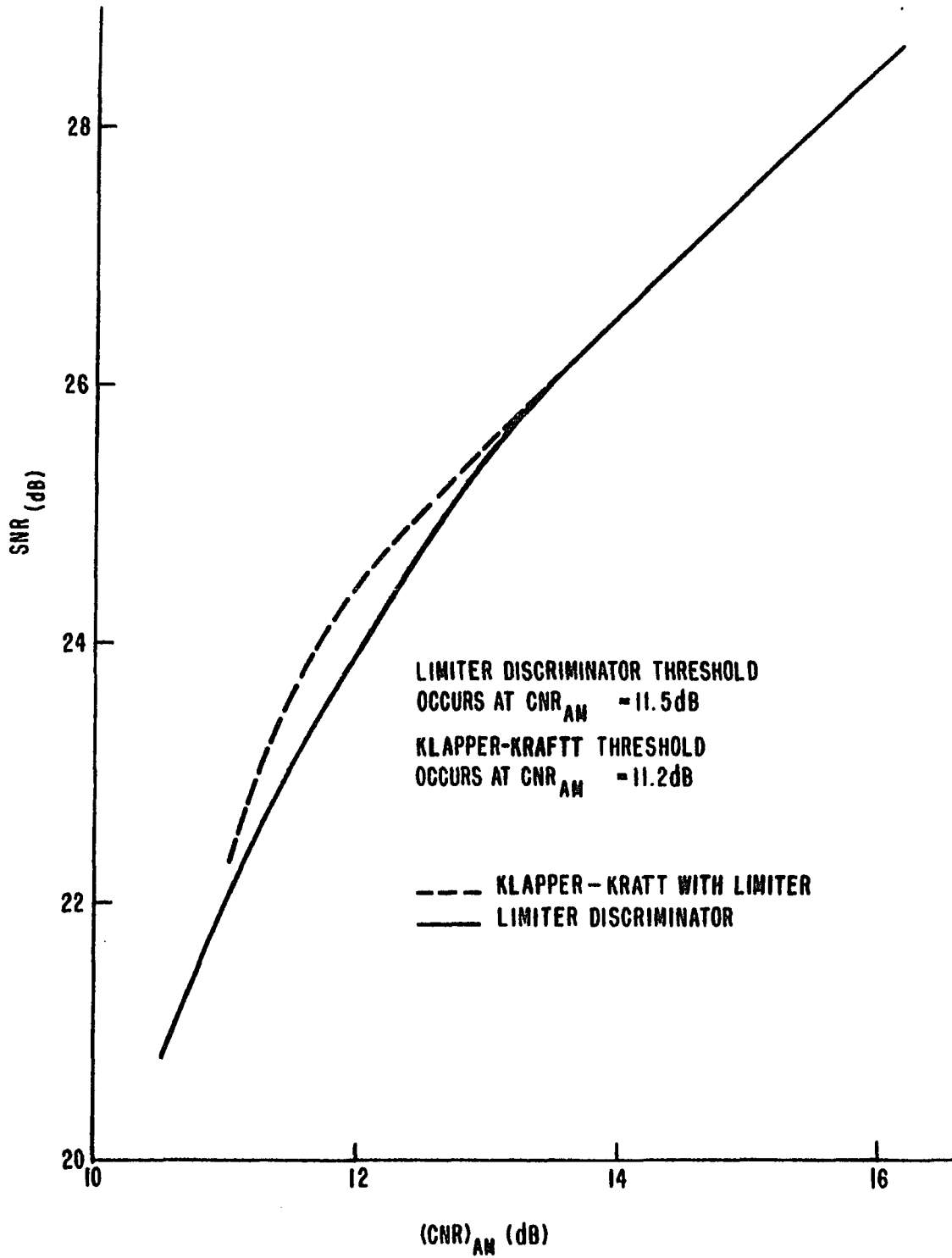


FIGURE 5-15. COMPARISON OF KLAPPER-KRAFT DEMODULATOR
 (WITH LIMITER) AND LIMITER DISCRIMINATOR

CHAPTER VI

CONCLUSIONS6.1 Conclusions

In the above threshold region the Klapper-Kratt detector performs identically to the limiter discriminator. Threshold in the Klapper-Kratt detector occurs at a higher CNR than that of the limiter discriminator (Figure 4-4). For small or moderate modulation indices, this difference in threshold performance is quite small. Small enough, in fact, that, in applications where a limiter is undesirable, the Klapper-Kratt detector would likely be a preferred alternative to the conventional limiter discriminator. The primary application for this demodulator is where absolute delay must be minimized.

The equation describing the performance of the Klapper-Kratt demodulator (Equation 4-26) and repeated below is very simple. This result is valid below threshold, at threshold, and throughout the linear improvement region.

$$\text{SNR} = \frac{\frac{3}{2} (\text{CNR}) B \beta^2 \frac{\omega_m^2}{\omega_b^3}}{1 + \frac{1}{8x(\text{CNR})} + \frac{1}{2(\text{CNR})} - \frac{3x}{4(\text{CNR})} + \frac{x^2}{2(\text{CNR})}} \quad (6-1)$$

where $x = B/\omega_b$.

Compare Equation 6-1 with the equations used by Middleton (Ref. 1) to describe the limiter discriminator performance, Equations 6-2 and 6-3. These equations are exceedingly complex and extremely hard to evaluate for specific system parameters.

$$\text{SNR}^2_{(\text{Low CNR})} = \frac{a_0^4 \langle \phi^2 \rangle}{2 \int_0^{\Delta f} df \int_0^{\infty} [(k_1^2 - k_0 k_2)_2 F_1(1, 1; 2; k_0^2) + O(a_0^2)] \cos \omega_t dt} \quad (6-2)$$

$$\text{SNR}^2 = \frac{b_0 a_0^2 \langle \dot{\phi}^2 \rangle}{\int_0^{\Delta f} \omega^2 df \sum_{\eta=0}^{\infty} A_{\eta} \left[W_{\eta}(\omega_0 + \eta\omega_a + \omega) + W_{\eta}(\omega_0 + \eta\omega_a - \omega) \right]} \quad (6-3)$$

6.2 Future Efforts

It is worthwhile to mention areas where future work should be directed. Below are several areas which seem appropriate at this time:

(1) Klapper-Kratt detector performance in terms of error rates for digital FM detection.

(2) A lowpass to bandpass transformation to make the detector more desirable at higher carrier frequencies.

(3) An extension into general networks, having outputs with opposing polarities but different amplitude versus frequency responses, as candidates for FM detection.

(4) An analysis into the relative merits of the various forms of the Klapper-Kratt detector.

References - Chapter VI

1. D. Middleton, An Introduction to Statistical Communication Theory, Chapter 15, Section 15.5-7, McGraw-Hill, 1960.

APPENDIX I

DETAILED DERIVATION OF

CNR - SNR RELATIONSHIP

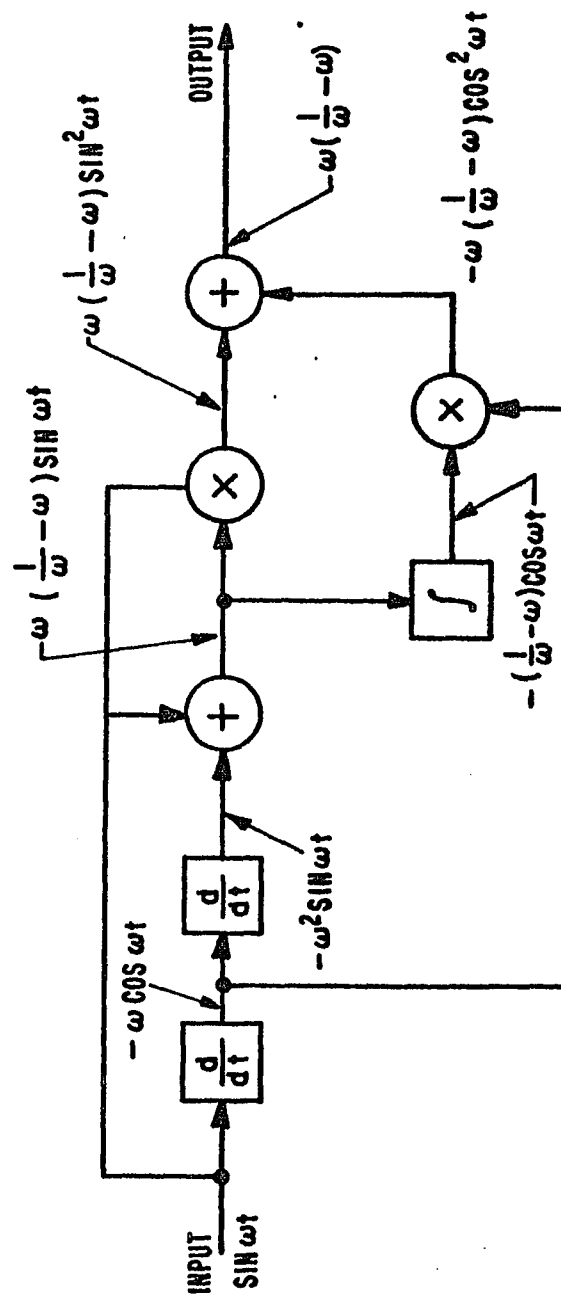
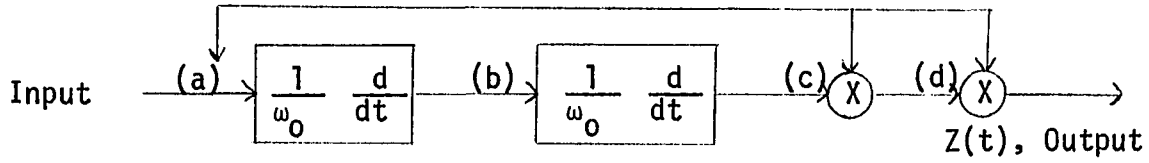


FIGURE I-1. DUAL DIFFERENTIATOR VERSION OF THE NEW FM DETECTOR FAMILY



$$\text{Input} = A \sin \omega_0 t + \overbrace{x(t) \cos \omega_0 t - y(t) \sin \omega_0 t}^{\text{Noise}} \quad (1)$$

At (b) we have

$$\frac{1}{\omega_0} \left[\omega_0 A \cos \omega_0 t + \dot{x}(t) \cos \omega_0 t - \omega_0 x(t) \sin \omega_0 t - \dot{y}(t) \sin \omega_0 t - \omega_0 y(t) \cos \omega_0 t. \right] \quad (2)$$

At (c),

$$\frac{1}{\omega_0^2} \left[-\omega_0^2 A \sin \omega_0 t + \ddot{x}(t) \cos \omega_0 t - \omega_0 \dot{x}(t) \sin \omega_0 t - \omega_0 \dot{x}(t) \sin \omega_0 t - \omega_0^2 x(t) \cos \omega_0 t - \ddot{y}(t) \sin \omega_0 t - \omega_0 \dot{y}(t) \cos \omega_0 t - \omega_0 \dot{y}(t) \cos \omega_0 t + \omega_0^2 y(t) \sin \omega_0 t \right] \quad (3)$$

or

$$\frac{1}{\omega_0^2} \left[-\omega_0^2 A \sin \omega_0 t + \ddot{x}(t) \cos \omega_0 t - 2 \omega_0 \dot{x}(t) \sin \omega_0 t - \omega_0^2 x(t) \cos \omega_0 t - \ddot{y}(t) \sin \omega_0 t - 2 \omega_0 \dot{y}(t) \cos \omega_0 t + \omega_0^2 y(t) \sin \omega_0 t \right] \quad (4)$$

$$\text{At point (d),} \quad (d) = (a) + (c) \quad (5)$$

or, $A \sin \omega_0 t + x \cos \omega_0 t - y \sin \omega_0 t$

$$\begin{aligned} & - A \sin \omega_0 t + \frac{1}{\omega_0^2} \ddot{x}(t) \cos \omega_0 t - \frac{2}{\omega_0} \dot{x}(t) \sin \omega_0 t \\ & - x(t) \cos \omega_0 t - \frac{1}{\omega_0^2} \ddot{y}(t) \sin \omega_0 t - \frac{2}{\omega_0} \dot{y}(t) \cos \omega_0 t \\ & + y(t) \sin \omega_0 t \end{aligned} \quad (6)$$

$$= \frac{\ddot{x}(t)}{\omega_0^2} \cos \omega_0 t - \frac{2}{\omega_0} \dot{x}(t) \sin \omega_0 t - \frac{\ddot{y}(t)}{\omega_0^2} \sin \omega_0 t - \frac{2\dot{y}(t)}{\omega_0} \cos \omega_0 t \quad (7)$$

(The carrier balances out.)

For $z(t)$, multiply (d) by (a)

$$\therefore \left[A \sin \omega_0 t + x(t) \cos \omega_0 t - y(t) \sin \omega_0 t \right] \times \left[\frac{\ddot{x}(t)}{\omega_0^2} \cos \omega_0 t - \frac{2}{\omega_0} \dot{x}(t) \sin \omega_0 t - \frac{\ddot{y}(t)}{\omega_0^2} \sin \omega_0 t - \frac{2\dot{y}(t)}{\omega_0} \cos \omega_0 t \right] \quad (8)$$

$$\begin{aligned} &= \left[A \sin \omega_0 t \right] \left[\frac{\ddot{x}(t)}{\omega_0^2} \cos \omega_0 t \right] - \left[A \sin \omega_0 t \right] \left[\frac{2}{\omega_0} \dot{x}(t) \sin \omega_0 t \right] \\ &- \left[A \sin \omega_0 t \right] \left[\frac{\ddot{y}(t)}{\omega_0^2} \sin \omega_0 t \right] - \left[A \sin \omega_0 t \right] \left[\frac{2\dot{y}(t)}{\omega_0} \cos \omega_0 t \right] \\ &+ \left[x(t) \cos \omega_0 t \right] \left[\frac{\ddot{x}(t)}{\omega_0^2} \cos \omega_0 t \right] - \left[x(t) \cos \omega_0 t \right] \left[\frac{2}{\omega_0} \dot{x}(t) \sin \omega_0 t \right] \\ &- \left[x(t) \cos \omega_0 t \right] \left[\frac{\ddot{y}(t)}{\omega_0^2} \sin \omega_0 t \right] - \left[x(t) \cos \omega_0 t \right] \left[\frac{2\dot{y}(t)}{\omega_0} \cos \omega_0 t \right] \\ &- \left[y(t) \sin \omega_0 t \right] \left[\frac{\ddot{x}(t)}{\omega_0^2} \cos \omega_0 t \right] + \left[y(t) \sin \omega_0 t \right] \left[\frac{2}{\omega_0} \dot{x}(t) \sin \omega_0 t \right] \\ &+ \left[y(t) \sin \omega_0 t \right] \left[\frac{\ddot{y}(t)}{\omega_0^2} \sin \omega_0 t \right] + \left[y(t) \sin \omega_0 t \right] \left[\frac{2\dot{y}(t)}{\omega_0} \cos \omega_0 t \right] \quad (9) \end{aligned}$$

$$\begin{aligned} &= \frac{A\ddot{x}(t)}{\omega_0^2} \sin \omega_0 t \cos \omega_0 t - \frac{2A\dot{x}(t)}{\omega_0} \sin^2 \omega_0 t \\ &- \frac{A\ddot{y}(t)}{\omega_0^2} \sin^2 \omega_0 t - \frac{2A\dot{y}(t)}{\omega_0} \sin \omega_0 t \cos \omega_0 t \\ &+ \frac{x(t)\ddot{x}(t)}{\omega_0^2} \cos^2 \omega_0 t - \frac{2x(t)\dot{x}(t)}{\omega_0} \sin \omega_0 t \cos \omega_0 t \end{aligned}$$

$$\begin{aligned}
& - \frac{x(t)\ddot{y}(t)}{\omega_0^2} \sin \omega_0 t \cos \omega_0 t - \frac{2x(t)\dot{y}(t)}{\omega_0} \cos^2 \omega_0 t \\
& - \frac{y(t)\ddot{x}(t)}{\omega_0^2} \sin \omega_0 t \cos \omega_0 t + \frac{2y(t)\dot{x}(t)}{\omega_0} \sin^2 \omega_0 t \\
& + \frac{y(t)\ddot{y}(t)}{\omega_0^2} \sin^2 \omega_0 t + \frac{2y(t)\dot{y}(t)}{\omega_0} \sin \omega_0 t \cos \omega_0 t
\end{aligned} \tag{10}$$

or

$$\begin{aligned}
& = \left[- \frac{2A\dot{x}(t)}{\omega_0} - \frac{A\ddot{y}(t)}{\omega_0^2} + \frac{2y(t)\dot{x}(t)}{\omega_0} + \frac{y(t)\ddot{y}(t)}{\omega_0^2} \right] \sin^2 \omega_0 t \\
& + \left[\frac{x(t)\ddot{x}(t)}{\omega_0^2} - \frac{2x(t)\dot{y}(t)}{\omega_0} \right] \cos^2 \omega_0 t \\
& + \left[\frac{A\ddot{x}(t)}{\omega_0^2} - \frac{2A\dot{y}(t)}{\omega_0} - \frac{2x(t)\dot{x}(t)}{\omega_0} - \frac{x(t)\ddot{y}(t)}{\omega_0^2} - \frac{y(t)\ddot{x}(t)}{\omega_0^2} + \frac{2y(t)\dot{y}(t)}{\omega_0} \right] \\
& \quad \sin \omega_0 t \cos \omega_0 t
\end{aligned} \tag{11}$$

Using trigonometric identities,

$$\sin^2 x = \frac{1}{2} (1 - \cos 2x) \tag{12}$$

$$\cos^2 x = \frac{1}{2} (1 + \cos 2x) \tag{13}$$

$$\sin x \cos x = \frac{1}{2} \sin 2x \tag{14}$$

We obtain

$$\begin{aligned}
& \left[- \frac{A\dot{x}(t)}{\omega_0} - \frac{A\ddot{y}(t)}{2\omega_0^2} + \frac{y(t)\dot{x}(t)}{\omega_0} + \frac{y(t)\ddot{y}(t)}{2\omega_0^2} \right] \\
& - \left[- \frac{A\dot{x}(t)}{\omega_0} - \frac{A\ddot{y}(t)}{2\omega_0^2} + \frac{y(t)\dot{x}(t)}{\omega_0} + \frac{y(t)\ddot{y}(t)}{2\omega_0^2} \right] \cos 2\omega_0 t
\end{aligned}$$

$$\begin{aligned}
& + \left[\frac{x(t)\ddot{x}(t)}{2\omega_0^2} - \frac{x(t)\dot{y}(t)}{\omega_0} \right] + \left[\frac{x(t)\dot{x}(t)}{2\omega_0^2} - \frac{x(t)\dot{y}(t)}{\omega_0} \right] \cos 2\omega_0 t \\
& + \left[\frac{A\ddot{x}(t)}{2\omega_0^2} - \frac{A\dot{y}(t)}{\omega_0} - \frac{x(t)\dot{x}(t)}{\omega_0} - \frac{x(t)\ddot{y}(t)}{2\omega_0^2} - \frac{y(t)\ddot{x}(t)}{2\omega_0^2} + \frac{y(t)\dot{y}(t)}{\omega_0} \right] \\
& \sin 2\omega_0 t
\end{aligned} \tag{15}$$

Taking baseband terms only,

$$\begin{aligned}
Z(t) = & -\frac{A\dot{x}(t)}{\omega_0} - \frac{A\ddot{y}(t)}{2\omega_0^2} + \frac{y(t)\dot{x}(t)}{\omega_0} + \frac{y(t)\dot{y}(t)}{2\omega_0^2} \\
& + \frac{x(t)\dot{x}(t)}{2\omega_0^2} - \frac{x(t)\dot{y}(t)}{\omega_0}
\end{aligned} \tag{16}$$

To determine the PSD of $Z(t)$ we must first find $R_{ZZ}(\tau)$, hence,

$$R_{ZZ}(\tau) = E \{ z(t)z(t + \tau) \} \tag{17}$$

$$\text{Let } B = \frac{-A}{\omega_0} ; C = \frac{-A}{2\omega_0^2} \tag{18}$$

$$D = \frac{1}{\omega_0} ; F = \frac{1}{2\omega_0^2} \tag{19}$$

Then

$$\begin{aligned}
z(t) = & B \dot{x}(t) + C \ddot{y}(t) + D y(t)\dot{x}(t) + F y(t)\dot{y}(t) \\
& + F x(t)\ddot{x}(t) - D x(t)\dot{y}(t)
\end{aligned} \tag{20}$$

$$\begin{aligned}
R_{ZZ}(\tau) = & E \left\{ \left[B \dot{x}(t) + C \ddot{y}(t) + D y(t)\dot{x}(t) + F y(t)\dot{y}(t) \right. \right. \\
& \left. \left. + F x(t)\ddot{x}(t) - D x(t)\dot{y}(t) \right] \left[B \dot{x}(t + \tau) + C \ddot{y}(t + \tau) \right. \right. \\
& \left. \left. - D \dot{x}(t + \tau)\dot{y}(t + \tau) \right] \right\} .
\end{aligned} \tag{21}$$

$$\begin{aligned}
&= E \left\{ \left[B^2 \dot{x}(t)\dot{x}(t + \tau) + BC \dot{x}(t)\dot{y}(t + \tau) + BD \dot{x}(t)y(t + \tau) \dot{x}(t + \tau) \right. \right. \\
&\quad + BF \dot{x}(t)y(t + \tau)\dot{y}(t + \tau) + BF \dot{x}(t)x(t + \tau)\ddot{x}(t + \tau) \\
&\quad \left. \left. - BD \dot{x}(t)x(t + \tau)\dot{y}(t + \tau) \right] + \left[BC \dot{y}(t)\dot{x}(t + \tau) \right. \right. \\
&\quad + C^2 \dot{y}(t)\dot{y}(t + \tau) + CD \dot{y}(t)y(t + \tau)\dot{x}(t + \tau) \\
&\quad + CF \dot{y}(t)y(t + \tau)\ddot{y}(t + \tau) + CF \dot{y}(t)x(t + \tau)\ddot{x}(t + \tau) \\
&\quad \left. \left. - CD \dot{y}(t)x(t + \tau)\dot{y}(t + \tau) \right] \right\} \\
&+ \left[BD y(t)\dot{x}(t)\dot{x}(t + \tau) + CD y(t)\dot{x}(t)\dot{y}(t + \tau) \right. \\
&\quad + D^2 y(t)\dot{x}(t)y(t + \tau)\dot{x}(t + \tau) + DF y(t)\dot{x}(t)y(t + \tau)\dot{y}(t + \tau) \\
&\quad \left. + DF y(t)\dot{x}(t)x(t + \tau)\ddot{x}(t + \tau) - D^2 y(t)\dot{x}(t)x(t + \tau)\dot{y}(t + \tau) \right] \\
&\quad \left[BF y(t)\dot{y}(t)\dot{x}(t + \tau) + CF y(t)\dot{y}(t)\ddot{y}(t + \tau) \right. \\
&\quad + DF y(t)\dot{y}(t)y(t + \tau)\dot{x}(t + \tau) + F^2 y(t)\dot{y}(t)y(t + \tau)\dot{y}(t + \tau) \\
&\quad \left. + F^2 y(t)\dot{y}(t)x(t + \tau)\ddot{x}(t + \tau) - DF y(t)\dot{y}(t)x(t + \tau)\dot{y}(t + \tau) \right] \\
&\quad + \left[BF x(t)\ddot{x}(t)\dot{x}(t + \tau) + CF x(t)\ddot{x}(t)\dot{y}(t + \tau) \right. \\
&\quad + DF x(t)\dot{x}(t)y(t + \tau)\dot{x}(t + \tau) + F^2 x(t)\dot{x}(t)y(t + \tau)\dot{y}(t + \tau) \\
&\quad \left. + F^2 x(t)\dot{x}(t)x(t + \tau)\ddot{x}(t + \tau) - DF x(t)\dot{x}(t)x(t + \tau)\dot{y}(t + \tau) \right] \\
&\quad + \left[-BD x(t)\dot{y}(t)\dot{x}(t + \tau) - CD x(t)\dot{y}(t)\ddot{y}(t + \tau) \right. \\
&\quad - D^2 x(t)\dot{y}(t)y(t + \tau)\dot{x}(t + \tau) - DF x(t)\dot{y}(t)y(t + \tau)\dot{y}(t + \tau) \\
&\quad \left. - DF x(t)\dot{y}(t)x(t + \tau)\ddot{x}(t + \tau) + D^2 x(t)\dot{y}(t)x(t + \tau)\dot{y}(t + \tau) \right] \Big\} \quad (22) \\
&= E \left[B^2 \dot{x}(t)\dot{x}(t + \tau) \right] + E \left[BF \dot{x}(t)x(t + \tau)\ddot{x}(t + \tau) \right] \\
&+ E \left[C^2 \dot{y}(t)\dot{y}(t + \tau) \right] + E \left[CF \dot{y}(t)y(t + \tau)\ddot{y}(t + \tau) \right]
\end{aligned}$$

$$\begin{aligned}
& + E \left[D^2 y(t) \dot{x}(t) y(t + \tau) \dot{x}(t + \tau) \right] - E \left[D^2 y(t) \dot{x}(t) x(t + \tau) \dot{y}(t + \tau) \right] \\
& + E \left[CF y(t) \ddot{y}(t) \ddot{y}(t + \tau) \right] + E \left[F^2 y(t) \ddot{y}(t) y(t + \tau) \ddot{y}(t + \tau) \right] \\
& + E \left[F^2 y(t) \ddot{y}(t) x(t + \tau) \ddot{x}(t + \tau) \right] \\
& + E \left[BF x(t) \ddot{x}(t) x(t + \tau) \right] + E \left[F^2 x(t) \ddot{x}(t) y(t + \tau) \ddot{y}(t + \tau) \right] \\
& + E \left[F^2 x(t) \ddot{x}(t) x(t + \tau) \ddot{x}(t + \tau) \right] - E \left[D^2 x(t) \dot{y}(t) y(t + \tau) \dot{x}(t + \tau) \right] \\
& + E \left[D^2 x(t) x(t + \tau) \dot{y}(t) \dot{y}(t + \tau) \right]. \tag{23}
\end{aligned}$$

Further simplification yields,

$$\begin{aligned}
R_{zz}(\tau) & = (B^2) R_{\dot{x}\dot{x}}(\tau) + (BF) E \left[\dot{x}(t) x(t + \tau) \ddot{x}(t + \tau) \right] \\
& + C^2 R_{\ddot{y}\ddot{y}}(\tau) + (CF) E \left[\ddot{y}(t) y(t + \tau) \ddot{y}(t + \tau) \right] \\
& + D^2 R_{yy}(\tau) R_{\dot{x}\dot{x}}(\tau) - (D^2) E \left[y(t) \dot{y}(t + \tau) \right] E \left[x(t + \tau) \dot{x}(t) \right] \\
& + (CF) E \left[y(t) \ddot{y}(t) \ddot{y}(t + \tau) \right] + (F^2) E \left[y(t) y(t + \tau) \ddot{y}(t) \ddot{y}(t + \tau) \right] \\
& + (F^2) E \left[y(t) \ddot{y}(t) \right] E \left[x(t + \tau) \ddot{x}(t + \tau) \right] \\
& + (BF) E \left[x(t) \ddot{x}(t) \dot{x}(t + \tau) \right] + (F^2) E \left[x(t) \ddot{x}(t) \right] E \left[y(t + \tau) \ddot{y}(t + \tau) \right] \\
& + (F^2) E \left[x(t) x(t + \tau) \ddot{x}(t) \ddot{x}(t + \tau) \right] \\
& - (D^2) E \left[x(t) \dot{x}(t + \tau) \right] E \left[\dot{y}(t) y(t + \tau) \right] \\
& + D^2 R_{xx}(\tau) R_{\dot{y}\dot{y}}(\tau). \tag{24} \\
& = B^2 R_{\dot{x}\dot{x}}(\tau) + (BF) E \left[\dot{x}(t) x(t + \tau) \ddot{x}(t + \tau) \right] \\
& + C^2 R_{\ddot{y}\ddot{y}}(\tau) + (CF) E \left[\ddot{y}(t) y(t + \tau) \ddot{y}(t + \tau) \right] \\
& + D^2 R_{yy}(\tau) R_{\dot{x}\dot{x}}(\tau) - (D^2) E^2 \left[x(t + \tau) \dot{x}(t) \right] \\
& + (CF) E \left[y(t) \ddot{y}(t) \ddot{y}(t + \tau) \right] + (F^2) E \left[y(t) y(t + \tau) \ddot{y}(t + \tau) \ddot{y}(t) \right]
\end{aligned}$$

$$\begin{aligned}
& + (F^2) E^2 \left[y(t)\ddot{y}(t) \right] + (BF) E \left[x(t)\dot{x}(t)\dot{x}(t + \tau) \right] \\
& + (F^2) E^2 \left[x(t)\ddot{x}(t) \right] + (F^2) E \left[x(t)x(t + \tau)\ddot{x}(t)\ddot{x}(t + \tau) \right] \\
& - (D^2) E^2 \left[x(t)\dot{x}(t + \tau) \right] + D^2 R_{xx}(\tau) R_{\dot{y}\dot{y}}(\tau). \tag{25}
\end{aligned}$$

Further simplifying,

$$\begin{aligned}
R_{ZZ}(\tau) & = B^2 R_{\dot{x}\dot{x}}(\tau) + (BF) E \left[\dot{x}(t)x(t + \tau)\ddot{x}(t + \tau) \right] \\
& + C^2 R_{\dot{y}\dot{y}}(\tau) + (CF) E \left[\dot{y}(t)y(t + \tau)\ddot{y}(t + \tau) \right] \\
& + 2D^2 R_{yy}(\tau) R_{\dot{x}\dot{x}}(\tau) - (2D^2) E^2 \left[x(t)\dot{x}(t + \tau) \right] \\
& + (CF) E \left[y(t)\ddot{y}(t)\ddot{y}(t + \tau) \right] + (2F^2) E \left[x(t)x(t + \tau)\ddot{x}(t)\ddot{x}(t + \tau) \right] \\
& + (2F^2) E^2 \left[x(t)\ddot{x}(t) \right] + (BF) E \left[x(t)\dot{x}(t)\dot{x}(t + \tau) \right]. \tag{26}
\end{aligned}$$

$$\text{Recall that } B = \frac{-A}{\omega_0} \quad C = \frac{-A}{2\omega_0^2} \tag{15}$$

$$D = \frac{1}{\omega_0} \quad F = \frac{1}{2\omega_0^2}$$

then,

$$\begin{aligned}
R_{ZZ}(\tau) & = (A^2/\omega_0^2) R_{\dot{x}\dot{x}}(\tau) - (A/2\omega_0^3) E \left[\dot{x}(t)x(t + \tau)\ddot{x}(t + \tau) \right] \\
& + (A^2/4\omega_0^4) R_{\dot{y}\dot{y}}(\tau) - (A/4\omega_0^4) E \left[\dot{y}(t)y(t + \tau)\ddot{y}(t + \tau) \right] \\
& + (2/\omega_0^2) R_{yy}(\tau) R_{\dot{x}\dot{x}}(\tau) - (2/\omega_0^2) E^2 \left[x(t)\dot{x}(t + \tau) \right] \\
& - (A/4\omega_0^4) E \left[y(t)\ddot{y}(t)\ddot{y}(t + \tau) \right] + (1/2\omega_0^4) E \left[x(t)x(t + \tau) \right] \\
& \left[\dot{x}(t)\dot{x}(t + \tau) \right] + (1/2\omega_0^4) E^2 \left[x(t)\ddot{x}(t) \right] \\
& (-A/2\omega_0^3) E \left[x(t)\dot{x}(t)\dot{x}(t + \tau) \right]. \tag{27}
\end{aligned}$$

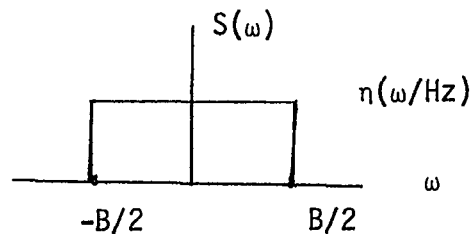
For high ω_0 Equation (27) becomes

$$R_{ZZ}(\tau) = \left(\frac{A^2}{\omega_0}\right) R_{\dot{x}\dot{x}}(\tau) + \left(\frac{2}{\omega_0}\right) R_{yy}(\tau) R_{\dot{x}\dot{x}}(\tau) - \left(\frac{2}{\omega_0}\right) E^2 \left[x(t)\dot{x}(t + \tau) \right]. \tag{28}$$

$$R_{zz}(\tau) \leftrightarrow S_{zz}(\omega) \text{ watts/Hz} \quad (29)$$

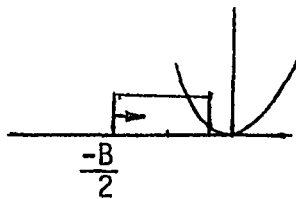
$$S_{zz}(\omega) = \left(\frac{A^2}{\omega_0}\right) \omega^2 S(\omega) + \left(\frac{2}{\omega_0}\right) \Psi \left[R_{yy}(\tau) R_{xx}(\tau) \right] - \left(\frac{2}{\omega_0}\right) \Psi \left\{ \left[\frac{dR_{xx}(\tau)}{d\tau} \right]^2 \right\} \quad (30)$$

where



The 2nd and 3rd terms of Equation (30) may be reduced as follows:

$$\Psi \left[R_{yy}(\tau) R_{xx}(\tau) \right] = \frac{1}{2\pi} \left[\begin{array}{c} S_{yy} = S(\omega) \\ \eta \\ \omega \\ \left[\begin{array}{c} -B/2 \\ +B/2 \end{array} \right] \end{array} * \begin{array}{c} S_{xx} = \omega^2 S(\omega) \\ \omega \\ \left[\begin{array}{c} -B/2 \\ B/2 \end{array} \right] \end{array} \right] \quad (31)$$



$$\frac{1}{2\pi} \left[S_{yy} * S_{xx} \right] = \frac{1}{2\pi} \int_{-B/2}^{t + B/2} \eta \omega^2 d\omega \quad -B \leq t < 0 \quad (32)$$

$$= \frac{\eta}{2\pi} \frac{\omega^3}{3} \Big|_{-B/2}^{t + B/2} = \frac{\eta}{6\pi} \left[\left(t + \frac{B}{2} \right)^3 + \left(\frac{B}{2} \right)^3 \right] \quad -B \leq t < 0 \quad (33)$$

Changing variables back to original,

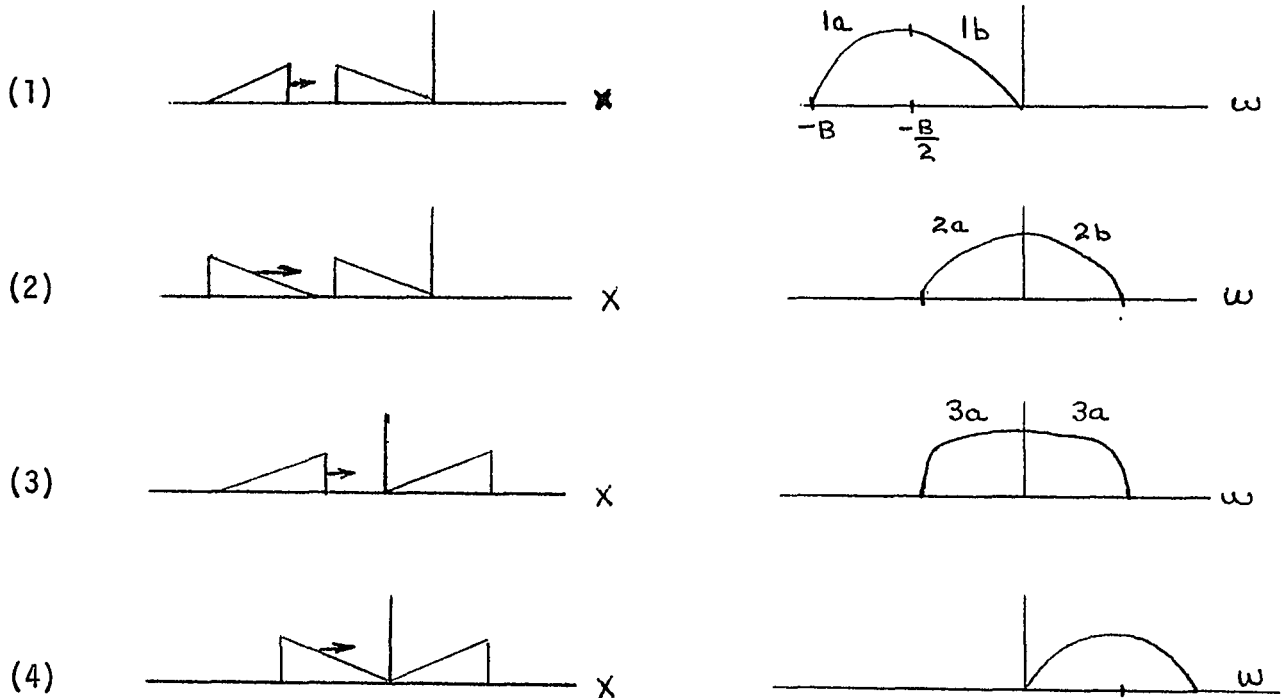
$$= \frac{n^2}{6\pi} \left[\left(\omega + \frac{B}{2}\right)^3 + \left(\frac{B}{2}\right)^3 \right] \quad -B \leq \omega < 0 \quad (34)$$

$$\frac{n^2}{6\pi} \left[\left(-\omega + \frac{B}{2}\right)^3 + \left(\frac{B}{2}\right)^3 \right] \quad 0 \leq \omega \leq B \quad (35)$$

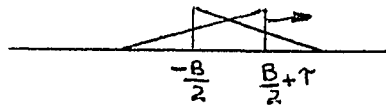
Next

$$(2\pi)^{\frac{1}{2}} \left\{ \left[\frac{d R_{XX}(\tau)}{d\tau} \right]^2 \right\} = \underbrace{\begin{array}{c} j\omega S(\omega) \\ \text{triangular plot from } -\frac{B}{2} \text{ to } \frac{B}{2} \end{array}}_{\times} \underbrace{\begin{array}{c} j\omega S(\omega) \\ \text{triangular plot from } -\frac{B}{2} \text{ to } \frac{B}{2} \end{array}}_{\times} \quad (36)$$

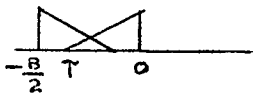
This convolution is symmetric about the $\omega = 0$ axis and can be broken into 4 parts, as follows:

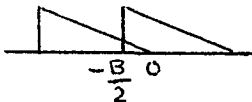


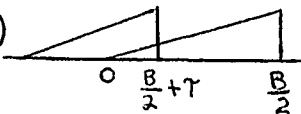
For (1a)



$$\frac{(j)^2}{2\pi} \int_{-\frac{B}{2}}^{\frac{B}{2} + \tau} (-\eta x) \eta (x - \tau) dx \quad -B \leq \tau \leq -\frac{B}{2} \quad (37)$$

(1b)  $\frac{(j)^2}{2\pi} \int_{\tau}^0 (-\eta x) \eta (x - \tau) dx \quad -\frac{B}{2} \leq \tau \leq 0 \quad (38)$

(2a)  $\frac{(j)^2}{2\pi} \int_{-\frac{B}{2}}^{\tau} (-\eta x) [-\eta (x - \tau)] dx \quad -\frac{B}{2} \leq \tau \leq 0 \quad (39)$

(3a)  $\frac{(j)^2}{2\pi} \int_0^{\frac{B}{2} + \tau} (\eta x) \eta (x - \tau) dx \quad -\frac{B}{2} \leq \tau \leq 0 \quad (40)$

Evaluating the (1a) contribution,

$$\frac{(-1)}{2\pi} \int_{-\frac{B}{2}}^{\frac{B}{2} + \tau} (-\eta x) \eta (x - \tau) dx = \frac{+\eta^2}{2\pi} \int_{-\frac{B}{2}}^{\frac{B}{2} + \tau} (x^2 - x\tau) dx \quad (41)$$

$$= \frac{1}{2\pi} \left[+\eta^2 \frac{x^3}{3} - \eta^2 \frac{x^2}{2} \tau \right] \Bigg|_{x = -\frac{B}{2}}^{\frac{B}{2} + \tau} \quad (42)$$

$$= \frac{\eta^2}{2\pi} \left[\frac{+(\frac{B}{2} + \tau)^3}{3} - \frac{(\frac{B}{2} + \tau)^2 \tau}{2} \right] - \frac{\eta^2}{2\pi} \left[\frac{-(\frac{B}{2})^3}{3} - \frac{(\frac{B}{2})^2 \tau}{2} \right] \quad (43)$$

$$= \frac{\eta^2}{2\pi} \left[\frac{+(\frac{B}{2} + \tau)^3}{3} - \frac{(\frac{B}{2} + \tau)^2 \tau}{2} + \frac{(\frac{B}{2})^3}{3} + \frac{(\frac{B}{2})^2 \tau}{2} \right] \quad (44)$$

$$= \frac{\eta^2}{2\pi} \left[\frac{+(\frac{B}{2})^3}{3} + \frac{(\frac{B}{2})^2 \tau}{2} + \frac{(\frac{B}{2}) \tau^2}{2} + \frac{\tau^3}{3} - \frac{(\frac{B}{2})^2 \tau}{2} - \frac{(\frac{B}{2}) \tau^2}{2} - \frac{\tau^3}{2} + \frac{(\frac{B}{2})^3}{3} + \frac{(\frac{B}{2})^2 \tau}{2} \right] \quad (45)$$

$$= \frac{\eta^2}{2\pi} \left[+ \frac{2}{3} \left(\frac{B}{2}\right)^3 + \left(\frac{B}{2}\right)^2 \tau - \frac{\tau^3}{6} \right]. \quad (46)$$

$$= \frac{\eta^2}{2\pi} \left[+ \frac{2}{3} \left(\frac{B}{2}\right)^3 + \left(\frac{B}{2}\right)^2 \omega - \frac{\omega^3}{6} \right] \quad -B \leq \omega \leq -\frac{B}{2} \quad (47)$$

Evaluating the (16) contribution:

$$\frac{(-1)}{2\pi} \int_{\tau}^0 (-\eta x) \eta (x-\tau) dx = \frac{+\eta^2}{2\pi} \int_{\tau}^0 x(x-\tau) dx \quad (48)$$

$$= \frac{1}{2\pi} \left[+ \eta^2 \frac{x^3}{3} - \frac{\eta^2 x^2}{2} \Big|_{x=\tau}^0 \right] \quad (49)$$

$$= \frac{\eta^2}{2\pi} \left[+ \frac{x^3}{3} - \frac{x^2}{2} \right] \Big|_{x=\tau}^0 = \frac{\eta^2}{2\pi} \left[(0) - \left(+ \frac{\tau^3}{3} - \frac{\tau^2}{2} \right) \right] \quad (50)$$

$$= \frac{1}{2\pi} \left[+ \eta^2 \frac{\tau^3}{6} \right] \quad (51)$$

Evaluating the (2a) term,

$$\frac{(-1)}{2\pi} \int_{-\frac{B}{2}}^{\tau} (-\eta x) - \eta (x-\tau) dx = \frac{-\eta^2}{2\pi} \int_{-\frac{B}{2}}^{\tau} x(x-\tau) dx \quad (52)$$

$$= \frac{-\eta^2}{2\pi} \left[\frac{x^3}{3} - \frac{x^2}{2} \tau \right] \Big|_{-\frac{B}{2}}^{\tau} = \frac{-\eta^2}{2\pi} \left\{ \left[\frac{\tau^3}{3} - \frac{\tau^3}{2} \right] - \left[\frac{-(\frac{B}{2})^3}{3} - \frac{(\frac{B}{2})^2 \tau}{2} \right] \right\} \quad (53)$$

$$= \frac{-\eta^2}{2\pi} \left[-\frac{\tau^3}{6} + \frac{(\frac{B}{2})^3}{3} + \frac{(\frac{B}{2})^2 \tau}{2} \right]. \quad (54)$$

Evaluating the (3a) term,

$$\frac{j^2}{2\pi} \int_0^{\frac{B}{2} + \tau} (\eta x) \eta (x-\tau) dx + \frac{\eta^2}{2\pi} \int_0^{\frac{B}{2} + \tau} x(x-\tau) dx \quad (55)$$

$$= \frac{1}{2\pi} \left\{ -\eta^2 \left[\frac{x^3}{3} - \frac{x^2}{2} \tau \right] \Big|_{x=0}^{\frac{B}{2} + \tau} \right\} \quad (56)$$

$$= \frac{1}{2\pi} \left\{ -\eta^2 \frac{(\frac{B}{2} + \tau)^3}{3} + \eta^2 \frac{(\frac{B}{2} + \tau)^2}{2} \tau \right\} \quad (57)$$

$$= -\frac{\eta^2}{2\pi} \left[\frac{(\frac{B}{2})^3}{3} + (\frac{B}{2})^2 \tau + (\frac{B}{2}) \tau^2 + \frac{\tau^3}{3} - \frac{(\frac{B}{2})^2 \tau}{2} - (\frac{B}{2}) \tau^2 - \frac{\tau^3}{2} \right] \quad (58)$$

$$= \frac{-\eta^2}{2\pi} \left[+ \frac{(\frac{B}{2})^3}{3} + \frac{(\frac{B}{2})^2 \tau}{2} - \frac{\tau^3}{6} \right]. \quad (59)$$

$$\therefore \text{for } -B \leq \omega \leq -\frac{B}{2} \longrightarrow \frac{n^2}{2\pi} \left[+\frac{2}{3} \left(\frac{B}{2}\right)^3 + \left(\frac{B}{2}\right)^2 \omega - \frac{\omega^3}{6} \right] \quad (60)$$

$$\frac{n^2}{2\pi} \left[+\frac{\omega^3}{6} + \frac{\omega^3}{6} - \frac{\left(\frac{B}{2}\right)^3}{3} - \frac{\left(\frac{B}{2}\right)^2 \omega}{2} - \frac{\left(\frac{B}{2}\right)^3}{3} - \frac{\left(\frac{B}{2}\right)^2 \omega}{2} + \frac{\omega^3}{6} \right] \quad (61)$$

$$= \frac{n^2}{2\pi} \left[\frac{\omega^3}{2} - \frac{2\left(\frac{B}{2}\right)^3}{3} - \left(\frac{B}{2}\right)^2 \omega \right] \quad (62)$$

$$\oint_{\pi} \left\{ \left[\frac{d R_{XX}(\tau)}{d\tau} \right]^2 \right\} = \left\{ \begin{array}{l} \frac{n^2}{2\pi} \left[\frac{\omega^3}{2} - \frac{2\left(\frac{B}{2}\right)^3}{3} - \left(\frac{B}{2}\right)^2 \omega \right], \quad -\frac{B}{2} \leq \omega \leq 0 \\ \frac{n^2}{2\pi} \left[\frac{2\left(\frac{B}{2}\right)^3}{3} + \left(\frac{B}{2}\right)^2 \omega - \frac{\omega^3}{6} \right], \quad -B \leq \omega \leq -\frac{B}{2} \end{array} \right\} \quad (63)$$

Now, Equation (30) may be written as

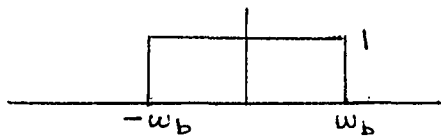
$$S_{ZZ}(\omega) = \frac{A^2}{\omega_0^2} \omega^2 S(\omega) + \frac{n^2}{3\pi\omega_0^2} \left[\begin{array}{l} \left(\omega + \frac{B}{2}\right)^3 + \left(\frac{B}{2}\right)^3 \quad -B \leq \omega \leq 0 \\ \left(-\omega + \frac{B}{2}\right)^3 + \left(\frac{B}{2}\right)^3 \quad 0 \leq \omega \leq B \end{array} \right]$$

$$- \frac{n^2}{\pi\omega_0^2} \left[\begin{array}{l} \frac{2}{3} \left(\frac{B}{2}\right)^3 + \left(\frac{B}{2}\right)^2 \omega - \frac{\omega^3}{6}, \quad -B \leq \omega \leq -\frac{B}{2} \\ \frac{\omega^3}{2} - \frac{2\left(\frac{B}{2}\right)^3}{3} - \left(\frac{B}{2}\right)^2 \omega, \quad -\frac{B}{2} \leq \omega \leq 0 \end{array} \right] \quad (64)$$

Symmetric in positive half-plane

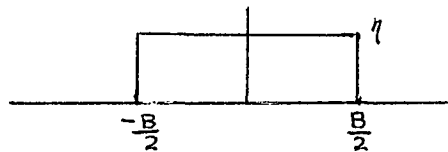
The total noise power at the detector output is equal to the integral of $1/2\pi S_{ZZ}(\omega)$ over the post detection filter bandwidth, or,

$$\frac{1}{2\pi} \int_{-\omega_b}^{\omega_b} S_{ZZ}(\omega) d\omega, \quad \omega_b \leq \frac{B}{2} \quad (65)$$



Post Detection Filter Response

$$\begin{aligned}
 &= \frac{1}{2\pi} \left[\frac{A^2}{\omega_0^2} \int_{-\omega_b}^{\omega_b} \omega^2 S(\omega) d\omega + \frac{2\eta^2}{3\pi\omega_0^2} \int_{-\omega_b}^0 \left[\left(\omega + \frac{B}{2}\right)^3 + \left(\frac{B}{2}\right)^3 \right] d\omega \right. \\
 &\quad \left. - \frac{2\eta^2}{\pi\omega_0^2} \int_{-\omega_b}^0 \left[\frac{\omega^3}{2} - \frac{2\left(\frac{B}{2}\right)^3}{3} - \left(\frac{B}{2}\right)^2 \omega \right] d\omega \right] \quad (66)
 \end{aligned}$$

Recall $S(\omega) \rightarrow$ 

where B is the IF bandwidth

$$\begin{aligned}
 \frac{1}{2\pi} \int S_{zz}(\omega) d\omega &= \frac{1}{2\pi} \left\{ \frac{A^2\eta}{\omega_0^2} \int_{-\omega_b}^{\omega_b} \omega^2 d\omega \right. \\
 &+ \frac{2\eta^2}{3\pi\omega_0^2} \int_{-\omega_b}^0 \left(\omega + \frac{B}{2}\right)^3 d\omega + \frac{2\eta^2}{3\pi\omega_0^2} \int_{-\omega_b}^0 \left(\frac{B}{2}\right)^3 d\omega \\
 &\left. - \frac{2\eta^2}{\pi\omega_0^2} \int_{-\omega_b}^0 \left[\frac{\omega^3}{2} - \frac{B^3}{12} - \frac{B^2}{4} \omega \right] d\omega \right\} \quad (67) \\
 &= \frac{1}{2\pi} \left[\frac{2A^2\eta}{\omega_0^2} \frac{\omega^3}{3} \Big|_0^{\omega_b} + \frac{2\eta^2}{3\pi\omega_0^2} \int_{-\omega_b}^0 \left(\omega^3 + \frac{3}{2}\omega^2 B + \frac{3}{4}\omega B^2 + \frac{B^3}{8} \right) d\omega \right.
 \end{aligned}$$

$$+ \frac{2\eta^2}{3\pi\omega_0^2} \left(\frac{B}{2}\right)^3 \omega \left[\begin{array}{l} 0 \\ -\omega_b \end{array} + \frac{\eta^2 \omega_b^4}{4\pi\omega_0^2} + \frac{\eta^2 B^3 \omega_b}{6\pi\omega_0^2} - \frac{\eta^2 B^2 \omega_0^2}{4\pi\omega_0^2} \right] \quad (68)$$

$$= \frac{1}{2\pi} \left[\begin{array}{l} \frac{2}{3} \frac{A^2 \eta \omega_b^2}{\omega_0^2} - \frac{\eta^2 \omega_b^4}{6\pi\omega_0^2} + \frac{\eta^2 \omega_b^3 B}{3\pi\omega_0^2} \\ - \frac{\eta^2 \omega_b^2 B^2}{4\pi\omega_0^2} + \frac{\eta^2 B^3 \omega_b}{12\pi\omega_0^2} + \frac{\eta^2 B^3 \omega_b}{12\pi\omega_0^2} \\ + \frac{\eta^2 \omega_b^4}{4\pi\omega_0^2} + \frac{\eta^2 B^3 \omega_b}{6\pi\omega_0^2} - \frac{\eta^2 B^2 \omega_b^2}{4\pi\omega_0^2} \end{array} \right] \quad (69)$$

$$\text{Noise Power} = \frac{A^2 \eta \omega_b^3}{3\pi\omega_0^2} + \frac{\eta^2 \omega_b^4}{24\pi^2 \omega_0^2} + \frac{\eta^2 \omega_b^3 B}{6\pi^2 \omega_0^2} \\ - \frac{\eta^2 \omega_b^2 B^2}{4\pi^2 \omega_0^2} + \frac{A^2 B^3 \omega_b}{6\pi^2 \omega_0^2} \quad (70)$$

Derivation of Signal Output Power from Demodulator for General Case

$$\text{Assume Input} = A \cos (\omega_0 t + \beta \sin \omega_m t) \quad (71)$$

where A = carrier amplitude

β = mod. index

ω_m = frequency of cosinusoidal modulating signal

At the output of the first differentiator, (point b),

$$(b) = \frac{-A}{\omega_0} (\omega_0 + \beta \omega_m \cos \omega_m t) \sin (\omega_0 t + \beta \sin \omega_m t) \quad (72)$$

$$= -A \sin (\omega_0 t + \beta \sin \omega_m t)$$

$$- \frac{A\beta\omega_m}{\omega_0} \cos \omega_m t \sin (\omega_0 t + \beta \sin \omega_m t) \quad (73)$$

At the output of the second differentiator, (point c),

$$(c) = \frac{-A}{\omega_0} (\omega_0 + \beta \omega_m \cos \omega_m t) \cos (\omega_0 t + \beta \sin \omega_m t)$$

$$- \frac{A\beta\omega_m}{\omega_0} \cos \omega_m t (\omega_0 + \beta \omega_m \cos \omega_m t) \cos (\omega_0 t + \beta \sin \omega_m t)$$

$$+ \frac{A\beta\omega_m^2}{\omega_0} \sin \omega_m t \sin (\omega_0 t + \beta \sin \omega_m t) \quad (74)$$

Summing, (point d),

$$(d) = A \cos (\omega_0 t + \beta \sin \omega_m t)$$

$$- \frac{A}{\omega_0} (\omega_0 + \beta \omega_m \cos \omega_m t) \cos (\omega_0 t + \beta \sin \omega_m t)$$

$$- \frac{A\beta\omega_m}{\omega_0} \cos \omega_m t (\omega_0 + \beta \omega_m \cos \omega_m t) \cos (\omega_0 t + \beta \sin \omega_m t)$$

$$+ \frac{A\beta\omega_m^2}{2\omega_0} \sin \omega_m t \sin (\omega_0 t + \beta \sin \omega_m t). \quad (75)$$

Multiplying yields the demodulator output

$$\begin{aligned} & A^2 \cos^2 (\omega_0 t + \beta \sin \omega_m t) \\ & - \frac{A^2}{\omega_0} (\omega_0 + \beta \omega_m \cos \omega_m t) \cos^2 (\omega_0 t + \beta \sin \omega_m t) \\ & - \frac{A^2 \beta \omega_m}{2\omega_0} (\omega_0 + \beta \omega_m \cos \omega_m t) \cos \omega_m t \cos^2 (\omega_0 t + \beta \sin \omega_m t) \\ & + \frac{A^2 \beta \omega_m^2}{2\omega_0} \sin \omega_m t \cos (\omega_0 t + \beta \sin \omega_m t) \sin (\omega_0 t + \beta \sin \omega_m t) \end{aligned} \quad (76)$$

Recall

$$\cos^2 x = 1/2 (1 + \cos 2x) \quad (77)$$

$$\sin x \cos x = 1/2 \sin 2x \quad (78)$$

then Equation (6) becomes

$$\begin{aligned} & = \frac{A^2}{2} \left[1 + \cos (2 \omega_0 t + 2 \beta \sin \omega_m t) \right] \\ & - \frac{A^2}{2\omega_0} (\omega_0 + \beta \omega_m \cos \omega_m t) \left[1 + \cos (2 \omega_0 t + 2 \beta \sin \omega_m t) \right] \\ & - \frac{A^2 \beta \omega_m}{2\omega_0} (\omega_0 + \beta \omega_m \cos \omega_m t) \cos \omega_m t \left[1 + \cos (2 \omega_0 t + 2 \beta \sin \omega_m t) \right] \\ & + \frac{A^2 \beta \omega_m^2}{2\omega_0} \sin \omega_m t \sin (2 \omega_0 t + 2 \beta \sin \omega_m t) \end{aligned} \quad (79)$$

Eliminating unwanted harmonics results in

$$= \frac{A^2}{2} - \frac{A^2}{2\omega_0} (\omega_0 + \beta \omega_m \cos \omega_m t)$$

$$- \frac{A^2 \beta \omega_m}{2\omega_0^2} (\omega_0 + \beta \omega_m \cos \omega_m t) \cos \omega_m t \quad (80)$$

$$= - \frac{A^2 \beta \omega_m}{2\omega_0} \cos \omega_m t - \frac{A^2 \beta^2 \omega_m^2}{2\omega_0^2} \cos^2 \omega_m t \quad (81)$$

$$= - \frac{A^2 \beta \omega_m}{\omega_0} \cos \omega_m t - \frac{A^2 \beta^2 \omega_m^2}{4\omega_0^2} (1 + \cos 2 \omega_m t) \quad (82)$$

and eliminating the $\cos 2 \omega_m t$ term and d.c. term,

$$\text{Desired Demod. Output Voltage} = - A^2 \frac{\beta \omega_m}{\omega_0} \cos \omega_m t \quad (83)$$

and,

$$\text{Power} = \frac{A^4 \beta^2 \omega_m^2}{2\omega_0^2} \quad (84)$$

General Expression for SNR as Function of CNR

$$\text{SNR} = \frac{\text{Signal Output}}{\text{Noise Output}} \quad (85)$$

$$= \frac{A^4 \beta^2 \omega_m^2}{2\omega_o^2} \left\{ \frac{A^2 \eta \omega_b^3}{3\pi \omega_o^2} + \frac{\eta^2 \omega_b^4}{24\pi^2 \omega_o^2} + \frac{\eta^2 \omega_b^3 B}{6\pi^2 \omega_o^2} - \frac{\eta^2 \omega_b^2 B^2}{4\pi^2 \omega_o^2} + \frac{\eta^2 B^3 \omega_b}{6\pi^2 \omega_o^2} \right\} \quad (86)$$

Divide numerator and denominator of (86) by

$$\frac{A^2 \eta \omega_b^2}{3\pi \omega_o^2},$$

$$\text{SNR} = \frac{\frac{A^4 \beta^2 \omega_m^2}{2\omega_o^2} \frac{3\pi \omega_o^2}{A^2 \eta \omega_b^3}}{1 + \frac{\eta \omega_b}{8\pi A^2} + \frac{\eta B}{2\pi A^2} - \frac{3\eta B^2}{4\pi A^2 \omega_b} + \frac{\eta B^3}{2\pi A^2 \omega_b^2}} \quad (87)$$

$$\text{CNR} = \frac{A^2/2}{\eta B/2\pi} = \frac{\pi A^2}{\eta B} \quad (88)$$

Writing (87) in terms of $\frac{\pi A^2}{\eta B} = \text{CNR}$,

$$\text{SNR} = \frac{\frac{3}{2} \left[\frac{\pi A^2}{\eta B} \right] \frac{\beta^2 \omega_m^2 B}{\omega_b^3}}{1 + \left[\frac{\eta B}{\pi A^2} \right] \frac{\omega_b \pi}{8\pi B} + \left[\frac{\eta B}{\pi A^2} \right] \frac{1}{2} - \frac{3}{2} \left[\frac{\eta B}{\pi A^2} \right] \frac{B}{2\omega_b} + \left[\frac{\eta B}{\pi A^2} \right] \frac{B^2}{2\omega_b^2}} \quad (89)$$

$$= \frac{\frac{3}{2} (\text{CNR}) B \beta^2 \frac{\omega_m^2}{\omega_b^3}}{1 + \frac{1}{8x(\text{CNR})} + \frac{1}{2(\text{CNR})} - \frac{3}{4} \frac{x}{(\text{CNR})} + \frac{x^2}{2(\text{CNR})}} \quad (90)$$

$$\text{where } x = \frac{B}{\omega_b}$$

Assume $H_i - \text{CNR}$,

$$\text{SNR}_{H_i - \text{CNR}} = \frac{3}{2} (\text{CNR}) B \beta^2 \frac{\omega_m^2}{\omega_b^3} \quad (91)$$

For optimum performance set $\omega_m = \omega_b$,
then

$$\text{SNR} = \frac{3}{2} (\text{CNR}) \frac{B \beta^2}{\omega_b} \quad (92)$$

$$\text{Recall that } \text{CNR} = (\text{CNR}_{AM}) \left(\frac{2\omega_b}{B}\right) \quad (93)$$

hence,

$$\text{SNR}_{H_i - \text{CNR}} = \frac{3}{2} (\text{CNR}_{AM}) \frac{2\omega_b}{B} \frac{B \beta^2}{\omega_b} \quad (94)$$

$$= 3 \beta^2 \text{CNR}_{AM} \quad (95)$$

which is identical to the expression for an L-D well above threshold.

APPENDIX II

REAL AND IDEAL DIFFERENTIATORS

The ideal differentiator would possess the perfect 90° phase shift of Figure II-1. However, real differentiators, due to their inherent frequency limitations, produce a phase shift different than 90° . The response of a real differentiator is shown in Figure II-2. In his project Kratt describes a simple method for correcting this phase error, as illustrated by Figures II-3 and II-4. A sample of the input signal, V_i , is added to the differentiator output to produce the desired 90° phase shift. This technique works very well. Laboratory measurements indicated that the phase errors of the differentiators of Chapter V with phase correction circuitry are less than $.75^\circ$ over the entire 20% bandwidth.

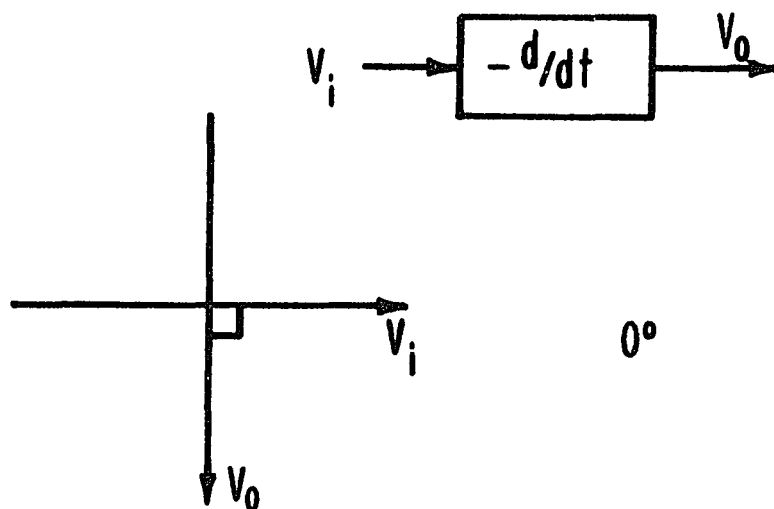


FIGURE II-1. IDEAL DIFFERENTIATOR

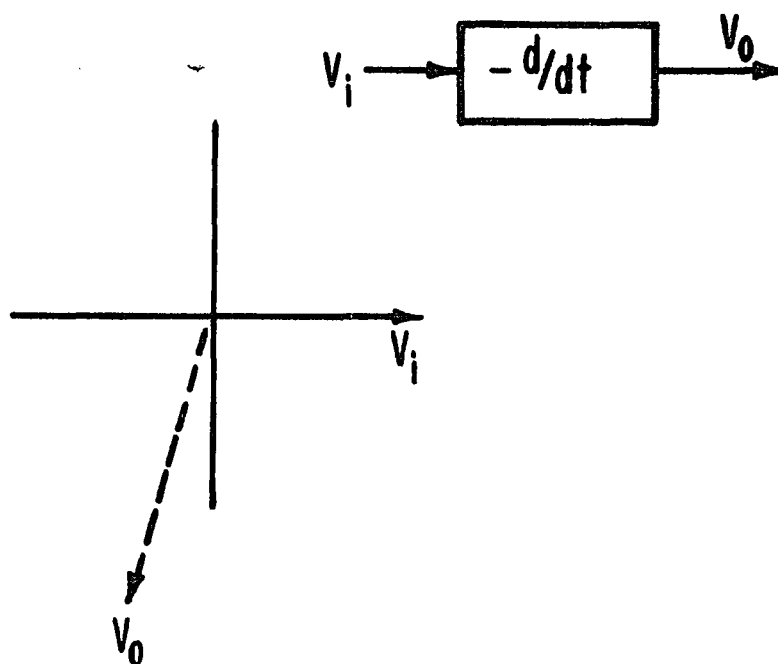


FIGURE II-2. REAL DIFFERENTIATOR

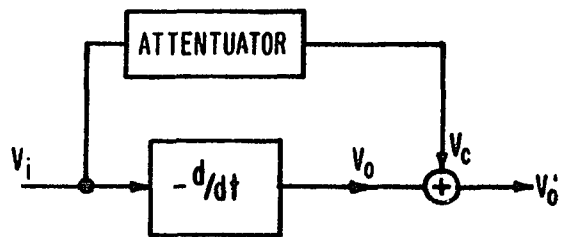


FIGURE II-3. BLOCK DIAGRAM OF REAL DIFFERENTIATOR WITH PHASE CORRECTION

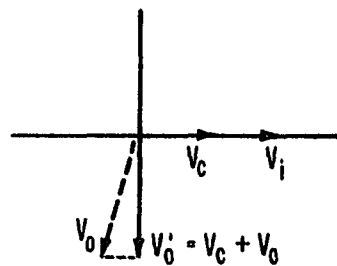


FIGURE II-4. PHASOR DIAGRAM FOR REAL DIFFERENTIATOR WITH PHASE CORRECTION

BIBLIOGRAPHY

BOOKS

1. Klapper & Frankle, Phased Locked and Frequency Feedback Systems, Academic Press, 1972.
2. Clark & Hess, Communications Circuits: Analysis and Design, Addison-Wesley, 1971.
3. Blachman, N., Noise and Its Effect on Communication, McGraw-Hill, 1966.
4. Papoulis, A., Probability, Random Variables, and Stochastic Processes, McGraw-Hill, 1965.
5. Middleton, D., Statistical Communication Theory, McGraw-Hill, 1960.
6. Schwartz, M., Information Transmission, Modulation, and Noise, McGraw-Hill, 1959.

PAPERS

1. Kersus, G., "Analysis of the Klapper-Kratt Detector," NJIT Master's Thesis, Newark, NJ, 1976.
2. Klapper & Kratt, "A New Family of Low Delay FM Detectors," NTC, 1975.
3. Park, J., "An FM Detector for Low S/N," IEEE Transactions on Communications Technology, Vol. COM-18, No. 2, April, 1970.
4. Patronis, D., "A Frequency Modulation Detector Using Operational Amplifiers," Audio Magazine, February, 1970.
5. Bedrosian & Rice, "Distortion and Crosstalk of Linearly Filtered, Angle Modulated Signals," Proc. IEEE, Vol. 56, No. 1, January, 1968.
6. Rice, S., "Noise in FM Receivers," in Time Series Analysis, ed. M. Rosenblatt, Wiley, 1963. Also in J. Klapper (Ed.), "Selected Papers on Frequency Modulation," Dover, 1970.
7. Develet, J., "A Threshold Criterion for Phase Lock Demodulation," Proc. IRE, Vol. 51, No. 2, February, 1963.

8. Enloe, L., "The Synthesis of Frequency Feedback Demodulators," Proc. Nat. Electron. Conf. 18; 477, 1962.
9. Enloe, L., "Decreasing the Threshold in FM by Frequency Feedback," Proc. IRE, Vol. 50, No. 1, January, 1962.
10. Blachman, N., "The Demodulation of a Frequency Modulated Carrier and Random Noise by a Discriminator," J. Appl. Phys., Vol. 20, No. 10, October, 1949.
11. Middleton, D., "On the Theoretical Signal to Noise Ratios in FM Receivers: A Comparison with AM," J. Appl. Phys., Vol. 20, April, 1949.
12. Rice, S., "Statistical Properties of a Sine Wave Plus Random Noise," Bell System Technical Journal, Vol. 27, No. 3, January, 1948.
13. Corrington, M., "Variation of Bandwidth with Modulation Index in Frequency Modulation," Proc. IRE, Vol. 35, No. 10, October, 1947.
14. Corrington, M., "Frequency Modulation Caused by Common and Adjacent Channel Interference," RCA Review, Vol. 7, No. 4, December, 1946.
15. van der Pol, B., "The Fundamental Principles of FM," Journal of IEE, Vol. 93, Pt. 3, No. 23, May, 1946.
16. Stumpers, F., "Theory of Frequency-Modulated Noise," Proc. IRE, Vol. 36, No. 9, September, 1948.